

## PDF hosted at the Radboud Repository of the Radboud University Nijmegen

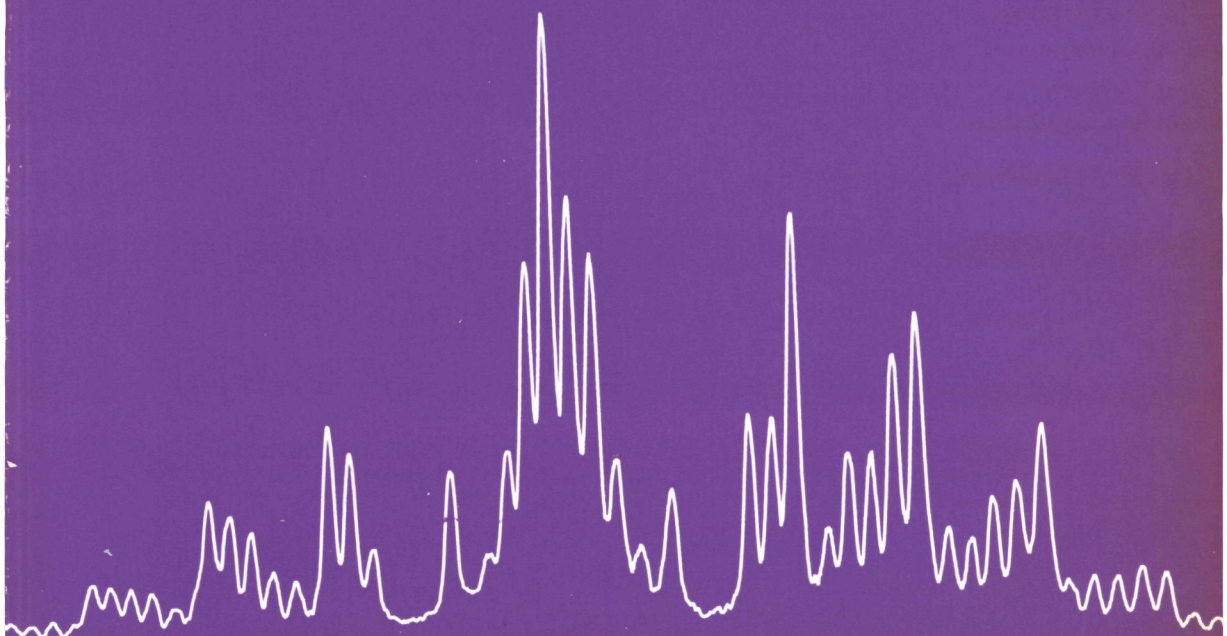
The following full text is a publisher's version.

For additional information about this publication click this link.

<http://hdl.handle.net/2066/146457>

Please be advised that this information was generated on 2017-03-14 and may be subject to change.

**HIGH RESOLUTION UV SPECTROSCOPY  
ON JET-COOLED MOLECULES**



Marcel Drabbels



**HIGH RESOLUTION UV SPECTROSCOPY  
ON JET-COOLED MOLECULES**

Drabbels, Marcel Mathias Johannes Elisabeth

**High resolution UV spectroscopy on jet-cooled molecules /  
Marcel Mathias Johannes Elisabeth Drabbels. - [S.l. :  
s.n.]. - I11.**

**Proefschrift Nijmegen. - Met lit. opg. - Met samenvatting  
in het Nederlands.**

**ISBN 90-9006299-8**

**Trefw.: moleculaire natuurkunde / spectroscopie.**

# **HIGH RESOLUTION UV SPECTROSCOPY ON JET-COOLED MOLECULES**

**EEN WETENSCHAPPELIJKE PROEVE OP HET GEBIED VAN  
DE NATUURWETENSCHAPPEN**

## **PROEFSCHRIFT**

**TER VERKRIJGING VAN DE GRAAD VAN DOCTOR  
AAN DE KATHOLIEKE UNIVERSITEIT NIJMEGEN,  
VOLGENS BESLUIT VAN HET COLLEGE VAN DECANEN  
IN HET OPENBAAR TE VERDEDIGEN  
OP WOENSDAG 22 SEPTEMBER 1993,  
DES NAMIDDAGS TE 3.30 UUR PRECIES**

door

**MARCEL MATHIAS JOHANNES ELISABETH DRABBELS**

**geboren op 31 maart 1966  
te Venray**

**Promotor** : **Prof. Dr. J. Reuss**

**Co-Promotores** : **Dr. J.J. ter Meulen**  
**Dr. W.L. Meerts**

aan Elly.





# Voorwoord

Op deze plaats zou ik graag iedereen willen bedanken die op directe of indirecte wijze een bijdrage heeft geleverd aan het welslagen van het onderzoek en het tot stand komen van dit proefschrift. Enkele van hen wil ik met naam noemen:

- Johannes Heinze voor de plezierige en intensieve samenwerking gedurende de eerste twee jaar van mijn promotie-onderzoek. Zijn inzet en geduld hebben ervoor gezorgd dat het PDA systeem zo'n succes is geworden.
- Mijn vaste begeleiders Hans ter Meulen en Leo Meerts die beide een belangrijke bijdrage hebben geleverd aan het welslagen van dit onderzoek.
- Jörg Reuss and Dave Parker voor hun altijd aanwezige belangstelling en de vele vruchtbare discussies.
- Gerard Meijer die altijd wel een antwoord had op mijn vele vragen en die me met veel enthousiasme heeft ingewijd in de wereld van georiënteerde moleculen.
- Maarten Ebben, Jean Schleipen en Michel Versluis voor de gezellige sfeer op de oude zit-, toen nog *koffiekamer* en voor de prettige samenwerking tijdens de nimmer overtroffen vrijdagmiddag experimenten.
- Steven Stolte die mij op onnavolgbare wijze duidelijk heeft weten te maken hoe  $\infty$  moleculen rechtop staan.
- Hanna Zuckermann who introduced me in the always surprising world of acetone. Thanks to her perseverance acetone had to reveal its secrets.
- Giel Berden en Harold Linnartz die altijd voor een gezellige, ietwat rumoerige maar ook zeker inspirerende sfeer op onze zitkamer wisten te zorgen. De introductie van de "*mini-multi-mixer-shaker*" heeft zeker bijgedragen tot een beter begrip van roterende en dissociërende moleculen.
- John Holtkamp, Frans van Rijn, Eugene van Leeuwen en Cor Sikkens die altijd wel een oplossing hadden voor de vele kleine en grote problemen van technische of electronische aard.
- John van Bladel, Daniela Consalvo, Ger van den Hoek, Paul Uit de Haag en Adrian Marijnissen voor de plezierige samenwerking tijdens de verschillende experimenten.
- Patrick Slavenburg voor zijn bijdrage als student aan de bouw van het PDA systeem.
- Alle medewerkers van de Glasblazerij, Instrumentmakerij, Quick-service, 'Zelf'-service, Illustratie en Fotografie van de Faculteit der Natuurwetenschappen.
- Mijn ouders die mij altijd in alles hebben gesteund.
- En natuurlijk Elly, wat zij voor mij betekent valt met geen pen of tekstverwerker te beschrijven.



# Contents

---

<b>1</b>	<b>General introduction</b>	<b>13</b>
	References . . . . .	17
<b>2</b>	<b>A high power Fourier transform limited laser system for high resolution spectroscopy</b>	<b>19</b>
2.1	Introduction . . . . .	20
2.2	Experimental setup . . . . .	21
2.3	Performance . . . . .	23
	2.3.1 Output power . . . . .	23
	2.3.2 Spatial beam profile . . . . .	23
	2.3.3 Bandwidth . . . . .	24
	2.3.4 ASE . . . . .	26
2.4	Conclusions . . . . .	27
	References . . . . .	29
<b>3</b>	<b>A study of the singlet-triplet perturbations in the <math>\tilde{A}^1A_u</math> state of acetylene by high resolution UV spectroscopy</b>	<b>31</b>
3.1	Introduction . . . . .	32
3.2	Experimental . . . . .	32
3.3	Results and discussion . . . . .	33
	3.3.1 Fermi perturbation . . . . .	38
	3.3.2 Singlet-triplet interactions . . . . .	39
	3.3.3 Hyperfine structure . . . . .	42
	3.3.4 Magnetic field measurements . . . . .	44
3.4	Summary . . . . .	46
	Acknowledgements . . . . .	47
	References . . . . .	48
<b>4</b>	<b>Acetone, a laser-induced fluorescence study with rotational resolution at 320 nm</b>	<b>51</b>
4.1	Introduction . . . . .	52
4.2	Experimental . . . . .	53
4.3	Spectroscopic Results and Analysis . . . . .	54
	4.3.1 Analysis of the $0_0^0$ band . . . . .	54
	4.3.2 Refined analysis of the $0_0^0$ band . . . . .	60
	4.3.3 Analysis of the torsional progression . . . . .	63
4.4	Other low energy modes . . . . .	66

4.4.1	First possibility . . . . .	67
4.4.2	Second possibility . . . . .	68
4.5	Discussion . . . . .	68
	Acknowledgements . . . . .	70
	References . . . . .	71
<b>5</b>	<b>High resolution laser induced fluorescence study of a cage molecule, 1,4-diazabicyclo[2,2,2]octane, DABCO</b>	<b>73</b>
5.1	Introduction . . . . .	74
5.2	Experimental . . . . .	74
5.3	Theoretical aspects . . . . .	75
5.4	Analysis . . . . .	77
5.5	Discussion . . . . .	81
5.6	Conclusion . . . . .	82
	Acknowledgements . . . . .	82
	References . . . . .	83
<b>6</b>	<b>Production of an intense pulsed beam of oriented metastable CO a <sup>3</sup>Π</b>	<b>85</b>
6.1	Introduction . . . . .	86
6.2	Method of production . . . . .	86
6.3	Experimental . . . . .	88
6.4	Results . . . . .	88
6.5	Conclusion . . . . .	91
	Acknowledgements . . . . .	91
	References . . . . .	92
<b>7</b>	<b>Determination of electric dipole moments and transition probabilities of low-lying singlet states of CO</b>	<b>93</b>
7.1	Introduction . . . . .	94
7.2	Experimental . . . . .	94
7.3	Results . . . . .	95
7.3.1	Spectroscopic . . . . .	95
7.3.2	Dipole moments . . . . .	97
7.3.3	Transition probabilities . . . . .	102
7.4	Summary . . . . .	105
	Acknowledgements . . . . .	105
	References . . . . .	106
<b>8</b>	<b>High resolution double-resonance spectroscopy on Rydberg states of CO</b>	<b>107</b>
8.1	Introduction . . . . .	108
8.2	Experimental . . . . .	109
8.3	Determination of predissociation rates . . . . .	110
8.4	Results . . . . .	113
8.4.1	B (3σ) <sup>1</sup> Σ <sup>+</sup> state . . . . .	113
8.4.2	L (4pπ) <sup>1</sup> Π(v = 0) state . . . . .	115
8.4.3	L' (3dπ) <sup>1</sup> Π(v = 1) state . . . . .	118

---

8.4.4	K ( $4p\sigma$ ) $^1\Sigma^+(v=0)$ state . . . . .	120
8.4.5	W ( $A^2\Pi$ ) ( $3s\sigma$ ) $^1\Pi(v=0)$ state . . . . .	121
8.4.6	W' $^1\Pi(v=2)$ state . . . . .	123
8.5	Discussion . . . . .	126
8.6	Summary . . . . .	127
	Acknowledgements . . . . .	127
	References . . . . .	129
<b>9</b>	<b>Pulsed-cw double-resonance spectroscopy on the B <math>^1\Sigma^+(v'=0) \leftarrow</math> A <math>^1\Pi(v''=0)</math> system of CO</b> . . . . .	<b>131</b>
9.1	Introduction . . . . .	132
9.2	Experimental . . . . .	132
9.3	Results . . . . .	133
9.4	Discussion . . . . .	136
	References . . . . .	138
	<b>Samenvatting</b> . . . . .	<b>139</b>
	<b>Curriculum Vitae</b> . . . . .	<b>141</b>
	<b>Publications</b> . . . . .	<b>143</b>



## General Introduction

Laser spectroscopy can provide detailed information on the dynamics and structure of molecules. Thanks to the rapid development in laser technology it is nowadays possible to study molecules from the microwave to the XUV region of the electromagnetic spectrum. Whereas microwave and infrared spectroscopy can yield very detailed information on the rotational and vibrational motions of molecules, visible and UV spectroscopy also give insight in the electronic structure. Depending on the resolution at which the molecules are studied different types of interactions between the various kinds of motion can be observed. For instance, the interaction between the electronic motion and the overall rotation of many molecules can already be observed with a resolution of the order of  $0.1 \text{ cm}^{-1}$ . The interaction between the electronic motion and the spins of the nuclei, on the other hand, is only observable with a resolution of the order of 100 MHz or better.

A variety of spectroscopic techniques has been developed to study the electronically excited states of atoms and molecules. One of the most common techniques in modern laser spectroscopy is laser-induced fluorescence (LIF). This technique is based on the detection of the fluorescence from an electronically excited state after it has been populated by a laser. LIF detection has the advantage, besides being very sensitive, that it can be applied in combination with both cw and pulsed lasers, this in contrast to other widely used techniques like resonance enhanced multiphoton ionization (REMPI) or degenerate four-wave mixing (DFWM) which require high laser powers, only available from pulsed lasers.

A very elegant way to perform high resolution spectroscopy on electronically excited states of molecules is by combining LIF detection using a single-frequency cw ring dye laser with molecular beam techniques. In a molecular beam the Doppler width is vastly reduced so that full advantage can be taken of the very narrow bandwidth ( $\sim 1 \text{ MHz}$ ) of the laser system. Already since many years this technique is successfully applied at the Nijmegen laboratory [1, 2, 3]. The wavelength region that can be covered by a cw ring dye laser is limited to the visible region of the electromagnetic spectrum. However, the wavelength range can be efficiently extended to wavelengths down to 295 nm by intra-cavity frequency doubling of the fundamental laser beam in an angle-tuned  $\text{LiIO}_3$  crystal [4]. Up to now almost no high resolution spectroscopy has been performed below this wavelength due to the lack of efficient non-linear crystals. With the recent development of



$\beta$ -BaB<sub>2</sub>O<sub>4</sub> (BBO) as a non-linear material this situation has changed. Now it is possible to cover the wavelength region down to 205 nm.

In Chapter 3 of this thesis an experiment is described in which the narrow bandwidth UV radiation obtained by intra-cavity frequency doubling in a BBO crystal is used to study the  $\tilde{A} \leftarrow \tilde{X}$  transition in acetylene at 220 nm with a resolution of 18 MHz. Due to a strong coupling with isoenergetic triplet states the spectrum is strongly perturbed. However, the resolution is high enough not only to resolve these perturbations but also to resolve the hyperfine structure of the perturbing triplet states. In this way detailed information on the character of the triplet states is obtained.

Due to the relatively low power the use of cw dye lasers in molecular spectroscopy is mostly limited to the study of electronically excited states that can be probed by one-photon allowed transitions. For the study of first-order forbidden electronic transitions or multiphoton transitions it would be advantageous to have a narrow bandwidth laser system with a high power. In 1977 Salour [5] succeeded in building such a system by combining a cw dye laser with a pulsed N<sub>2</sub> laser. The narrow bandwidth radiation of the cw laser was amplified in three stages by the pulsed N<sub>2</sub> laser, yielding an amplified laser beam with a peak power of 100 kW. The bandwidth of the

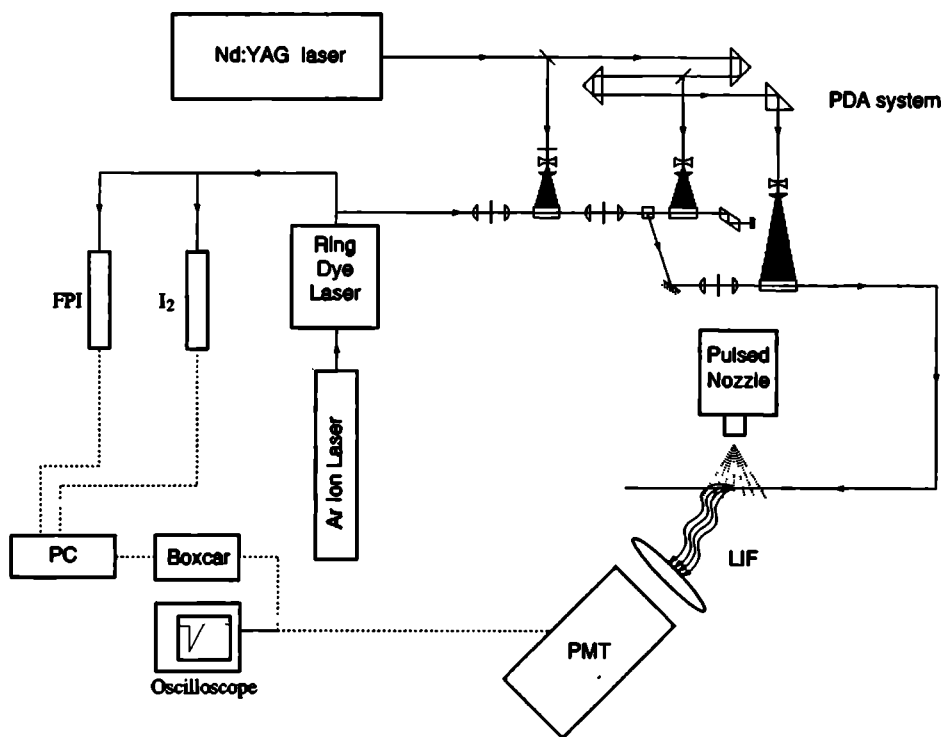


Figure 1.1: Schematic overview of the experimental setup used in most experiments.

amplified radiation was solely determined by the Fourier transform of the temporal profile of the pump laser and amounted to 60 MHz. Recently, a similar pulsed dye amplifier (PDA) system has been built at the Nijmegen laboratory. The radiation of a single-frequency cw ring dye laser is amplified in three stages, of which the second stage is used in a double-pass configuration, by a Q-switched Nd:YAG laser. In this way radiation with a peak power up to 30 MW per pulse and a bandwidth of 135 MHz is obtained. A full description of the Nijmegen PDA system is given in Chapter 2 of this thesis. Taking full advantage of the bandwidth of this type of laser system does not require an expensive molecular beam apparatus; the reduction of the Doppler width in a free jet expansion is already sufficient. The high density of molecules in a jet makes the combination of a free jet expansion with a PDA laser system an ideal technique to study weak electronic transitions in molecules at a relatively high resolution. Figure 1.1 gives a schematic overview of such an experimental setup used in most experiments described in this thesis.

Chapter 4 describes an experiment on acetone,  $\text{CO}(\text{CH}_3)_2$ . The very weak  $S_1 \leftarrow S_0$  transition at 320 nm has been studied with a resolution of 270 MHz using the PDA system. The individual rovibronic transitions show very complex splittings due to the internal rotation of the two methyl groups and a coupling of these rotations with vibrational modes. From the analysis of these splittings the barrier height for the internal rotation of the two methyl groups in both the  $S_0$  and  $S_1$  electronic state could be determined.

In Chapter 5 it is shown that it is possible with the PDA system to resolve even the rotational structure of an electronic transition involving a 20-atom molecule, DABCO. Due to the high spectral brightness of the laser system not only electric dipole transitions were observed but also the extremely weak electric quadrupole transitions could be detected.

Chapter 6 describes an experiment in which full use of the characteristics of the PDA system, *i.e.* narrow bandwidth and high peak power, is being made. Using the pulsed dye amplifier system CO molecules in a free jet are resonantly excited in the presence of an electric field to the metastable a  $^3\Pi(v=0)$  state. Due to the electric field the  $M$ -degeneracy of the rotational levels is lifted. By populating one specific rotational  $M$ -sublevel it is possible to orient the carbon monoxide molecules with respect to the applied electric field. Due to the long lifetime of the excited state a beam of oriented metastable a  $^3\Pi(v=0)$  carbon monoxide molecules can be produced, which can be used to study for example steric effects in reactive molecular scattering.

The second part of this thesis deals with the spectroscopy of highly excited electronic states of the CO molecule. Transitions from the electronic ground state to these high-lying electronic states fall in the VUV ( $100 \text{ nm} < \lambda < 200 \text{ nm}$ ) and XUV ( $\lambda < 100 \text{ nm}$ ) region of the electromagnetic spectrum. Spectroscopy in this region of the spectrum is hampered by the lack of intense and tunable light sources. Whereas laser light with a wavelength above 188 nm can efficiently be generated by frequency doubling or mixing of visible laser light in non-linear crystals like BBO this is no longer possible for wavelengths below this value due to self absorption of the generated UV light by the crystal. A well-known method for the generation of coherent tunable VUV and XUV radiation is third-order frequency conversion in atomic or molecular gases [6]. However, a rather expensive and complicated experimental setup is required and the conversion efficiencies that can be obtained are relatively low. Very attractive alternatives for direct one-photon VUV or XUV spectroscopy on high-lying electronic states are multiphoton and double-resonance spectroscopy.

The sensitivity of multiphoton spectroscopy depends strongly on the number of absorbed photons. In case of two-photon spectroscopy the sensitivity is comparable with that of direct VUV spectroscopy using the presently available sources. This offers the possibility to study electronic

states in the energy region between 50 000 and 100 000  $\text{cm}^{-1}$  with a relatively simple experimental setup using a single laser system. Due to the relatively low excitation rates two-photon spectroscopy on highly excited electronic states in the VUV region is mostly performed with pulsed lasers. In some favorable cases it is possible to use continuous lasers [7] as well, in which case the electronic states can be studied at high resolution. The spectroscopic information obtained by one- and two-photon excitation is for diatomic molecules in most cases identical. However, due to the difference in selection rules between one- and two-photon excitation, it is sometimes possible to observe electronic states by two-photon spectroscopy that can not be observed by one-photon spectroscopy.

In Chapter 7 an experiment on highly excited electronic states of carbon monoxide is described, showing the power of two-photon spectroscopy in combination with a Fourier transform limited laser system. The CO molecules are excited from the electronic ground state to electronic states around 90 000  $\text{cm}^{-1}$  in the presence of an electric field. Due to the Stark effect the  $M$ -degeneracy is lifted. By measuring the splittings and lineshifts of the rotational levels as a function of the applied electric field the permanent electric dipole moments of these states could be determined.

Double-resonance spectroscopy offers the possibility to study electronically excited states in molecules with a resolution of several MHz. In a first step one specific rovibronic level in an electronically excited state is populated by a pump laser. In a second step a transition between the level populated by the pump laser and a higher electronic state is induced. Using a single-frequency cw dye laser in the second step both electronically excited states can be studied at high resolution. This technique has already successfully been employed to study Rydberg states in NO in the region around 65 000  $\text{cm}^{-1}$  [8, 9]. In principle it is possible to study with this technique electronic states up to 150 000  $\text{cm}^{-1}$  with a resolution of a few MHz if in the first step a highly excited electronic state is populated via a two-photon transition. Double-resonance spectroscopy not only offers the possibility to study electronic states at high resolution, it can also be used to study strongly predissociating states. Whereas direct spectroscopy on such states becomes difficult due to the fact that the fluorescence from the predissociating state is vastly reduced, this is not the case for double-resonance spectroscopy where the problem of the reduced fluorescence can be circumvented by monitoring the fluorescence from the intermediate state. In this case a transition induced to the upper predissociating state can be detected by a decrease of the fluorescence from the intermediate state.

In Chapter 8 an experiment is described in which this technique has been used to study Rydberg states of CO in the energy region around 103 000  $\text{cm}^{-1}$ . After populating a rotational level in the  $B^1\Sigma^+(v=0)$  state with a "normal" pulsed laser via a two-photon transition, the Rydberg states are probed in the second step by the PDA system. Thanks to the narrow bandwidth of the PDA system the linewidths of these transitions could be accurately determined yielding precise values for the predissociation rates of the Rydberg states.

The last chapter of this thesis describes a similar experiment on the  $B^1\Sigma^+(v=0)$  electronic state of CO. In the first step a rotational level of the  $A^1\Pi(v=0)$  state is populated after which the B state is probed by a narrow bandwidth cw dye laser. In this way the energy levels of the strongly perturbed intermediate  $A^1\Pi(v=0)$  state could be accurately determined.

**References**

1. W. Ubachs, *Ph.D. Thesis*, Katholieke Universiteit Nijmegen (1986)
2. W.M. van Herpen, *Ph.D. Thesis*, Katholieke Universiteit Nijmegen (1988)
3. P. Uijt de Haag, *Ph.D. Thesis*, Katholieke Universiteit Nijmegen (1990)
4. W.A. Majewski, *Opt. Comm.* **45**, 201 (1983)
5. M.M. Salour, *Opt. Comm.* **22**, 202 (1977)
6. C.R. Vidal, in *"Topics in Applied Physics, Volume 59: Tunable Lasers"*, Eds. L.F. Mollenauer and J.C. White, Springer Verlag, Berlin (1987)
7. R.G. Beausoleil, D.H. McIntyre, C.J. Foot, E.A. Hildum, B. Couillaud and T.W. Hänsch, *Phys. Rev. A* **39**, 4591 (1989)  
C. Zimmermann, R. Kallenbach and T.W. Hänsch, *Phys. Rev. Lett.* **65**, 571 (1990)
8. G. Meijer, M. Ebben and J.J. ter Meulen, *Chem. Phys. Lett.* **147**, 525 (1988)  
G. Meijer, M. Ebben and J.J. ter Meulen, *Chem. Phys.* **127**, 173 (1988)
9. R.J. Miller and B.A. Bushaw, *J. Chem. Phys.* **92**, 3245 (1990)



### **A High Power Fourier Transform Limited Laser System For High Resolution Spectroscopy**

#### **Abstract**

Radiation with a high peak power and a near Fourier transform limited bandwidth is obtained by pulsed amplification of narrow bandwidth radiation of a cw ring dye laser. Employing a Q-switched Nd:YAG laser as pump laser amplified radiation with an output energy up to 150 mJ per pulse is obtained. The bandwidth has been measured to be 135 MHz when the system is pumped by the second harmonic and 235 MHz when pumped by the third harmonic of the Nd:YAG laser.

## 2.1 Introduction

In modern laser spectroscopy two different tunable laser systems are often used for the study of electronically excited states of atoms and molecules, *i.e.* cw ring dye lasers and pulsed dye lasers. As can be seen in Table 2.1 the properties of both systems are very different. Whereas a cw dye laser has a very narrow bandwidth and a relatively low output power a pulsed dye laser has a relatively large bandwidth and a very high peak power. Consequently, both laser systems are used for different types of spectroscopy.

The combination of narrow bandwidth cw ring dye lasers with molecular beam techniques makes it possible to observe electronic transitions in molecules with a resolution of a few MHz. In this way very weak interactions, such as hyperfine interactions, can be studied in diatomic molecules [1]. With this resolution it is also possible to resolve the rotational structure of electronic transitions of polyatomic molecules [2, 3] and even of complexes of these molecules with rare gas atoms [2] so that information about the geometrical structure of these molecules and complexes can be obtained. Since the output of a cw dye laser is in the visible and near UV region of the spectrum usually only the lowest electronically excited states can be studied.

Pulsed dye lasers are, because of their high peak powers, often used to study high-lying electronically excited states of molecules by multiphoton spectroscopy [4]. The spectral range of these lasers can, because of their high peak powers, be extended to the VUV and even XUV region of the electromagnetic spectrum via non linear techniques [5]. In this way direct one-photon spectroscopy on high-lying electronically excited states of molecules can be performed. Due to the relatively large bandwidth of pulsed dye lasers their use is mostly limited to spectroscopy on diatomic and small polyatomic molecules.

To perform high resolution spectroscopy on high-lying electronically excited states of diatomic and polyatomic molecules it would be advantageous to have a laser system which combines the narrow bandwidth of a cw dye laser with the high peak power of a pulsed dye laser. As early as 1977 Salour [6] succeeded in building such a laser system. The narrow bandwidth radiation of a cw dye laser was amplified in three stages by a pulsed laser. The bandwidth of the pulsed amplified radiation is in this case determined by the Fourier transform of the temporal profile of the pump laser. Employing a  $N_2$  laser as pump laser for the pulsed dye amplifier (PDA) system radiation with a bandwidth of 60 MHz and a peak power of 100 kW was obtained. By replacing the  $N_2$  pump laser by a more powerful Nd:YAG laser Drell and Chu [7] obtained one year later narrow bandwidth radiation with a peak power exceeding 5 MW. Recently Cromwell *et al.* [8] built a high power PDA system making use of the latest technical novelties. This system is used to generate via non-linear processes XUV radiation with a bandwidth of about 200 MHz.

System	Bandwidth	(Peak) Power
cw ring dye laser	$\sim 1$ MHz	$\sim 1$ W
pulsed dye laser	$> 1$ GHz	$\sim 1$ MW
pulsed dye amplifier	$\sim 100$ MHz	$\sim 1$ MW

Table 2.1: Characteristics of different types of laser systems.

The pulsed dye amplifier system described here is quite similar to the system of Cromwell *et al.* but is built in a more compact way. Furthermore, the wavelength range at which the system can operate is extended to the blue region of the spectrum.

## 2.2 Experimental setup

The starting point of our system is a single-frequency cw ring dye laser (Spectra Physics 380D) pumped by a powerful argon ion laser (Spectra Physics 2045-15). The ring dye laser can at present be operated either in the red (540-670 nm), when pumped by the visible lines of the argon ion laser, or in the blue (410-470 nm) region of the spectrum, when pumped by the UV lines of the argon ion laser. The bandwidth of this laser system is less than 1 MHz and the output power is typically 500 mW in the red and 200 mW in the blue.

The second key component of the laser system is a high power Q-switched Nd:YAG laser (Quantel YG681-10C) which serves as pump laser. The second harmonic of the Nd:YAG laser,  $\lambda=532$  nm, has a pulse energy of 550 mJ and is used to pump the PDA system when operated in the red. The third harmonic,  $\lambda=355$  nm, which is used to pump the system when operated in the blue, has an output energy of 200 mJ per pulse. The most important limiting factor on the bandwidth of the PDA system is the temporal profile of the amplified laser beam which is directly related to the temporal profile of the pump laser. The output of the unseeded Nd:YAG laser consists of fast spikes with a Gaussian envelope. The effective pulse length of the second

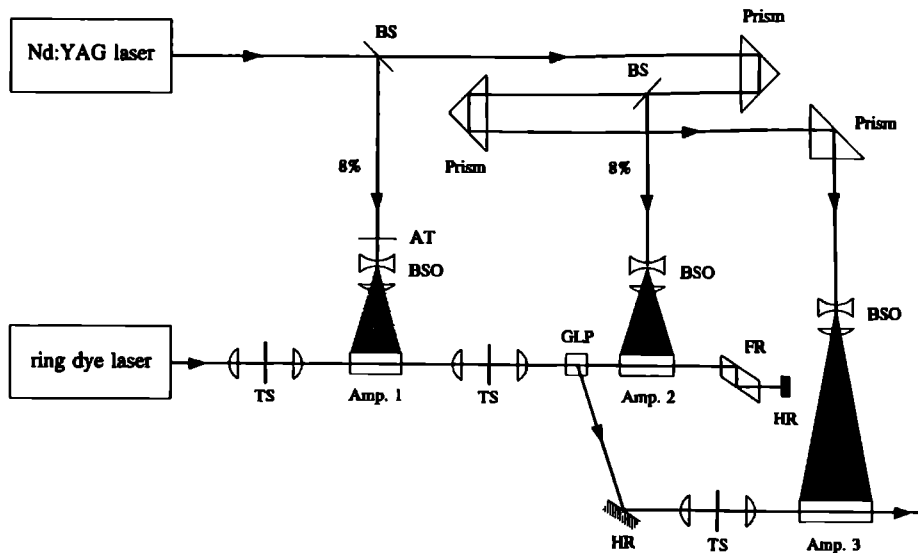


Figure 2.1: Schematic overview of the pulsed dye amplifier (PDA) system. BS: beam splitter, BSO: beam shaping optics, AT: attenuator, TS: telescope, Amp: amplifier, GLP: Glan-laser polarizer, FR:  $\lambda/4$  Fresnel rhomb, HR: high reflector.



harmonic is in the order of 5 ns. That of the third harmonic is considerably shorter, 3-4 ns and consequently the bandwidth of the amplified laser beam will be larger when the third harmonic is used to pump the PDA system.

In our setup the distance between the ring dye laser and PDA system is more than 10 m and as a result the system can operated without a Faraday optical isolator which is usually used to optically decouple the ring dye laser from the PDA system [7, 8]. The Nd:YAG laser is positioned as close as possible to the PDA system in order to avoid damage of the steering and beam shaping optics due to the presence of hot spots in the laser beam at large distances.

A schematic overview of the PDA system is given in Figure 2.1. The cw radiation is amplified in three stages, where the second stage is used in a double-pass configuration. After having passed the second amplifier for the first time the polarization of the laser beam is rotated  $90^\circ$  by means of a  $\lambda/4$  Fresnel rhomb and a mirror. After the laser beam has passed the second amplifier for the second time it is directed to the third amplifier by a Glan-laser polarizer.

To obtain a homogeneous beam profile Bethune dye cells are used [9]. These cells are based on standard  $45^\circ$  right angle, fused silica prisms with a hole drilled through in which the dye solution flows. The unfocussed laser beam enters from the left with a height of four times the diameter of the bore, as indicated in Figure 2.2. The four segments of the pump beam irradiate the four different sides of the dye cylinder via internal reflections at the surfaces of the prism. In our system three such dye cells of different size are used. The first cell has a bore size of  $\phi$  1 mm and a length of 20 mm. The second cell has a  $\phi$  3 mm  $\times$  30 mm bore and the final amplifier has a bore of  $\phi$  6 mm and a length of 60 mm. In order to obtain a homogeneous and in time stable spatial beam profile each dye cell is connected to a separate dye circulator with dye cooling circuit. To minimize

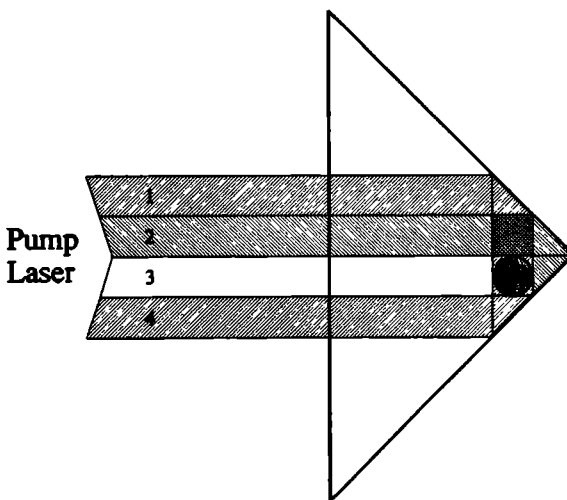


**Figure 2.2:** Side view of the Bethune dye cell. The four segments (1-4) of the pump laser, coming from the left, pump the top, back, front and bottom of the dye solution.

the growth of amplified stimulated emission (ASE) the windows of the dye cells are AR-coated and placed under a small angle. Telescopes consisting of a lens-pinhole-lens combination are used to spatially filter the laser beam to further reduce the growth of ASE and to maintain a diffraction limited beam profile with low divergence. These telescopes, with amplification powers of  $1\times$ ,  $3\times$  and  $2\times$ , also serve to match the shape of the amplified laser beam to the diameter of the different dye cells.

To obtain radiation with an as small as possible bandwidth the amplified laser beam and the pump beam have to temporally overlap at each dye cell. A delay line consisting of retro-reflectors is used to match the delay between the Nd:YAG laser and the amplified laser beam. The pump energy is distributed by two beam splitters over the three amplifier stages with a ratio of 8:8:84. Usually the pump beam for the first amplifier is attenuated by a factor of 2-10 using neutral density filters to minimize the growth of ASE, see section 2.3.4. The pump laser beam is then shaped by AR-coated negative spherical and positive cylindrical lenses to match the size of the laser beam to the length and bore diameter of each dye cell.

## 2.3 Performance

### 2.3.1 Output power

The output power of the PDA system is mainly determined by the pulse energy of the pump laser and the efficiency and concentration of the laser dye used. Since the beam profile of the amplified laser beam depends also on the dye concentration (see section 2.3.2) a compromise between spatial beam profile and pulse energy is necessary. The output power of the system hardly depends on the power of the cw seed laser. A cw laser power of 1 mW, the output of a HeNe laser, is already enough to produce an amplified laser beam with an energy of 40 mJ per pulse. If the power of the cw laser exceeds 25 mW the output power of the PDA system is independent of the power of the seed laser. The output energy of the PDA system is typically 80-150 mJ per pulse when efficient red laser dyes (Rhodamine and DCM) are used which are pumped by the second harmonic of the Nd:YAG laser. To extend the wavelength to the UV region of the spectrum the output of the PDA system is frequency doubled in a KDP crystal. The output energy after frequency doubling is typically 20-30 mJ. When the system is operated in the blue region of the spectrum and less efficient laser dyes (Coumarin) are used which have to be pumped by the third harmonic of the Nd:YAG laser, the output is much less, typically 10-20 mJ. After frequency doubling in a BBO crystal an UV laser beam with a pulse energy of 1-2.5 mJ results.

The shot-to-shot fluctuations of the laser system are mainly determined by the stability of the pump laser and are in the order of 10%. However, when the distance between the cw laser and the PDA systems is very large ( $>25$  m) the shot-to-shot fluctuations are larger due to the beam pointing instability of the seed laser.

### 2.3.2 Spatial beam profile

In the present setup Bethune prisms are used as dye cells [9]. These cells have the advantage that the dye volumes can be pumped fairly uniformly, resulting in a cylindrically symmetric spatial beam profile. The radial intensity distribution of the amplified laser beam is largely determined by the dye concentration. At high dye concentrations most of the pump light is absorbed near the edges of the dye cell and as a consequence the laser beam has a donut-like spatial beam profile

with high intensities near the edges and almost no intensity at the center of the laser beam. At low dye concentrations the amount of absorbed pump light is almost equal over the entire dye volume. The laser beam then has a nearly uniform spatial beam profile with sharp edges. However, at low concentrations the total amount of absorbed pump light is relatively low and consequently the output power of the system is rather low. It can be shown that the intensity at the center of the laser beam is maximum when the absorption coefficient of the dye solution is equal to one over the bore radius of the dye cell. In this case nearly all the pump light, 86%, is absorbed and a fairly uniform laser beam with slightly higher intensity at the edges is obtained.

In case the system is operated with efficient red dyes a nearly uniform amplified laser beam with low divergence and high output energy can be obtained. The spatial beam profile shows, however, some diffraction fringes arising from the aperturing of the near Gaussian beam by the bore of the amplifier cells. This effect can be minimized by reducing the beam diameter of the cw dye laser, which causes, however, also a loss in output energy. A compromise between spatial beam quality and output energy is therefore required. When the system is operated with the less efficient blue dyes the gain in the amplifiers is much lower and in order to be able to amplify the cw laser beam it is necessary to use rather high dye concentrations in the amplifier cells. As a result a laser beam with a donut-like spatial beam profile is obtained.

### 2.3.3 Bandwidth

The bandwidth of the amplified radiation is directly related to the temporal profile of the amplified laser beam by a Fourier transformation. Under the assumption that the Nd:YAG laser has a Gaussian temporal profile and that the temporal profile of the amplified laser beam resembles that

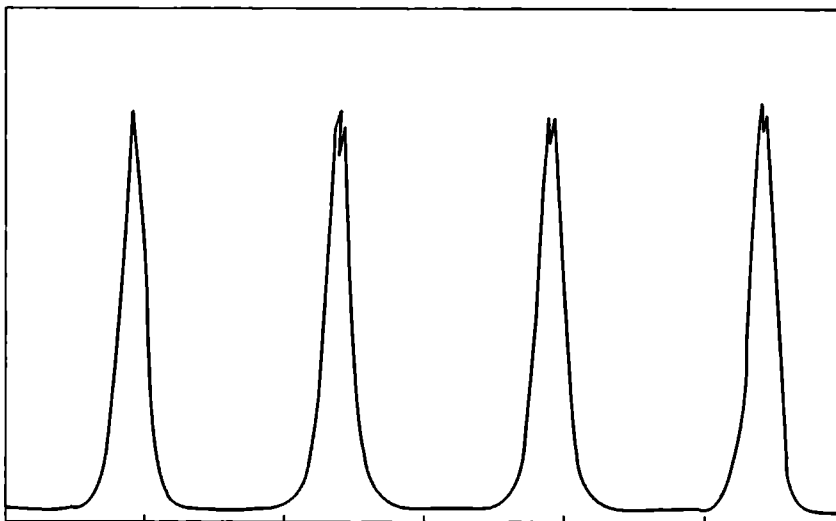


**Figure 2.3:** Wavelength scan of the PDA laser system around 460 nm through a high finesse etalon with a free spectral range of 1.5 GHz. The frequency is marked every GHz.

of the pump laser, the bandwidth of the amplified radiation,  $\Delta\nu$ , is related to the pulse length,  $\tau$ , of the pump laser by:

$$\Delta\nu = \frac{2 \ln 2}{\pi\tau} \quad (2.1)$$

This implies that the minimum bandwidth of our PDA system is limited to 88 MHz, assuming a pulse length of 5 ns for the pump laser.

The bandwidth of the PDA system has been determined by recording the transmission fringes of a Fabry-Perot interferometer (FPI) with a free spectral range of 1.5 GHz and a finesse of 200. Figure 2.3 shows the transmission fringes of the FPI obtained by scanning the wavelength of the PDA system, which in this case is pumped by the third harmonic of the Nd:YAG laser. The width of the fringes is mainly determined by the bandwidth of the amplified radiation since the contribution of the FPI to the observed width is in the order of a few MHz. The bandwidth has been analyzed by fitting the observed fringe pattern to a Voigt profile. It is found that the bandwidth of the system is 135 MHz when pumped by the second harmonic of the Nd:YAG laser and 235 MHz when pumped by the third harmonic. In both cases the bandwidth has a large Gaussian contribution (>90%) and a small Lorentzian contribution (<10%). The difference in bandwidth found when the system is pumped by the second or third harmonic of the Nd:YAG laser is clearly due to a difference in pulse length. Figure 2.4 shows the temporal profile of the amplified radiation measured with a detection system with a response time of 4 ns. Although it is not possible to exactly analyze the temporal profile it is clear that the pulse length is a factor of  $\sim 1.5$  shorter when the PDA is pumped by the third harmonic of the Nd:YAG laser. This is in perfect agreement with the observed difference in bandwidth.

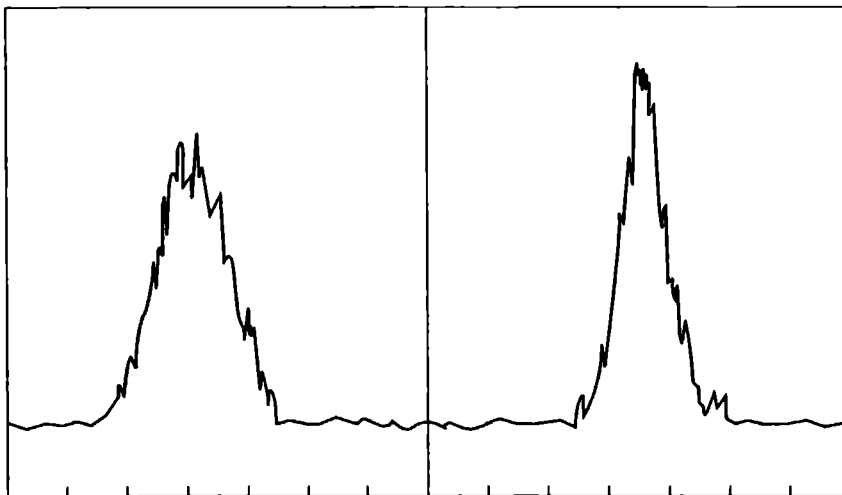


**Figure 2.4:** Temporal profile of the amplified laser beam when the PDA system is pumped by the second harmonic (left part) and by the third harmonic (right part) of the Nd:YAG laser. The markers are indicated every 2 ns.

## 2.3.4 ASE

Great care has been taken to minimize the growth of amplified spontaneous emission (ASE) in the PDA system (see section 2.2) since this would reduce the gain of the cw laser beam. It is well-known that the amount of ASE produced in the system can not simply be determined by measuring the difference between the output energy of the system with and without cw seed laser, since the ASE is reduced when the system operates with seed laser. One way of measuring the ASE is by means of an etalon with a rather low finesse, 10-20. The amount of ASE can then be determined from the intensity ratio of the transmission peaks and the background caused by the ASE, which has typically a bandwidth of several nm. Figure 2.5 shows a wavelength scan of the laser system through a FPI with a free spectral range of  $0.66 \text{ cm}^{-1}$  and a finesse of 20. The left part of Figure 2.5 is recorded while 8% of the total pump energy is used to pump the first amplifier stage. From the observed intensity ratio of the transmission fringes and the background the ASE is determined to be 20%. By reducing the pump energy of the first amplifier stage by a factor of 10 the ASE can be reduced considerably as can be seen in the right part of Figure 2.5. Whereas the amount of ASE is reduced to less than the detection limit of 5% by reducing the pump energy of the first amplifier stage, the output power is not reduced and thus the effective output energy of the PDA system is increased by 20%.

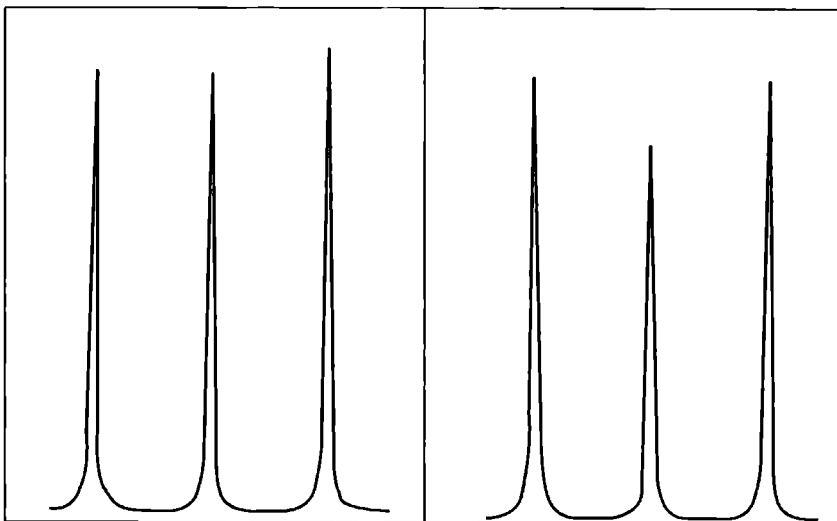


**Figure 2.5:** Wavelength scan of the laser around 580 nm through an etalon with a free spectral range of  $0.66 \text{ cm}^{-1}$  and a finesse of 20. The left part: The first amplifier stage is pumped by 8% (45 mJ) of the total pump energy. The right part: The first amplifier stage is pumped by less than 1% (5 mJ) of the total energy.

## 2.4 Conclusions

A laser system is described with a high output power, near Fourier transform limited bandwidth and a near Gaussian spatial beam profile. The performance of the system is quite different when operated in the blue or red region of the spectrum. The differences are mainly caused by the difference in pulse energy and pulse length of the second and third harmonic of the Nd:YAG laser. The main characteristics of the laser system are summarized in Table 2.2.

	Red	Blue
Wavelength cw dye laser	540-670 nm	410-470 nm
Power cw dye laser	500 mW	200 mW
Bandwidth cw dye laser	<1 MHz	<1 MHz
Wavelength pump laser	532 nm	355 nm
Pump energy	550 mJ	200 mJ
Pulse length pump laser	5 ns	3-4 ns
Output energy	80-150 mJ	10-20 mJ
Output energy $2h\nu$	20-30 mJ	1-2.5 mJ
Shot-to-shot fluctuations	10%	10%
Spatial beam profile	near Gaussian	Donut-like
Bandwidth	135 MHz	235 MHz
ASE	<5%	<5%

**Table 2.2:** Characteristics of the pulsed dye amplifier (PDA) system.

The wavelength range that can be covered at present is limited by the scanning range of the cw ring dye laser. In the near future this range will be extended so that the whole wavelength range between 410 and 900 nm can be covered. Via non-linear techniques it will then be possible to generate light with a high spectral brightness from the deep UV (196 nm) to the near infrared (900 nm) region of the spectrum.

The bandwidth of the PDA system is determined by the pulse length of the pump laser. In principle, the bandwidth of the system can only be reduced by replacing Nd:YAG laser by another pump laser with a longer pulse length. Table 2.3 summarizes the possible pump sources. The most attractive alternative is an Excimer laser which has a typical pulse length of 15 ns and a pulse energy that is nearly equal to that of a Nd:YAG laser. Using this type of pump laser would yield an amplified laser beam with a Fourier limited bandwidth of only 29 MHz. Another alternative is a Copper vapour laser which has even a longer pulse length and an extremely high repetition rate of 20 kHz. However, the output energy of this laser is considerably lower than that of a Nd:YAG laser. A completely different pump source is a flashlamp which has a typical pulse length of 100  $\mu$ s. Due to the long pulse length the peak power is relatively low. Another very attractive and less radical way to reduce the bandwidth of the amplified laser beam is by injection seeding the Nd:YAG pump laser. Injection seeding the Nd:YAG laser has not only the advantage that it

<b>Pump laser</b>	<b>Pulse energy</b>	<b>Pulse length</b>	<b>Bandwidth</b>
Nd:YAG laser, Quantel	550 mJ	5 ns	88 MHz
Nd:YAG laser, Quanta-Ray	500 mJ	8 ns	55 MHz
Excimer laser	400 mJ	15 ns	29 MHz
Copper vapour laser	10 mJ	40 ns	11 MHz
Flashlamp	50 J	100 $\mu$ s	<1 MHz

**Table 2.3:** Possible pump sources for the PDA system with their characteristics and the calculated bandwidth of the amplified laser beam.

produces an output pulse with a Gaussian temporal profile but it also tends to lengthen the output pulse. In case of the presently used Nd:YAG laser the pulse length would increase to 6-7 ns, which would yield a bandwidth of 70 MHz for the amplified laser beam.

## References

1. W. Ubachs, *Ph.D. Thesis*, Katholieke Universiteit Nijmegen (1986)
2. W.M. van Herpen, *Ph.D. Thesis*, Katholieke Universiteit Nijmegen (1988)
3. P. Uijt de Haag, *Ph.D. Thesis*, Katholieke Universiteit Nijmegen (1990)
4. G. van den Hoek, *Ph.D Thesis*, Katholieke Universiteit Nijmegen (1993)
5. C.R. Vidal, in "*Topics in Applied Physics, Volume 59: Tunable Lasers*", Eds. L.F. Mollenauer and J.C. White, Springer Verlag, Berlin (1987)
6. M.M. Salour, *Opt. Comm.* **22**, 202 (1977)
7. P. Drell and S. Chu, *Opt. Comm.* **28**, 343 (1978)
8. E. Cromwell, T. Trickl, Y.T. Lee and A.H. Kung, *Rev. Sci. Instr.* **60**, 2888 (1989)
9. D.S. Bethune, *Appl. Opt.* **20**, 1897 (1981)





### A Study Of The Singlet-Triplet Perturbations In The $\tilde{A} \ ^1A_u$ State Of Acetylene By High Resolution UV Spectroscopy

*M. Drabbels, J. Heinze and W.L. Meerts*

*Department of Molecular and Laser Physics, University of Nijmegen,  
Toernooiveld, 6525 ED Nijmegen, The Netherlands*

#### Abstract

Laser-induced fluorescence spectra of the  $3_0^3 K_0^1$  and  $3_0^4 K_0^1$  vibronic bands of the  $\tilde{A} \ ^1A_u \leftarrow \tilde{X} \ ^1\Sigma_g^-$  transition in acetylene have been recorded with a resolution of 18 MHz. Each rotational transition consists of a group of lines due to coupling of the electronically excited singlet state with isoenergetic triplet states. Using the standard deconvolution procedure the singlet-triplet coupling element and the density of coupled triplet states are derived for rotational levels up to  $J=4$  in both bands. From the density of coupled triplet states it is concluded that the  $\tilde{A} \ ^1A_u$  state is perturbed by the  $T_1 \ ^3B_2$  state. Magnetic field measurements have shown that the predissociation of acetylene in the  $4\nu_3'$  vibrational level of the  $\tilde{A}$  state is caused by a coupling via the  $T_1 \ ^3B_2$  state with predissociating vibrational levels of the electronic ground state.

### 3.1 Introduction

Acetylene plays an important role in bridging the gap between diatomic and large polyatomic molecules and is therefore one of the most intensively studied small polyatomic species. The  $\tilde{A}^1A_u \leftarrow \tilde{X}^1\Sigma_g^+$  band system of acetylene has been well analyzed spectroscopically [1, 2, 3, 4, 5]. On the basis of these studies it was concluded that acetylene has a *trans*-bent geometrical structure in the electronically excited  $\tilde{A}$  state, in contrast to the linear structure in the electronic ground state. A laser-induced fluorescence (LIF) study by Schrerer *et al.* [6] showed that the rotational structure of the  $\tilde{A} 3\nu_3'$  vibrational level is strongly perturbed. An extensive analysis of the perturbation showed that it arises from a Fermi interaction between the  $3\nu_3'$  and the  $\nu_2' + 2\nu_4'$  vibrational levels. The observation of quantum beats in other LIF studies indicated that this level is also perturbed by other interactions [7]. A study of these quantum beat phenomena in the presence of a magnetic field revealed that the  $3\nu_3'$  level is perturbed by a singlet-triplet interaction [8, 9]. Recently, extensive studies on this singlet-triplet interaction in the vibronic levels of the  $\tilde{A}$  state were reported by Dupre *et al.* [10] and by Ochi and Tsuchiya [11]. Both experiments not only showed that a strong interaction ( $\sim$ GHz) is present between the rovibronic levels of the  $\tilde{A}$  state and isoenergetic triplet states but also showed the existence of a weak coupling ( $\sim$ MHz) between triplet states and high-lying vibrational levels of the electronic ground state.

In the present experiment we have recorded the LIF spectrum of the  $3_0^3 K_0^1$  and  $3_0^4 K_0^1$  vibronic bands of the  $\tilde{A}^1A_u \leftarrow \tilde{X}^1\Sigma_g^+$  transition in acetylene with a resolution of 18 MHz. This resolution is sufficient to resolve the splitting of rotational lines due to the singlet-triplet interactions. Using the standard deconvolution procedure the coupling elements and the density of coupled triplet states can be obtained from the recorded spectra, giving information on the coupling mechanism and the identity of the coupled triplet state.

### 3.2 Experimental

The laser system and molecular beam apparatus have been extensively described before [12]. Therefore, only the relevant features will be given here. The laser system consists of a single-frequency cw ring dye laser (Spectra Physics 380D) which is operated with Stilbene 3 dye and is pumped by an Argon ion laser (Spectra Physics 2045-15) with a maximum UV output of 7 W. For the generation of narrow bandwidth UV radiation in the wavelength range of 213-225 nm, an angle-tuned  $\beta$ -BaB<sub>2</sub>O<sub>4</sub> (BBO) crystal is placed in the auxiliary beam waist of the laser cavity. Due to the non-linear properties of the crystal, UV radiation is generated at the second harmonic of the fundamental laser frequency. In order to minimize the losses in the laser cavity the crystal is placed at Brewster angle. In this way UV radiation with a bandwidth of less than 1 MHz and a power up to 150  $\mu$ W is obtained. For relative frequency calibration the transmission fringes of a temperature and pressure stabilized Fabry-Perot interferometer with a free spectral range of 149.72 MHz are recorded along with the excitation spectrum. For absolute frequency calibration the absorption spectrum of the Te<sub>2</sub> molecule [13] at the fundamental laser frequency is recorded.

The molecular beam is formed by a continuous expansion of pure acetylene or acetylene seeded in argon through a nozzle with a diameter of 100  $\mu$ m. The backing pressure applied is typically 1 atm. The rotational temperature in the molecular beam was found to vary between 3 and 9 K depending on the acetylene concentration. The molecular beam is skimmed twice and enters a differential pumped LIF detection chamber about 30 cm downstream of the nozzle. The molecular beam is at that point crossed perpendicularly by the weakly focused UV laser beam which

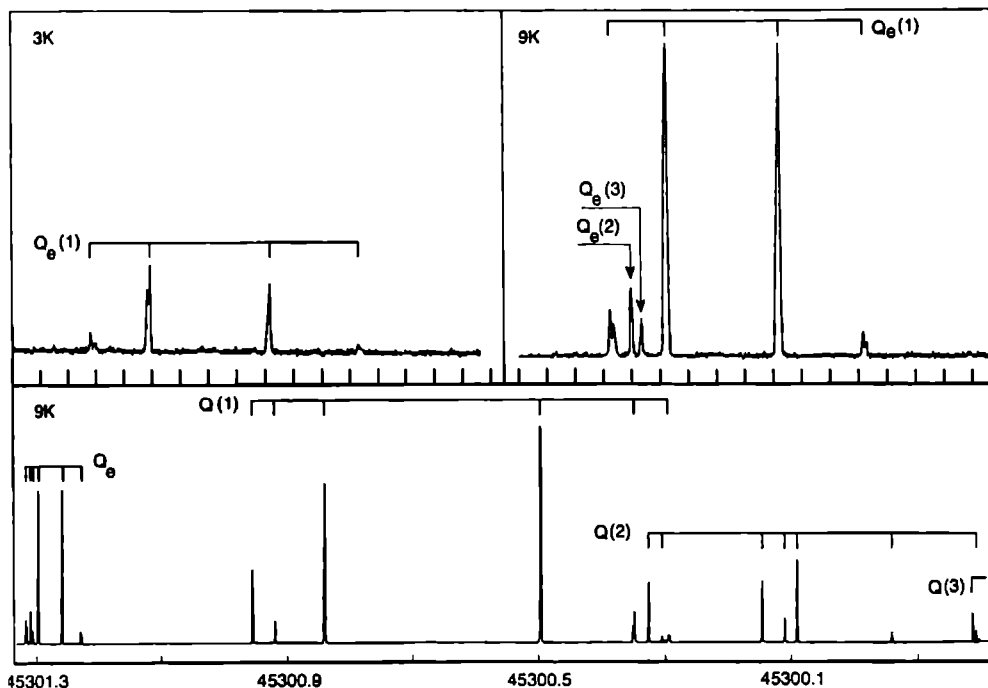


**Figure 3.1:** Lower panel: Q-branch of the  $3_0^3 K_0^1$  vibronic band of the  $\tilde{A} \ ^1A_u \leftarrow \tilde{X} \ ^1\Sigma_g^+$  electronic transition in acetylene recorded at an estimated rotational temperature of 9 K. Upper panel: Recording of the  $Q_e$ -branch at rotational temperatures of 3 K (left part) and 9 K (right part). The frequency is marked every 300 MHz and increases from right to left.

resonantly excites the molecules from the electronic ground state  $\tilde{X} \ ^1\Sigma_g^+$  to the  $\tilde{A} \ ^1A_u$  ( $\nu_3' = 3, 4$ ) state. The undispersed laser-induced fluorescence is collected by two spherical mirrors and imaged onto a photomultiplier. The linewidth of the individual transitions in the recorded LIF spectra amounts to 18 MHz. This linewidth is mainly determined by the residual Doppler width in the molecular beam in combination with the spatial sensitivity of the collection optics.

For measurements in a magnetic field a pair of coils in a non-Helmholtz configuration are mounted. With this setup it is possible to generate magnetic fields up to 100 Gauss with an accuracy of 5%. The direction of the magnetic field is parallel the laser beam.

### 3.3 Results and discussion

Two vibronic bands of the  $\tilde{A} \ ^1A_u \leftarrow \tilde{X} \ ^1\Sigma_g^+$  transition in acetylene have been recorded at high resolution, i.e. the  $3_0^3 K_0^1$  band at 221 nm and the  $3_0^4 K_0^1$  band at 216 nm. Each band consists of a P-, Q- and R-branch, characteristic for a  $\Delta K=1$  transition. Figure 3.1 shows a part of the Q-branch of the  $3_0^3 K_0^1$  band recorded at different temperatures.

Transition		Freq <sup>a)</sup>	$ C_s ^2$	$V_{st}$ <sup>b)</sup>	$A_{eff}$ <sup>c)</sup>	$ g_{eff} $ <sup>d)</sup>	$\frac{A_{eff}}{ g_{eff} }$
$3^3_0 K^1_0$	R(0)	45 302 7299	0 02	489	-	<0 05	-
		2 7397	0 04	1873	-	0 48	-
		2 7866	0 04	2561	-	0 34	-
		2 9032	0 06	2574	-	1 06	-
		3 1653	0 48	-	-	0 47	-
	3 2120	0 36	752	-	0 60	-	
	R <sub>e</sub> (0)	45 303 5710	0 09	958	-	<0 05	-
		3 6518	0 01	1	-	1 95	-
		3 6820	0 90	-	-	0 15	-
	Q(1)	45 300 3134	0 02	824	17 3	1 18	14 6
		0 3650	0 08	1905	18 7	1 08	17 3
		0 5172	0 48	-	9 7	0 56	17 3
		0 8335	0 26	5 152	11 0	0 88	12 5
		0 9102	0 04	1 586	<	<0 05	-
		0 9458	0 12	1 328	<	0 16	-
Q <sub>e</sub> (1)	45 301 2420	0 04	324	12 0	0 77	15 6	
	1 2839	0 40	524	<	<0 05	-	
	1 3168	0 45	-	5 0	0 22	22 6	
	1 3407	0 12	313	16 5	0 93	17 8	
R(1)	45 304 9428	0 06	1 499	15 0	0 80	18 8	
	4 9993	0 06	1 759	15 0	0 80	18 8	
	5 0713	0 06	1 301	<	0 22	-	
	5 1113	0 05	1 603	<	<0 05	-	
	5 1848	0 06	722	15 0	0 84	17 8	
	5 2140	0 07	426	<	0 11	-	
	5 2272	0 10	846	3 6	0 38	-	
	5 2630	0 24	-	6 0	0 43	14 0	
	5 3239	0 14	1 282	<	<0 05	-	
	5 3583	0 16	844	2 0	0 16	12 5	
	R <sub>e</sub> (1)	45 305 9406	0 07	387	10 0	-	-
5 9905		0 93	-	<	0 09	-	
Q(2)	45 299 8147	0 04	2037	-	0 55	-	
	9 9587	0 04	1 257	-	<0 05	-	
	0 1139	0 33	-	-	0 33	-	
	0 1325	0 09	412	-	<0 05	-	
	0 1649	0 26	713	-	<0 05	-	
	0 3257	0 02	441	-	<0 05	-	
	0 3464	0 23	2 740	-	0 16	-	
Q <sub>e</sub> (2)	45 301 3277	1 00	-	-	<0 05	-	
R(2)	45 306 9844	0 03	503	-	<0 03	-	
	6 9966	0 03	929	-	0 28	-	
	7 0591	0 02	193	-	-	-	
	7 0849	0 49	-	-	0 16	-	
	7 1411	0 01	412	-	0 08	-	
	7 2983	0 30	3 238	-	0 43	-	
	7 3190	0 03	311	-	0 25	-	
	7 3439	0 06	704	-	0 10	-	
	7 3497	0 03	209	-	0 04	-	

Transition		Freq <sup>a)</sup>	$ C_s ^2$	$V_{st}$ <sup>b)</sup>	$A_{eff}$ <sup>c)</sup>	$ g_{eff} $ <sup>d)</sup>	$\frac{A_{eff}}{ g_{eff} }$	
$3_0^3 K_0^1$	R <sub>e</sub> (2)	45 308 3830	1 00	-	-	-	-	
	Q(3)	45 298 8097	0 04	3 672	10 3	0 58	17 6	
		8 9228	0 01	1 702	<	-	-	
		9 2587	0 01	494	<	0 20	-	
		9 3149	0 01	340	<	<0 05	-	
		9 3890	0 16	674	6 2	0 31	19 6	
		9 4385	0 59	-	<	<0 05	-	
		9 4612	0 02	135	<	0 18	-	
		9 4785	0 03	276	<	0 11	-	
		9 6334	0 05	1 848	<	0 26	-	
		9 6826	0 03	1 374	<	0 43	-	
		9 6971	0 01	482	<	-	-	
		9 8200	0 06	2 452	<	0 05	-	
		Q <sub>e</sub> (3)	45 301 3315	1 00	-	~3	<0 05	-
		R(3)	45 308 5101	0 02	1 016	<	-	-
			8 5245	0 01	1 734	<	-	-
			8 7110	0 01	278	<	0 20	-
			8 7493	0 02	290	<	0 29	-
	8 7802		0 33	-	<	0 19	-	
	8 8397		0 08	1 341	<	0 13	-	
	8 8507		0 02	378	<	0 26	-	
	8 9261		0 09	1 340	<	0 30	-	
	8 9772		0 22	2 312	<	0 20	-	
	9 0454		0 06	1 301	5 5	0 37	14 9	
	9 0744		0 05	860	12 3	0 82	15 0	
	9 1786		0 01	556	<	0 34	-	
	9 2206		0 01	984	<	0 24	-	
	9 2512		0 02	3 268	<	0 17	-	
	9 3231		0 06	34	11 6	0 70	-	
	Q(4)	45 297 9482	0 03	2 635	-	-	-	
		8 1892	0 03	922	-	-	-	
		8 2319	0 10	2 828	-	-	-	
8 3930		0 04	498	-	-	-		
8 4096		0 07	1 136	-	-	-		
8 4716		0 21	600	-	-	-		
8 4975		0 20	2 823	-	-	-		
8 6582		0 28	-	-	-	-		
8 6998		0 04	558	-	-	-		
$3_0^4 K_0^1$	R(0)	46 290 1903	0 01	698	-	-		
	0 3278	0 14	597	-	0 05	-		
	0 3563	0 25	2 289	-	0 17	-		
	0 5047	0 58	-	-	0 23	-		
	0 5346	0 08	121	-	-	-		
	0 7135	0 08	673	-	-	-		

Transition	Freq. <sup>a)</sup>	$ C_s ^2$	$V_{st}$ <sup>b)</sup>	$A_{eff}$ <sup>c)</sup>	$ g_{eff} $ <sup>d)</sup>	$\frac{A_{eff}}{ g_{eff} }$
$3_0^4 K_0^1$ Q(1)	46 287.7308	0.01	399	<	-	-
	7.9211	0.50	-	<	0.19	-
	8.0625	0.46	2154	9.3	0.37	25.1
	8.2089	0.01	712	19.0	-	-
	8.2958	0.02	1152	19.0	-	-
R(1)	46 292.2675	0.01	629	<	-	-
	2.2932	0.01	695	<	-	-
	2.4368	0.20	914	7.2	0.23	31.3
	2.4880	0.23	704	<	0.19	-
	2.5202	0.19	711	6.4	0.31	20.6
	2.5562	0.36	-	<	0.06	-
	7.2690	0.02	1143	-	-	-
Q(2)	46 287.2059	0.06	1970	-	-	-
	7.2690	0.02	1143	-	-	-
	7.3156	0.01	701	-	-	-
	7.3345	0.01	372	-	-	-
	7.3384	0.01	898	-	-	-
	7.4782	0.01	143	-	-	-
	7.5145	0.76	-	-	0.02	-
	7.5298	0.01	100	-	-	-
	7.6395	0.12	1290	-	0.41	-
	7.6395	0.12	1290	-	0.41	-
R(2)	46 294.0436	0.01	770	-	-	-
	4.2301	0.02	449	-	-	-
	4.2966	0.32	-	-	0.48	-
	4.3450	0.09	765	-	0.06	-
	4.3802	0.21	1089	-	0.05	-
	4.3970	0.26	362	-	0.08	-
	4.4798	0.05	783	-	0.63	-
	4.6158	0.01	939	-	-	-
	4.7296	0.01	1328	-	-	-
	4.7965	0.01	1176	-	-	-
	4.7965	0.01	1176	-	-	-
Q(3)	46 286.5354	0.07	1549	7.7	0.31	24.8
	6.6016	0.02	723	<	0.15	-
	6.6641	0.11	734	<	0.06	-
	6.6809	0.01	325	<	0.12	-
	6.6914	0.08	1093	<	0.15	-
	6.7310	0.11	1205	<	<0.02	-
	6.7951	0.23	-	4.9	0.25	19.6
	6.8069	0.17	274	5.7	0.19	30.0
	6.8220	0.07	307	8.2	0.22	37.3
	6.8557	0.10	661	14.7	0.58	25.3
	6.9875	0.01	754	<	-	-
	7.1287	0.03	1670	18.0	-	-

Transition	Freq <sup>a)</sup>	$ C_S ^2$	$V_{st}$ <sup>b)</sup>	$A_{eff}$ <sup>c)</sup>	$ g_{eff} $ <sup>d)</sup>	$\frac{A_{eff}}{ g_{eff} }$	
$3_0^4 K_0^1$	R(3) 46 296 0003	0 42	–	6 6	0 39	–	
	6 0747	0 28	1 318	3 3	0 17	19 4	
	6 0977	0 05	387	<	<0 03	–	
	6 1135	0 02	310	<	0 06	–	
	6 1851	0.15	1 612	8 4	0 40	21 0	
	6 2839	0 01	541	9 8	–	–	
	6 3366	0 01	816	12 8	–	–	
	6 4175	0 09	2 796	<	0 30	–	
	Q(4)	46 285 5305	0 02	214	–	–	–
		5 5463	0 12	540	–	0 14	–
5 5608		0 01	239	–	–	–	
5 6009		0 69	–	–	<0 02	–	
5 6143		0 02	86	–	–	–	
5 6270		0.12	285	–	0 19	–	
5 6428		0 02	153	–	–	–	

<sup>a)</sup> The relative accuracy in the line positions is  $0.0005 \text{ cm}^{-1}$ . The absolute accuracy is  $0.002 \text{ cm}^{-1}$ .

<sup>b)</sup> The coupling matrix elements given at a molecular eigenstate correspond to the interaction strength between the zero-order singlet level and the triplet state having the largest contribution to the molecular eigenstate.

<sup>c)</sup> The error in the effective Fermi contact parameter is 10%. – indicates no hyperfine structure present, < indicates hyperfine structure not observable.

<sup>d)</sup> The error in the gyromagnetic factor is 10% for states having no hyperfine structure and 20% for states having hyperfine structure.

**Table 3.1:** Transition frequency ( $\text{cm}^{-1}$ ), amount of  $\tilde{A}^1 A_u$  state character,  $|C_S|^2$ , singlet-triplet coupling matrix elements,  $V_{ST}$ , (MHz), effective Fermi contact parameter,  $A_{eff}$ , (MHz) and the gyromagnetic factor,  $g_{eff}$ , of the individual molecular eigenstates as obtained from the study of the  $\tilde{A}^1 A_u \leftarrow \tilde{X}^1 \Sigma_g^+$  system.

It can directly be seen that this band is strongly perturbed since each rotational line is split into a large number of lines. The same conclusion is valid for the  $3_0^4 K_0^1$  band. It has been well established that the rotational levels in both bands are perturbed by a strong interaction with isoenergetic triplet states [9, 10, 11]. The observed line positions and their assignments are given in Table 3.1. The rotational assignment for the P and R transitions has been verified by comparison of the P- and R-branch combination differences to the well-known ground state combination differences [14]. The P transitions have not been incorporated in this table since they give no substantial new information. The frequencies of the P transitions can easily be calculated from the reported R transitions and the well-known ground state constants [14]. The assignment for the Q lines can not be verified by combination differences. The assignment of these lines has been checked by comparing the intensities of the different lines at various rotational temperatures.



## 3.3.1 Fermi perturbation

From the low resolution work of Scherer *et al.* [6] it is known that the  $3\nu'_3$  level in the  $\tilde{A}$  state is perturbed, most probably by a Fermi interaction with the  $\nu'_2 + 2\nu'_4$  vibrational level. All the so-called "extra"  $P_e$ ,  $Q_e$  and  $R_e$  transitions induced by this perturbation that were observed by Scherer *et al.* are also observed in the present high resolution study and most of them consist of several lines, see Table 3.1. The high resolution spectra confirm the previous assignments of the  $P_e$  and  $R_e$  transitions. However, for the  $Q_e$  transitions the assignment has to be revised. The transition previously assigned as "extra"  $Q_e(1)$  appears to consist of several lines that involve transitions from higher rotational levels, as can be seen in Figure 3.1. On the basis of the temperature dependence of the intensities of these lines they are assigned to  $Q_e(2)$  and  $Q_e(3)$  transitions. On the same basis it has to be concluded that the transition previously assigned as "extra"  $Q_e(2)$  consists of lines belonging to the  $Q(1)$  transition. Another indication that these lines belong to the  $Q(1)$  transition is provided by the fact that some of the lines show a hyperfine splitting, which can only be present in  $Q$  transitions involving odd  $J$ -levels, see section 3.3.3.

Vibr. level	Trans.	Freq. $ S_1\rangle$	$\langle V_{ST} \rangle$	$\rho_T$
$3\nu'_3$	R(0)	45 302.1277	1 653	8.7
	R(1)	45 305.2192	1 142	20.6
	R(2)	45 307.1762	812	19.4
	R(3)	45 308.9112	1 124	16.1
	Q(1)	45 300.6482	2 159	6.6
	Q(2)	45 300.1657	1 267	10.0
	Q(3)	45 299.4453	1 219	10.4
	Q(4)	45 298.4806	1 500	9.6
$\nu'_2 + 2\nu'_4$	$R_e(0)$	45 303.6698	479	19.0
	$R_e(1)$	45 305.9893	387	–
	$R_e(2)$	45 308.3830	–	–
	$Q_e(1)$	45 301.3038	387	21.5
	$Q_e(2)$	45 301.3277	–	–
	$Q_e(3)$	45 301.3315	–	–
$4\nu'_3$	R(0)	46 290.4412	876	7.7
	R(1)	46 292.5046	731	15.0
	R(2)	46 294.3663	851	10.7
	R(3)	46 296.0949	1 111	17.3
	Q(1)	46 287.9963	1 104	5.4
	Q(2)	46 287.5014	827	17.5
	Q(3)	46 286.7662	845	17.5
	Q(4)	46 285.5971	253	45.3

**Table 3.2:** Calculated transition frequencies of zero-order singlet states ( $\text{cm}^{-1}$ ), the average singlet-triplet coupling matrix elements,  $\langle V_{ST} \rangle$ , (MHz) and the density of coupled triplet states,  $\rho_T$ , (states/ $\text{cm}^{-1}$ ) for the observed transitions.

	$3\nu_3$	$\nu_2 + 2\nu_4$	$4\nu_3$
$B'$	1.031(2)	1.178(3)	1.017(3)
$C'$	1 131(2)	1.179(3)	1.125(2)
$T_0$	45 300.90(3)	45 301.30(3)	46 288.26(3)

**Table 3.3:** Molecular constants ( $\text{cm}^{-1}$ ) of three vibrational levels in the  $\bar{A}^1A_u$  state of acetylene.

It has been pointed out by Scherer *et al.* [6] that it is very unlikely that the observed "extra" lines are due to transitions to a hitherto unobserved singlet state or due to transition to triplet states. Consequently, it has to be assumed that the "extra" transitions arise from a Fermi interaction of the  $3\nu_3$  level with another vibrational level of the  $\bar{A}$  state, most probably the  $\nu_2 + 2\nu_4$  combination band. In order to analyze this Fermi perturbation it is necessary to know the energy levels of the unperturbed singlet states. We therefore have determined the center of gravity of lines in the excitation spectrum belonging to the same rotational transition. The line positions of the singlet levels can be found in Table 3.2. These line positions of both the  $3\nu_3$  state and perturbing state have been fit to an effective Hamiltonian as described by Scherer *et al.* [6]. In the least squares fit the rotational constants of the ground state were kept fixed at the accurate values determined by infrared spectroscopy [14]. Since there are insufficient data to determine the  $A'$  rotational constants we decided to determine the effective term values. It turned out the Fermi interaction parameter could not be determined from the observed data, indicating that the model used is not correct. Analysis in terms of a Coriolis interaction did not improve the situation. Using constrained values for the Fermi interaction parameter showed that the best fit resulted when the interaction strength was set equal to zero. The molecular constants obtained from the fit with the interaction strength set to zero are listed in Table 3.3. The standard deviation of the fit is about  $0.02 \text{ cm}^{-1}$ . In view of the interval of  $0.5 \text{ cm}^{-1}$  over which the lines belonging to the same rotational transition extends, the fit is quite satisfactory. For comparison the constants for the  $4\nu_3$  level are also given.

The rotational constants found for the  $3\nu_3$  and  $4\nu_3$  levels agree to a reasonable extent with former studies [3, 4, 6]. The constants of the perturbing state, however, differ strongly from the constants obtained by Scherer *et al.* [6], as might be expected. The fact that the rotational constants found for the perturbing state are so different from those of other vibrational levels in the  $\bar{A}$  state indicates that the model used is not correct and that the  $3\nu_3$  and/or the perturbing state are probably perturbed by a third state. In conclusion we can say that although the assignment of some "extra" rotational lines has been changed, there is no need to change the proposed assignment [6] of the perturbing state as  $\nu_2 + 2\nu_4$ .

### 3.3.2 Singlet-triplet interactions

Due to a strong singlet-triplet interaction every rotational level in the electronically excited  $\bar{A}$  state is split into several components, the so-called molecular eigenstates. These molecular eigenstates,  $|ME\rangle$ , can be described as a linear combination of a zero-order  $\bar{A}$  state singlet level,  $|S_1\rangle$ , and

zero-order triplet states,  $|T_i\rangle$ :

$$|ME\rangle = C_S|S_1\rangle + \sum_{i=1}^n C_{T_i}|T_i\rangle \quad (3.1)$$

In order to deduce the zero-order singlet and triplet states, the density of coupled triplet states,  $\rho_T$ , and the singlet-triplet coupling matrix elements,  $V_{ST}$ , from the observed spectra we adopt the deconvolution procedure of Lawrance and Knight [15]. This method is in principle only applicable to a spectrum with known absorption intensities, whereas we have measured the laser-induced fluorescence excitation spectrum. It can be shown that the absorption intensity of the molecular eigenstate is proportional to the intensity of the molecular eigenstate in the LIF excitation spectrum in the case where the decay rates of the zero-order triplet states are negligible with respect to the decay rate of the zero-order singlet state [16].

It is well-known that the radiative decay rates of triplet states in acetylene are much smaller than the radiative decay rate of the  $\tilde{A}$  singlet state [17]. A comparison of our excitation intensities with the lifetime measurements by Ochi and Tsuchiya [11] shows that for the  $3_0^3$  and  $2_0^1 4_0^2$  vibronic bands the absorption intensities are proportional to the excitation intensities. A comparison of both experiments for the  $3_0^3$  band shows that this not the case for this vibronic band, indicating that the decay rates of the triplet states are no longer negligible. Fluorescence yield measurements [18] and lifetime measurements [19] have shown that the  $4\nu_3'$  level predissociates and that indeed triplet states are involved in this predissociation. Yet, we assume for our deperturbation analysis that for all three vibrational levels the excitation and absorption intensities are equal, since no information on the lifetimes of the individual molecular eigenstates is available. With this assumption we are now able to deconvolute the spectra into zero-order singlet and triplet states. The results of the deconvolution procedure for the three vibrational levels,  $3\nu_3'$ ,  $4\nu_3'$  and  $\nu_2' + 2\nu_4'$ , are listed in Tables 3.1 and 3.2.

The density of coupled triplet states,  $\rho_T$ , can be defined from the set of coupled zero-order triplet states as:

$$\rho_T = \frac{n-1}{\Delta E} \quad (3.2)$$

Here  $n$  is the number of coupled zero-order triplet states and  $\Delta E$  is the energy difference between the highest and lowest energy zero-order triplet state. Using this expression the density of coupled triplet states has been determined for every individual rotational level. The results can be found in Table 3.2.

It can be seen from from Table 3.2 that for the  $3\nu_3'$  and  $4\nu_3'$  levels the average interaction coupling matrix elements  $\langle V_{ST} \rangle$  do not systematically depend on the rotational quantum number  $J$ . This indicates that no Coriolis-induced intersystem crossing is present in acetylene. The average coupling strengths for the  $3\nu_3'$  and  $4\nu_3'$  are found to be 1 281 MHz and 823 MHz, respectively. The small decrease in the coupling constant can be attributed to a diminishing Franck-Condon overlap between the singlet states and the vibronically excited triplet states. In order to determine whether the vibrational states in the triplet state are completely mixed, in which case an averaging of the coupling strength is expected, we have calculated the number:

$$\frac{1}{n} \sum_{i=1}^n \frac{(V_{ST} - \langle V_{ST} \rangle)^2}{\langle V_{ST} \rangle^2} \quad (3.3)$$

This number amounts to 0.68 for the  $3\nu_3'$  and to 0.49 for the  $4\nu_3'$  state. We therefore conclude that

the vibrational wavefunctions of the triplet states are only very weakly mixed and that the increase in vibrational excess energy results in a small additional mixing of the coupled triplet states.

For the  $\nu'_2 + 2\nu'_4$  level the coupling strength varies strongly with  $J$ . The variation in coupling strength appears to be proportional to the amount of  $3\nu'_3$  character in this level, indicating that the coupling strength between the pure  $\nu'_2 + 2\nu'_4$  state and the triplet states is much smaller. This difference in coupling strength between the two vibrational levels at the same energy directly reflects the difference in Franck-Condon overlap between these two singlet states and the triplet states. An analysis of the vibrational modes involved shows that the Franck-Condon overlap is largest when the molecule tends to be linear.

As can be seen in Table 3.2 the density of coupled triplet states,  $\rho_T$ , depends on the rotational quantum number. For  $J=1$  the number of coupled states is approximately a factor of two less than for  $J \neq 1$ . This difference in coupled triplet states arises from the selection rules involved in the singlet-triplet interaction. Since the coupling is induced by a spin-orbit interaction the following selection rules apply:  $\Delta J=0$ ,  $\Delta N=0, \pm 1$  and  $\Delta K_a=0, \pm 1$ . In order to deduce the density of triplet states,  $\rho_T^y$  from the observed density of coupled states,  $\rho_T$ , these selection rules have to be taken into account. Since in the case of acetylene the rotational  $A'$  constant is in the order of  $10 \text{ cm}^{-1}$  only one out of the possible three  $K$  levels is expected to interact with the singlet state. With these assumptions the density of triplet states is found to be  $\rho_T^y=4.9$  and  $\rho_T^y=6.3 \text{ states/cm}^{-1}$  for the  $3\nu'_3$  and  $4\nu'_3$  vibrational level, respectively. These values differ considerably from those obtained by Zeeman anticrossing (ZAC) spectroscopy [10], where the density of coupled states for these vibrational levels was found to be more than  $100 \text{ states/cm}^{-1}$ . This density was explained by a coupling of the  $|S_1\rangle$  states via the triplet states with high vibrational levels of the electronic ground state,  $|S_0\rangle$ . The coupling matrix elements between the triplet states and the  $|S_0\rangle$  levels was found to be in the order of a few MHz. Since this coupling is so weak the  $|S_0\rangle$  states can not be observed with the resolution and signal-to-noise ratio in the present experiment. The observed density of coupled states is therefore fully determined by the density of triplet states this in contrast to the

Vibr. level	Electr. state	Energy <sup>a)</sup>	Calc. density <sup>b)</sup>	Obs. density
$3\nu'_3$	$T_1 \ ^3B_2 \ cis$	16 150	4.7	4.9
	$T_1 \ ^3B_u \ trans$	13 950	2.6	
	$T_2 \ ^3A_u \ trans$	10 450	1.0	
	$T_2 \ ^3A_2 \ cis$	7 750	0.3	
$4\nu'_3$	$T_1 \ ^3B_2 \ cis$	17 150	6.0	6.3
	$T_1 \ ^3B_u \ trans$	14 950	3.5	
	$T_2 \ ^3A_u \ trans$	11 450	1.3	
	$T_2 \ ^3A_2 \ cis$	8 750	0.5	

<sup>a)</sup> Energy difference ( $\text{cm}^{-1}$ ) between the minimum of the potential energy surface of the triplet state and the vibrational level in the  $\bar{A}$  state.

<sup>b)</sup> In the calculations the normal mode frequencies of the  $\bar{A}$  state are used [24].

**Table 3.4:** Calculated density of triplet states ( $\text{states/cm}^{-1}$ ) for different electronic triplet states.

ZAC experiment.

*Ab initio* calculations have shown that two triplet states lie below the  $\tilde{A}^1A_u$  state [20, 21, 22]. Both triplet states are expected to have minima in the *cis*- and *trans*-bent configurations. The calculated potential energy minima of these triplet states agree reasonably well with the few published experimental values [17, 23]. In order to determine which triplet state is responsible for the observed intersystem crossing we have computed, by direct level count, the density of states at the energies of the  $3\nu'_2$  and  $4\nu'_2$  vibrational levels. Since only very little experimental information is available on the triplet states we have used in this calculation the normal mode frequencies of the  $\tilde{A}$  state [24] and the potential energy minima calculated by Lischka and Karpfen [22]. In these computations we have ignored the vibrational selection rules imposed by the spin-orbit coupling. The results of the calculations are listed in Table 3.4.

Comparing the observed and computed densities of triplet states it is clear that only the  $T_1^3B_2$  (*cis*) state can be responsible for the observed density of states, although it can not be excluded that also other triplet states contribute. Another indication that the  $T_1^3B_2$  (*cis*) state is involved in the perturbation is provided by the vibrational dependence of the coupling strength, *i.e.* the Franck-Condon overlap between the wavefunctions of the singlet and triplet states. As has been pointed out by Dupre *et al.* [10], the Franck-Condon overlap between the wavefunctions of the *trans*-bent  $\tilde{A}$  state and the *cis*-bent  $T_1$  state is expected to be large when the molecule tends to be linear, especially in the neighborhood of the *cis-trans* isomerization barrier of the triplet state. This has indeed been observed. Hence, we conclude that the observed perturbations in the  $3\nu'_2$  and  $4\nu'_2$  vibrational levels in the  $\tilde{A}^1A_u$  state of acetylene are due to a spin-orbit interaction with excited vibrational levels of the  $T_1^3B_2$  (*cis*) state.

### 3.3.3 Hyperfine structure

The rotational levels in the  $\tilde{A} n\nu'_2$  state with even  $K_c$  quantum numbers have a total nuclear spin,  $I=0$ , whereas the rotational levels with odd  $K_c$  quantum numbers have a total nuclear spin  $I=1$ . The nuclear spin  $\tilde{I}$  of these states may couple with the angular momentum  $\tilde{J}$  to form the resulting vector  $\tilde{F} = \tilde{J} + \tilde{I}$ . For a  $^1\Sigma$  state this coupling is very weak, in the order of a few kHz, and as a result the hyperfine structure of the  $\tilde{A}$  state of acetylene, which corresponds to  $^1\Sigma_u^-$  in  $D_{\infty h}$ , can not be resolved with the present resolution. However, for triplet states this coupling is much stronger, in the order of 100 MHz. Due to the strong singlet-triplet interaction in acetylene the hyperfine structure of the triplet states becomes observable in the  $\tilde{A} \leftarrow \tilde{X}$  excitation spectrum. Most of the molecular eigenstates involving rotational levels having a nuclear spin  $I=1$  are split into three hyperfine components. This hyperfine splitting is usually largest for the weak lines, which are expected to have the largest amount of triplet character. Figure 3.2 shows an example of such a hyperfine splitting.

Comparing acetylene with other small hydrocarbons like glyoxal and propynal it can be expected that the hyperfine splitting in the triplet state is largely determined by the the Fermi contact parameter [25, 26]. Assuming that the triplet states in acetylene can be represented by the  $(b_{\beta J})$  coupling case the hyperfine structure of a rotational level in the triplet state is given by:

$$\langle T | \hat{H}_{HF} | T \rangle = A_{FC} \frac{J(J+1) + S(S+1) - N(N+1)}{2J(J+1)} \frac{1}{2} [F(F+1) - J(J+1) - I(I+1)] \quad (3.4)$$

Here  $A_{FC}$  is the Fermi contact parameter,  $N$  the angular momentum due to the rotational motion,  $S$  the electron spin angular momentum and  $\tilde{J} = \tilde{N} + \tilde{S}$  the total angular momentum apart from nuclear spin.

The hyperfine structure of a molecular eigenstate is obtained by combining equation (3.1) and (3.4) yielding:

$$\begin{aligned} \langle ME | \hat{H}_{HF} | ME \rangle &= \sum_{i=1}^n |C_{T_i}|^2 \langle T_i | \hat{H}_{HF} | T_i \rangle \\ &= A_{eff} \frac{1}{2} [F(F+1) - J(J+1) - I(I+1)] \end{aligned} \quad (3.5)$$

where  $A_{eff}$  is defined by:

$$A_{eff} = \sum_{i=1}^n |C_{T_i}|^2 A_{FC} \frac{J(J+1) + S(S+1) - N(N+1)}{2J(J+1)} \quad (3.6)$$

Here we have assumed that the  $\hat{H}_{HF}$  acts only on triplet states and is diagonal in  $|T\rangle$ . Unfortunately, our experiments give no information on the  $N$  values of the coupled triplet states, except that  $N$  is restricted to  $N=J, J\pm 1$ . Therefore, it is not possible to determine directly the Fermi contact parameter,  $A_{FC}$ , from the observed spectra. Only the effective parameter,  $A_{eff}$ , can be determined for every individual eigenstate. The values found for this parameter can be found in Table 3.1

By setting  $N=J-1$  for every zero-order triplet state it is possible to determine a lower limit for  $A_{FC}$  from the effective values of the individual molecular eigenstates. For the triplet states probed via the  $3\nu'_3$  level a lower limit of  $A_{FC} \geq 30$  MHz is found, whereas for the triplet states probed via the  $4\nu'_3$  level a lower limit of  $A_{FC} \geq 50$  MHz is found. A more accurate value for  $A_{FC}$  can be obtained by comparing the effective hyperfine contact parameter,  $A_{eff}$  with the effective gyromagnetic factor,  $g_{eff}$  of a molecular eigenstate. This g-factor has been determined for all the individual lines by magnetic field measurements, see section 3.3.4. Since  $A_{eff}$  and  $g_{eff}$  depend in the same way on the rotational quantum numbers of the triplet state, see also section 3.3.4, the ratio  $A_{eff}/g_{eff}$  is equal to the ratio  $A_{FC}/g_e$ . Knowing that  $g_e = 2.0023$ , the Fermi contact parameter can be determined to be  $A_{FC} = 33 \pm 5$  MHz and  $A_{FC} = 51 \pm 12$  MHz for the triplet states probed at the  $3\nu'_3$  level and  $4\nu'_3$  level, respectively. The value of 51 MHz for the  $4\nu'_3$  level is

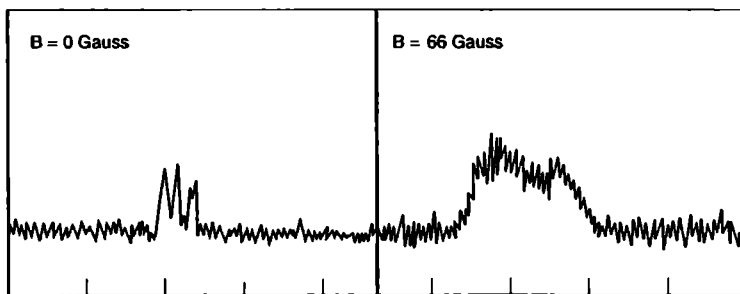


Figure 3.2: Left panel: Recording of the  $R(3)$  transition of the  $3_0^3$  band at  $45\,309.0744\text{ cm}^{-1}$  showing clearly three hyperfine components ( $A_{eff}=8.4$  MHz). Right panel: The same transition recorded in a magnetic field of 66 Gauss.

in good agreement with the values determined by ZAC spectroscopy for other vibrational levels in the  $\tilde{A}$  state [8, 27]. The value of 33 MHz for the  $3\nu'_3$  level is, however, considerably smaller than the value of 57.7 MHz determined via ZAC spectroscopy [8] for this vibrational level. The analysis of the singlet-triplet perturbations has shown that there is no substantial difference in the interaction of the  $3\nu'_3$  and the  $4\nu'_3$  vibronic levels with the triplet states which could have explained the observed difference. The small value of  $A_{FC}$  determined via the  $3\nu'_3$  vibrational level in the present experiment therefore remains an enigma.

### 3.3.4 Magnetic field measurements

To gain a better insight into the character of the coupled states we have studied the molecular eigenstates in the presence of a magnetic field. The interaction of zero-order singlet levels with a magnetic field is too weak to produce effects that can be resolved with the present resolution. Therefore the magnetic field effects that are observed have to be attributed to the interaction of zero-order triplet states with the magnetic field. The energy shift of a rotational level in a triplet state can, with the weak magnetic fields used in the present experiment, be described by the first-order Zeeman effect:

$$\langle T | \hat{H}_Z | T \rangle = g_e \frac{J(J+1) + S(S+1) - N(N+1)}{2J(J+1)} \mu_B B M_J \quad (3.7)$$

Here  $g_e = 2.0023$  is the gyromagnetic ratio,  $\mu_B$  the Bohr magneton,  $B$  the magnetic field strength and  $M_J$  the projection of  $J$  on the magnetic field. Just as in the case for the hyperfine structure only an effective  $g_{eff}$  value can be determined from the observed spectra. The Zeeman splitting of the molecular eigenstate is given by:

$$\langle M E | \hat{H}_Z | M E \rangle = g_{eff} \mu_B B M_J \quad (3.8)$$

where  $g_{eff}$  is defined as:

$$g_{eff} = \sum_{i=1}^n |C_{T_i}|^2 g_e \frac{J(J+1) + S(S+1) - N(N+1)}{2J(J+1)} \quad (3.9)$$

In the case where no hyperfine structure is present the lines in the spectrum show a Zeeman splitting in a magnetic field according to equation (3.8). Figure 3.3 shows two typical examples of such a splitting. The  $g_{eff}$  values derived from these splittings are listed in Table 3.1. The agreement between the values obtained in the present high resolution experiment and those found in the quantum beat experiment of Ochi and Tsuchiya [11] is striking.

However, if hyperfine structure is present equation (3.7) is no longer valid and has to be replaced by an expression which also includes the hyperfine interaction. Since the structure of the lines in a magnetic field can not be fully resolved, as can be seen in Figure 3.2, the Zeeman pattern can not be exactly analyzed. We therefore decided to determine  $g_{eff}$  from the total width of the lines assuming that the splitting can be treated in the high-field (Paschen-Back) limit. In this limit equation (3.7) has to be replaced by:

$$\langle T | \hat{H}_Z | T \rangle = g_e \frac{J(J+1) + S(S+1) - N(N+1)}{2J(J+1)} \mu_B B M_J + A_{FC} M_J M_I \quad (3.10)$$

Here  $A_{FC}$  is the Fermi contact parameter and  $M_I$  the projection of the nuclear spin onto the magnetic field. Numerical calculations have shown that the error introduced by this assumption

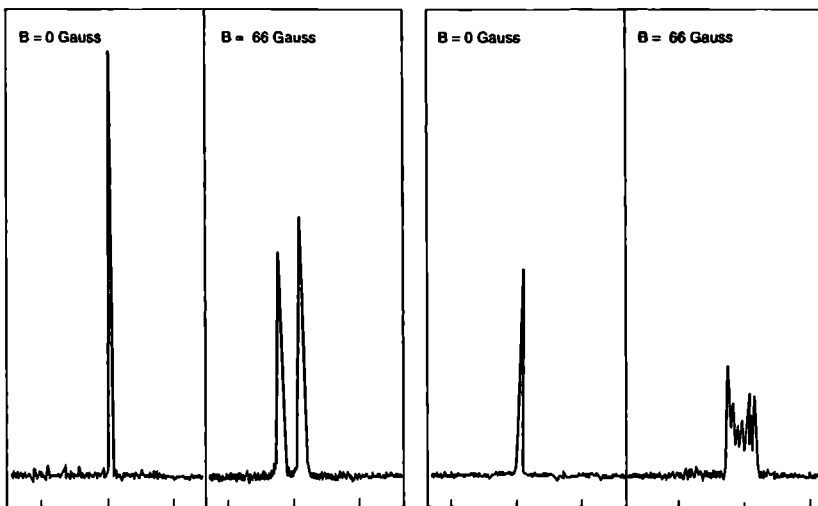


**Figure 3.3:** Left panel: The  $R(0)$  transition at  $45\,303.1653\text{ cm}^{-1}$  at zero field and in a magnetic field of 66 Gauss. Only two components are observed,  $M = -1$  and  $M = +1$ , due to selection rules. Right panel: The  $R(2)$  transition at  $46\,294.2966\text{ cm}^{-1}$  in a magnetic field of 0 and 66 Gauss. The seven  $M$ -sublevels can just be resolved.

is in the order of 10-20%, which is only slightly more than the error introduced by the uncertainty in the line splittings. The results of this analysis can be found in Table 3.1.

All the molecular eigenstates studied in a magnetic field, except two, show a Zeeman splitting that can be fully explained by equation (3.8). If a weak magnetic field is applied the  $R(0)$   $3_0^4 K_0^1$  transition at  $46\,290.5047\text{ cm}^{-1}$  splits into two components,  $M = -1$  and  $M = +1$ , as expected. When the magnetic field is increased some weak extra lines appear at higher energy and the intensity of the  $M = +1$  component decreases dramatically, see Figure 3.4. A similar effect is observed for the  $R(3)$   $3_0^3 K_0^1$  transition at  $45\,308.9261\text{ cm}^{-1}$ . Also here weak extra lines appear if a magnetic field is applied but in this case no dramatic loss in intensity is observed.

The extra lines that appear when a magnetic field is applied are most likely due to a magnetic field induced interaction of the molecular eigenstates with "dark" states. From the observed line positions and intensities the interaction strength can be estimated to be in the order of 10 MHz. Although it is difficult to determine the density of coupled "dark" states from the present observations, it can be estimated to be more than 100 states/ $\text{cm}^{-1}$ . Both the high density of coupled states and the value for the interaction strength indicate that the "dark" states are high-lying vibrational levels of the electronic ground state,  $|S_0\rangle$ . In principle, the  $|S_0\rangle$  levels are observable around every molecular eigenstate. The observation of these states is, however, limited by the experimental linewidth and signal-to-noise ratio in our experiment. Consequently, only those  $|S_0\rangle$  levels that have a relatively strong interaction with a molecular eigenstate can be observed.

Due to the interaction between the molecular eigenstate and the dark  $|S_0\rangle$  levels the intensity of the molecular eigenstate is distributed over the  $|S_0\rangle$  levels. However, for the  $R(0)$   $4_0^3$  transition



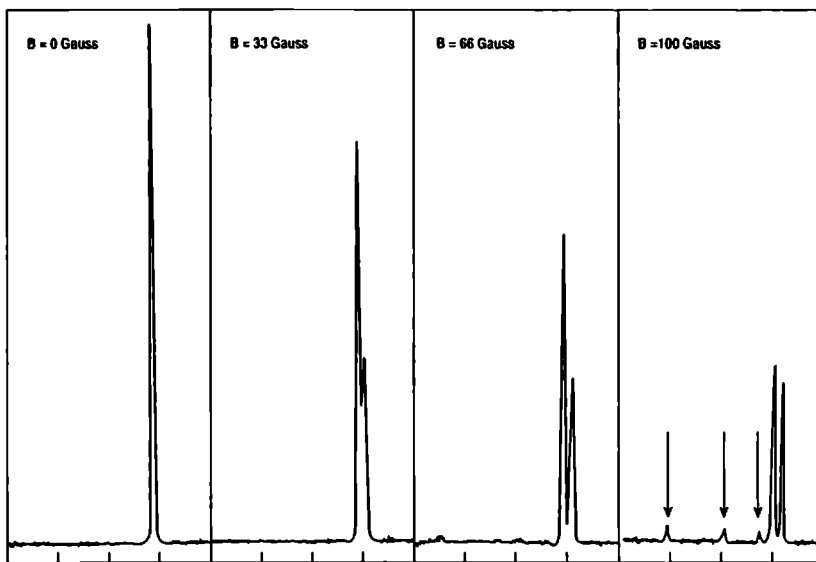


**Figure 3.4:** Recording of the  $R(0)$  transition of the  $3_0^4$  vibronic band at  $46\,290.5047\text{ cm}^{-1}$  in magnetic fields up to 100 Gauss. The arrows indicate the coupled  $|S_0\rangle$  levels. The frequency is marked every 300 MHz and increases from right to left.

the intensity gained by the  $|S_0\rangle$  levels is smaller than the intensity loss of the molecular eigenstate. This indicates that the coupled  $|S_0\rangle$  levels have a relatively large non-radiative decay rate. In order to check the validity of this hypothesis it is necessary to perform lifetime measurements on the molecular eigenstate and the individual  $|S_0\rangle$  levels. Unfortunately, this is not possible with the present experimental setup. However, lifetime measurements on this rotational level performed with a broadband laser have shown that the lifetime of this level indeed decreases when a magnetic field is applied [19]. Hence, it can be concluded that the coupled ground state levels indeed have a relatively large non-radiative decay rate. However, it is not possible to decide on ground of these observations what kind of non-radiative processes are taking place. But since the probed levels are above the theoretically [28, 29, 30] and experimentally determined [18, 31, 32] dissociation limit of acetylene it is very likely that the  $|S_0\rangle$  levels predissociate. This implies that one possible pathway for the predissociation of acetylene is a coupling of  $\tilde{A}$  state rovibronic levels via the  $T_1\ ^3B_2$  state with predissociating vibrational levels of the electronic ground state. A similar mechanism has been suggested by Satyapal and Bersohn [33] in order to explain the results obtained in their photodissociation experiments.

### 3.4 Summary

Laser-induced fluorescence spectra of the  $3_0^3 K_0^1$  and  $3_0^4 K_0^1$  vibronic bands of the  $\tilde{A}\ ^1A_u \leftarrow \tilde{X}\ ^1\Sigma_g^+$  transition of acetylene have been recorded in a molecular beam with a resolution of 18 MHz. Each

rotational transition appears to consist of a group of lines due to an interaction with isoenergetic triplet states. From the deconvolution of the excitation spectrum the singlet-triplet coupling matrix elements and the density of coupled triplet states have been determined. The singlet-triplet coupling elements are found to be in the order of 1 GHz for both vibrational levels. Comparison of the observed density of coupled triplet states with the calculated density of several low-lying triplet states shows that the  $T_1 \ ^3B_2$  state is involved in the perturbation of the  $\tilde{A} \ ^1A_u$  state.

The Fermi interaction between the  $3\nu_1'$  and  $\nu_2' + 2\nu_4'$  vibrational level has been reinvestigated. Although some of the rotational transitions have been reassigned the conclusions drawn by Scherer *et al.* [6] are still valid.

Magnetic field measurements have shown that most of the lines in the excitation spectrum have large magnetic moments, confirming that the states involved in the perturbation are indeed triplet states. Furthermore, the magnetic field measurements have shown that the triplet states can also couple to high-lying vibrational levels of the electronic ground state. The coupling constants for this interaction are found to be in the order of several MHz. Evidence has been found that some electronic ground state vibrational levels predissociate at an excess energy of  $46\,290\text{ cm}^{-1}$ . This implies that the  $\tilde{A}$  state of acetylene can predissociate by coupling via triplet states to these predissociating vibrational levels of the electronic ground state.

The Fermi contact parameter of the triplet states involved in the interaction with the  $\tilde{A}$  state has been determined from the hyperfine structure observed in the excitation spectrum and the  $g$ -factor found by the magnetic field measurements and is in reasonable agreement with the values determined by Zeeman anticrossing spectroscopy.

### Acknowledgements

This research was made possible by the financial support of the Dutch Organization for Fundamental Research of Matter (FOM).

### References

1. C.K. Ingold and G.W. King, *J. Chem. Soc.*, 2702 (1953)
2. K.K. Innes, *J. Chem. Phys.* **22**, 863 (1954)
3. J.K.G. Watson, M. Herman, J.C. van Craen and R. Colin, *J. Mol. Spectrosc.* **95**, 101 (1982)
4. J.C. van Craen, M. Herman, R. Colin and J.K.G. Watson, *J. Mol. Spectrosc.* **111**, 185 (1985)
5. J.C. van Craen, M. Herman, R. Colin and J.K.G. Watson, *J. Mol. Spectrosc.* **119**, 137 (1986)
6. G.J. Scherer, Y. Chen, R.L. Redington, J.L. Kinsey and R.W. Field, *J. Chem. Phys.* **85**, 6315 (1986)
7. E. Abramson, C. Kittrell, J.L. Kinsey and R.W. Field, *J. Chem. Phys.* **76**, 2293 (1982)
8. E. Abramson, *Ph.D. Thesis*, M.I.T., Cambridge (1985)
9. N. Ochi and S. Tsuchiya, *Chem. Phys. Lett.* **140**, 20 (1987)
10. P. Dupre, R. Jost, M. Lombardi, P.G. Green, E. Abramson and R.W. Field, *Chem. Phys.* **152**, 293 (1991)
11. N. Ochi and S. Tsuchiya, *Chem. Phys.* **152**, 319 (1991)
12. W.A. Majewski and W.L. Meerts, *J. Mol. Spectrosc.* **104**, 271 (1984)
13. J. Cariou and P. Luc, *"Atlas de spectroscopie d'absorption de la molecule tellure"*, CNRS, Paris (1980)
14. K.F. Palmer, M.E. Michelson and K.N. Rao, *J. Mol. Spectrosc.* **44**, 131 (1972)
15. W.D. Lawrance and A.E.W. Knight, *J. Phys. Chem.* **89**, 917 (1985)
16. W.M. van Herpen, W.L. Meerts, K.E. Drabe and J. Commandeur, *J. Chem. Phys.* **86**, 4396 (1987)
17. H.R. Wendt, H. Hipler and H.E. Hunziker, *J. Chem. Phys.* **70**, 4044 (1979)
18. M. Fujii, A. Haijima and M. Ito, *Chem. Phys. Lett* **150**, 380 (1988)  
A. Haijima, M. Fujii and M. Ito, *J. Chem. Phys.* **92**, 959 (1990)
19. Y. Chen, D.M. Jonas, C.E. Hamilton, P. Green, J.L. Kinsey and R.W. Field, *Ber. Bunsenges. Phys. Chem.* **92**, 329 (1988)
20. R.W. Wetmore and H.F. Schaefer III, *J. Chem. Phys.* **69**, 1648 (1978)
21. M. Peric, R.J. Buenker and S.D. Peyerimhoff, *Mol. Phys.* **53**, 1177 (1984)
22. H. Lishka and A. Karpfen, *Chem. Phys.* **102**, 77 (1986)
23. J.M. Lisy and W. Klemperer, *J. Chem. Phys.* **72**, 3880 (1979)

24. J. Vander Auwera, T.R. Huet, M. Herman, C. Hamilton, J.L. Kinsrey and R.W. Field, *J. Mol. Spectrosc.* **137**, 381 (1989)
25. M. Lombardi, R. Jost, C. Michel and A. Tramer, *Chem Phys.* **57**, 341 (1981)
26. H. Bitto, M.P. Docker, P. Schmidt and J.R. Huber, *J. Chem. Phys.* **92**, 187 (1990)
27. P. Dupre, *Ph.D. Thesis*, L'Université Joseph Fourier, Grenoble (1992)
28. J.A. Montgomery Jr. and G.A. Petersson, *Chem. Phys. Lett.* **168**, 75 (1990)
29. Y. Osamura, F. Mitsuhashi and S. Iwata, *Chem. Phys. Lett.* **164**, 205 (1989)
30. C.W. Bauschlicher Jr., S.R. Langhoff and P.R. Taylor, *Chem. Phys. Lett.* **171**, 42 (1990)
31. A.M. Wodtke and Y.T. Lee, *J. Phys. Chem.* **89**, 4744 (1985)
32. D.P. Baldwin, M.A. Buntine and D.W. Chandler, *J. Chem. Phys.* **93**, 6578 (1990)
33. S. Satyapal and R. Bersohn, *J. Phys. Chem.* **95**, 8004 (1991)



## Acetone, A Laser-Induced Fluorescence Study With Rotational Resolution At 320 nm

*H. Zuckermann and Y. Haas*

*Department of Physical Chemistry and Farkas Center of Light Induced Processes,  
The Hebrew University, Jerusalem 91904, Israel*

*M. Drabbels, J. Heinze, W.L. Meerts and J. Reuss*

*Department of Molecular and Laser Physics, University of Nijmegen,  
Toernooiveld, 6525 ED Nijmegen, The Netherlands*

*J. van Bladel*

*Department of Theoretical Chemistry, University of Nijmegen,  
Toernooiveld, 6525 ED Nijmegen, The Netherlands*

### Abstract

The symmetry forbidden  $S_1 \leftarrow S_0$  transition of acetone has been investigated by laser-induced fluorescence spectroscopy with a resolution of 270 MHz. The rotational structure demonstrates that one deals with a-type transitions and that there is a strong coupling between the torsional motion of the two  $\text{CH}_3$  groups and the out-of-plane wagging motion ( $\nu'_{23}$ ) of acetone. The interpretation of torsional-vibrational combination bands is less conclusive.

## 4.1 Introduction

Transitions from the electronic ground state to the lowest energy  ${}^1\pi^*$  state of formaldehyde ( $\text{H}_2\text{CO}$ ) are strictly forbidden in  $C_{2v}$  and are therefore extremely weak,  $f \approx 1 \cdot 10^{-3}$ . The observed intensity of the  $S_1(A_2) \leftarrow S_0(A_1)$  transition is vibronically induced by the C=O out-of-plane wagging motion ( $\nu_4'$ ) of  $b_1$  symmetry via intensity borrowing from the higher lying  ${}^1\sigma^*$  state of  $B_2$  symmetry [1, 2]. Proof of this mechanism was provided by the observation of a-type rovibronic structure in the high resolution electronic spectrum of  $\text{H}_2\text{CO}$  [3].

A similar mechanism was expected to apply to acetone,  $(\text{CH}_3)_2\text{CO}$ , where the  $S_1(A_2) \leftarrow S_0(A_1)$  transition is also very weak,  $f \approx 4 \cdot 10^{-4}$  [4]. But Baba, Hanazaki and Nagashima (BHN) [5] and Zuckermann *et al.* [6, 7] concluded from low resolution laser-induced fluorescence studies on acetone that many of the bands are c-type. Therefore, it appeared that the vibronic coupling mechanism responsible for the observed intensity in the  $S_1 \leftarrow S_0$  transition of acetone is different from that in formaldehyde.

The previous experiments on acetone were performed at a resolution of  $0.2 \text{ cm}^{-1}$ . Now, contour analysis of weak transitions is potentially subjected to errors due to fluctuations in laser intensity and to mode hopping within the bandwidth. For this reason, we have re-examined the  $S_1 \leftarrow S_0$  spectrum of acetone at high resolution,  $0.01 \text{ cm}^{-1}$ . We find that the low-lying bands are all pure a-type, a result that is consistent with the earlier results on formaldehyde. Additionally, for the lowest vibrational  $S_1$  level we find a constant threefold splitting of each rotational line. More complex splitting patterns are observed in higher energy bands. We show in this paper that these splittings have their origin in the methyl group torsional motion.

In addition to the torsional motion we concern ourselves here also with other low frequency vibrations in the  $S_1$  state of acetone. Table 4.1 summarizes the available data on the five lowest frequency vibrational modes in the electronic ground state of acetone. The inertial axes and the torsional angles are shown in Figure 4.1. The two torsional fundamentals have been assigned only recently, and fitted to a hindered two rotor potential [14]. The assignment of the  $385 \text{ cm}^{-1}$  vibration to the C-C-C bending motion and the  $484 \text{ cm}^{-1}$  vibration to the C=O out-of-plane wagging motion has been controversial [10, 11, 12, 13].

Mode	Symm. ( $C_{2v}$ )	Description	Frequency ( $\text{cm}^{-1}$ )	Reference
$\nu_{12}$	$a_2$	"anti-gearing" torsion	77	[8]
$\nu_{24}$	$b_1$	"gearing" torsion	124	[9]
$\nu_8$	$a_1$	C-C-C bending	385	[10, 11] <sup>a)</sup>
$\nu_{23}$	$b_1$	C=O out-of-plane wagging	484	[12] <sup>b)</sup>
$\nu_{19}$	$b_2$	C=O in-plane-wagging	530	[11] <sup>c)</sup>

<sup>a)</sup> In reference [12] the assignment of  $\nu_8''$  and  $\nu_{23}''$  is reversed, but reference [13] reconfirms the present assignment.

<sup>b)</sup> In reference [12] this vibration is of  $b_2$  symmetry.

<sup>c)</sup> In reference [12] this vibration is of  $b_1$  symmetry.

Table 4.1: Low frequency vibrational modes of acetone in the electronic ground state.

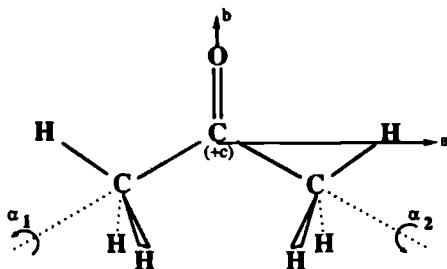


Figure 4.1: Schematic presentation of the structure of acetone.

The ground state torsional potential has been calculated by several authors [15, 16, 17, 18] in an attempt to account for the microwave spectrum. The  $\nu''_{12}$  vibration, which is infrared inactive and very weakly Raman active, has been observed by two-photon jet spectroscopy involving Rydberg transitions [8], leading to a revised calculation [14], in which complete geometry optimization for each conformer was allowed. This calculation, using only four terms in the torsional potential ( $V_3, V_{33}, V'_{33}$  and  $V_6$ ), led to good agreement with the experimental results and to an effective torsional barrier ( $V_{eff} = V_3 - V_{33}$ ) of  $240 \text{ cm}^{-1}$ , somewhat lower than the previously determined barrier of  $270 \text{ cm}^{-1}$  [15, 16].

In the  $S_1(A_2)$  state the  $\nu'_{23}$  vibration is described by a double-well potential and thus subject to tunnel splitting, in contrast to the ground state. A complete analysis of the spectrum thus involves two multiple-well potentials that may lead to tunnel splitting: that of the torsion of the two methyl rotors ( $3^2$ -fold) and of the C=O out-of-plane wagging motion (2-fold). It turns out that some interaction between these two modes is required to account for the rotational fine structure in certain bands. In all bands, the  $\nu'_{23}$  mode is involved via at least one of its tunnel split levels.

## 4.2 Experimental

Narrow bandwidth radiation with a high peak power is obtained by pulsed amplification of radiation from a single-frequency cw ring dye laser. The ring dye laser (Spectra Physics 380D) is pumped by an Argon ion laser (Spectra Physics 2045-15) and operated on DCM dye (620-660 nm). The bandwidth of the ring dye laser is less than 0.5 MHz and the output power is typically 400 mW. This radiation is amplified by a home-built four stage pulsed dye amplifier (PDA) system similar to the system described by Cromwell *et al.* [19]. A frequency doubled Q-switched Nd:YAG laser (Quantel YG 681C-10) with a pulse length of 5 ns and a pulse energy of 550 mJ pumps the PDA system. The pulse energy of the amplified laser beam is 100 mJ. The bandwidth, which is merely determined by the Fourier limit of the pulsed pump laser is measured with a 300 MHz Fabry-Perot interferometer and amounts to 135 MHz. This light is frequency doubled in a KDP crystal yielding UV radiation with a pulse energy of 20 mJ. For absolute frequency calibration the iodine absorption spectrum [20] is recorded at the fundamental frequency simultaneously with the excitation spectrum. For relative frequency calibration the transmission fringes of a temperature stabilized Fabry-Perot interferometer with a free spectral range of 598.82 MHz are recorded.



A molecular beam of acetone is formed by expanding a 5% mixture of acetone in 2 atm argon through a modified electromagnetic fuel injector valve (Bosch) with an orifice diameter of 1 mm into a vacuum chamber. During operation the background pressure in the vacuum chamber is  $5 \cdot 10^{-5}$  torr. The laser beam with a diameter of 3 mm crosses the molecular beam 45 mm downstream of the nozzle. The laser-induced fluorescence is collected by a quartz lens system and imaged onto the photocathode of a photomultiplier (EMI 9863B). To reduce the scattered laser light a Schott KV 370 glass filter is placed in front of the photomultiplier. The fluorescence signal is processed by a digital oscilloscope (LeCroy 7400) and a boxcar integrator (SRS 250) interfaced with a PDP 11/23 computer.

### 4.3 Spectroscopic Results and Analysis

We have studied at high resolution the first 14 bands reported by BHN. Figures 4.2, 4.3 and 4.4 show the fluorescence excitation spectra of some bands with their tunnel splitting fine structure. These are the bands where a satisfactory fit to an asymmetric rotor Hamiltonian could be obtained. In Table 4.2 we summarize the main features of the bands, using BHN's line numbering system. Three main conclusions may be drawn from the results:

1. All transitions are *a*-type, namely polarized in the molecular plane, perpendicular to the C=O bond. (In  $C_{2v}$ , this polarization belongs to the  $B_2$  irreducible representation).
2. The largest change of the inertial moment on excitation to  $S_1$  is with respect to the *b*-axis, i.e. along the C=O bond, as expressed by the relatively large change in the *B* rotational constant. This is indeed expected if the excited state is non-planar, as in formaldehyde, with the central carbon atom becoming the apex of a pyramid whose base is formed by the two other carbon atoms and the oxygen atom.
3. Each of the rotational lines is split into a multiplet.

#### 4.3.1 Analysis of the $0_0^0$ band

The lowest frequency transition observed, line 1 in Table 4.2, was assigned by BHN as the  $0_0^0$  band. We have studied it with a resolution of 270 MHz, and Figure 4.2 shows the fluorescence excitation spectrum. Within the experimental error of 50 MHz every observed rotational line in the spectrum could be fit to the asymmetric rotor Hamiltonian. The observed triplet splitting remains constant for all rotational quantum numbers and amounts to 2.3 GHz. This splitting arises from either (or both) tunnel splittings expected in this system: the one due to the threefold potential of the  $CH_3$  torsional motion, and the one due to the double-well potential of the C=O out-of-plane wagging. The former is expected to be present in both  $S_0$  and  $S_1$ , and the latter only in  $S_1$ .

Since the transition is pure *a*-type, we can determine the symmetry species of the excited state. We shall begin by assuming that the system can be discussed within the  $C_{2v}$  point group as far as the  $\pi^* \leftarrow n$  transition is concerned. The main justification for this assumption is the fact that the  $S_1 \leftarrow S_0$  oscillator strength in acetone is very small, similar to that of formaldehyde. The physical reason is that the local symmetry of the C=O bond is close enough to  $C_{2v}$ , so that  $C_{2v}$  selection rules hold almost rigorously. Furthermore, the fact that the two pyramidal forms of  $S_1$  are interconverting by tunneling motion means that  $C_{2v}$  should be used rather than  $C_s$ . As we shall see, predictions based on these rules agree well with experimental observations.

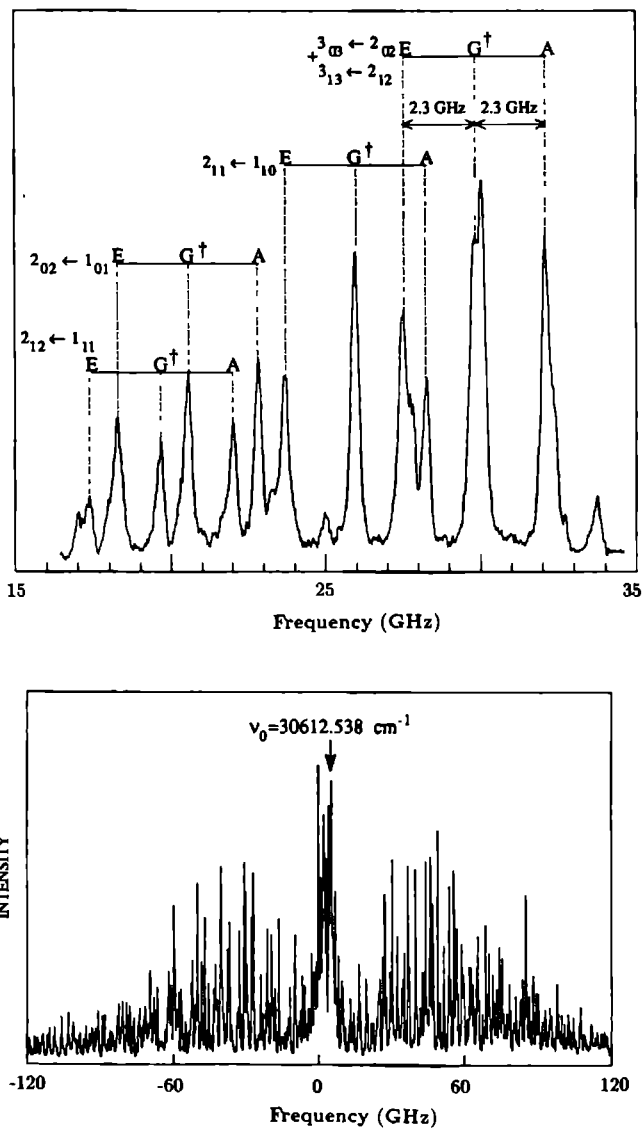


**Figure 4.2:** Lower panel: the high resolution spectrum of line 1, the band origin indicated in the figure is determined for the transitions of G symmetry, of which some are shown in the upper panel. Upper Panel: measured splittings (GHz) and proposed assignments of the fine structure. The splitting, shown for some multiplets only, holds for the entire spectrum.

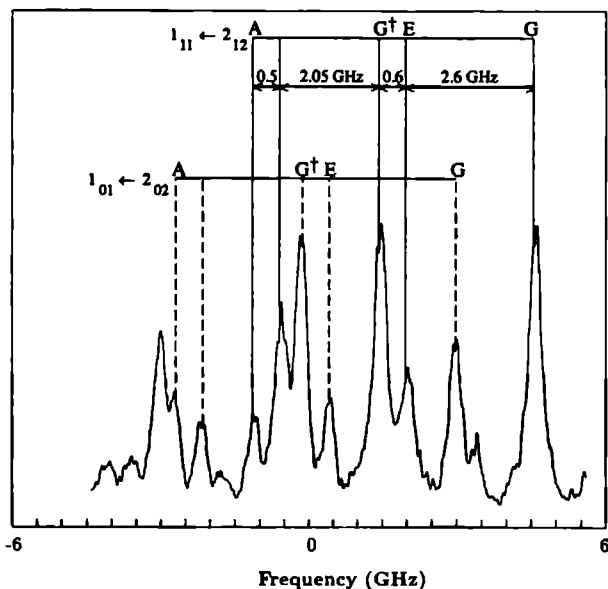


Figure 4.3: Measured splittings (GHz) and proposed assignment of the fine structure for line 2.

In the jet experiments, all transitions are assumed to originate from the vibrational ground state, which is of  $A_1$  symmetry. The  ${}^1\pi^*$  electronic state transforms as  $A_2$ . We write the transition dipole moment as:

$$\mu_{fi} = \langle \Psi'_{ev} | \hat{\mu} | \Psi''_{ev} \rangle \quad (4.1)$$

where  $\Psi'_{ev}$  and  $\Psi''_{ev}$  are the electronic-vibronic wave functions of the upper and lower electronic states, respectively. The direct product of the irreducible representations (irreps) of the terms appearing in equation (4.1) is:

$$\begin{aligned} A_1 &= \Gamma(\Psi'_e) \otimes \Gamma(\hat{\mu}) \otimes \Gamma(\Psi''_e) \otimes \Gamma(X'_v) \otimes \Gamma(X''_v) \\ &= A_2 \otimes B_2 \otimes A_1 \otimes \Gamma(X'_v) \otimes A_1 \\ &= B_1 \otimes \Gamma(X'_v) \end{aligned} \quad (4.2)$$

( $A_3 \otimes A_4 \otimes A_1 \otimes \Gamma(X'_v) \otimes A_1 = A_2 \otimes \Gamma(X'_v)$  in  $G_{36}$ , see below.) Since  $\mu_{fi}$  is of  $A_1$  symmetry the vibrational wavefunction  $X'_v$  of  $S_1$  must transform as  $B_1$  ( $A_2$  in  $G_{36}$ ) in order to make the transition allowed. The real zero point vibrational wavefunction is totally symmetric ( $A_1$ ). A transition to this lowest state is therefore forbidden. The first observed transition will be to the a low vibrational level of  $B_1$  symmetry, which *e.g.* might arise from tunnel splitting of one of the multiple-well motions.

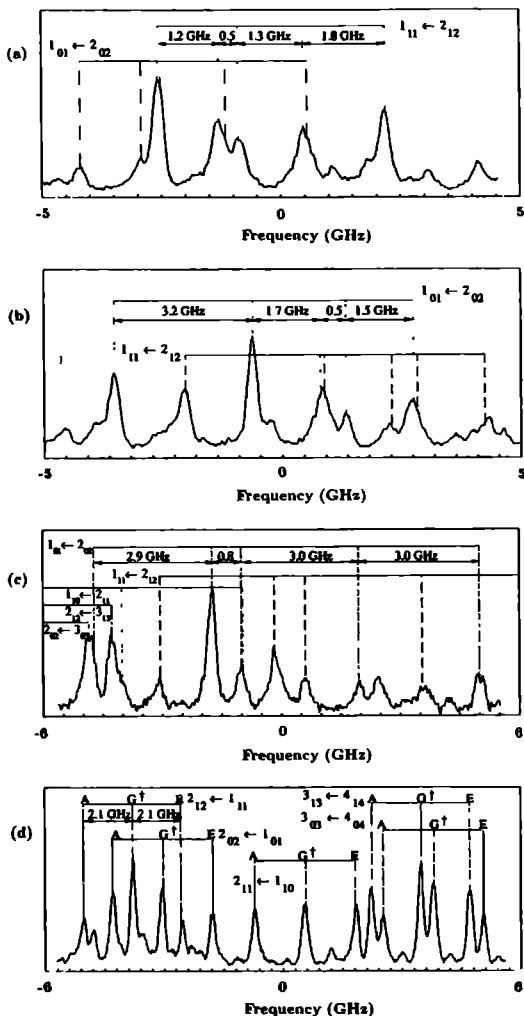


**Figure 4.4:** (a) As in Figure 4.2 for line 4. The symmetry species of the quintets have not been assigned. (b) As in Figure 4.2 for line 5. The symmetry species of the quintets have not been assigned. (c) As in Figure 4.2 for line 6. The symmetry species of the quintets have not been assigned. (d) As in Figure 4.2 for line 7. A triplet structure has been found.

Line <sup>a)</sup>	Frequency <sup>b)</sup> (cm <sup>-1</sup> )	Type <sup>c)</sup>	Rotational constants <sup>d)</sup> (MHz)			Fine structure
			$\Delta A$	$\Delta B$	$\Delta C$	
1	0	a	60.2(7.1)	-341.9(3.4)	-14.4(1.1)	triplet
2	172.624	a	78.8(5.7)	-351.5(2.8)	10.9(0.6)	quintet
3	not observed					
4	314.546	a	68.1(7.5)	-362.9(2.7)	-29.7(1.2)	quintet
5	333.559	a	87.4(6.2)	-371.3(3.0)	-32.0(0.3)	quintet
6	346.393	a	23.8(8.9)	-381.9(5.2)	-23.8(1.2)	quintet
7	373	a				triplet
8	473.4	a				>quintet
	474.4	a				
9	486.7	a				quintet <sup>e)</sup>
10	509.728	a	42.4(6.1)	-437.4(6.1)	-23.9(1.8)	
	510.117	a	140.0(9.8)	-525.4(6.7)	-20.5(1.3)	
	510.372	a	53.4(8.0)	-408.9(6.9)	-37.1(0.6)	
11	544					
12	578					
13a	621.76	a	107(11)	-303.7(7.2)	-40.9(0.6)	
13b	624					quintet <sup>f)</sup>
14a	641					
14b	645					

<sup>a)</sup> The numbering system is the same as used by BHN [5].

<sup>b)</sup> frequencies above the 0<sub>0</sub><sup>0</sup> transition at 30 439.915 cm<sup>-1</sup>. The error in the observed band origins is 0.005 cm<sup>-1</sup>.

<sup>c)</sup> Using the axis convention of Figure 4.1.

<sup>d)</sup> Listed are the changes in the three principal rotational constants with respect to the ground state constants which are (MHz):  $A''=10\,165.6$ ,  $B''=8\,514.9$  and  $C''=4\,910.2$ . The standard deviation of the fit is given in parentheses.

<sup>e)</sup> Five components are observed with approximate relative shifts of 20, 9, 13 and 9 GHz.

<sup>f)</sup> Five components are observed with approximate relative shifts of 16, 8, 4 and 9 GHz.

Table 4.2: Main experimental results for the observed vibronic bands of acetone.

We start the theoretical analysis of the torsional vibrations with the assumption that interactions between torsional vibrations and other normal vibrations of the molecule can be neglected. In this case, it is sufficient to consider only the following terms of the Hamiltonian [15]:

$$H = H_R + H_{T_1} + H_{T_2} + H_{T_1 T_2} + H_{RT} \quad (4.3)$$

The terms  $H_R$  and  $H_{T_i}$  ( $i=1,2$ ) stand for pure rotation and torsional vibration of top  $i$ , respectively.  $H_{T_1 T_2}$  describes the interaction between the two CH<sub>3</sub> tops and  $H_{RT}$  describes the interaction between overall rotation and the torsional vibrations. In the analysis of our spectra we will ignore the  $H_{RT}$  interaction term so that the rotational energy levels are merely superimposed on the energy levels of the torsional vibrations. This is permitted since in our measurements, the triplet splitting remains constant for all rotational quantum numbers. The torsional Hamiltonian consists, then, of three parts:

$$H_{T_k} = F P_{\alpha_k}^2 + \frac{1}{2} [V_3(1 - \cos 3\alpha_k) + V_6(1 - \cos 6\alpha_k)], \quad k = 1, 2$$

$$H_{T_1 T_2} = F' P_{\alpha_1} P_{\alpha_2} + \frac{1}{2} \{V_+[1 - \cos(3\alpha_1 + 3\alpha_2)] + V_-[1 - \cos(3\alpha_1 - 3\alpha_2)] + \dots\} \quad (4.4)$$

Here  $H_{T_k}$  describes the motion of the  $k$ -th methyl group with momentum  $P_{\alpha_k}$  conjugated to the torsional angle  $\alpha_k$ . The parameters  $V_3$  and  $V_6$  describe the frame-top interaction, whereas  $V_+$  and  $V_-$  we call the anti-g geared and geared top-top interactions.  $F$  and  $F'$  are determined by the molecular geometry only. Note that there is a simple correspondence between our notation and that used in references [14, 15, 21]:  $V_+ = \frac{1}{2}(V'_{33} - V_{33})$  and  $V_- = -\frac{1}{2}(V'_{33} + V_{33})$ .

Since the torsional barrier in  $S_0$  is relatively low, about  $250 \text{ cm}^{-1}$  [15, 16], we cannot neglect the splitting caused by tunnelling. Thus, a complete analysis of the spectrum requires the use of the  $G_{36}$  molecular symmetry group for the ground state, instead of  $C_{2v}$ . To the  $C_s$  symmetry of a pyramidal geometry corresponds the symmetry group of  $G_{18}$  [22]. However, the finite inversion barrier, as will be shown later, requires actually the use of  $G_{36}$  also for the  $S_1$  surface. The correlation between  $C_{2v}$  and  $G_{36}$  is reproduced in Table 4.4, as taken from Bunker [23, 24]. In the high-barrier limit, each torsional wavefunction associated with a given rotational level is ninefold degenerate. As the barrier height is lowered, this degenerate level is split into a non-degenerate  $A_i$ ,  $i \in \{1..4\}$  level, two doubly degenerate  $E_i$ ,  $i \in \{1..4\}$  levels and a fourfold degenerate  $G$  level. If the  $H_{T_1 T_2}$  interaction term is also neglected, the two  $E_i$  states are degenerate so that torsional triplets are obtained. All low-lying torsional levels actually possess this triplet structure, for reasonable assumptions concerning the torsional potential including also an  $H_{T_1 T_2}$  term.

Figure 4.5 shows the fine structure for the (pseudo)  $0_0^0$  electronic transition. The rule according to which the allowed transitions were determined is that the initial overall vibrational wavefunctions ( $A_1, E_1, E_3, G$ ) should transform into ( $A_2, E_1, E_4, G$ ) i.e.  $A \leftrightarrow A$ ,  $E \leftrightarrow E$ ,  $G \leftrightarrow G$ . The direct product of the irreps of the vibrational wavefunctions,  $\Gamma(X_v)$ , transforms as  $\Gamma(\text{torsion}) \otimes \Gamma(\text{wag})$ , since all other vibrational modes are in their ground state. Therefore, it is the second inversion-tunnelling component,  $\Gamma(\text{wag})=A_2$  ( $B_1$  in  $C_{2v}$ ), that is responsible for the observation of line 1 whereas the fine structure mainly reflects the torsion tunnel-splitting in the ground torsional state. The triplet splitting of the lines in the observed spectrum,  $\Delta E = |\Delta E' - \Delta E''|$ , is determined by the difference in torsional energy splittings in the upper and lower electronic states. Figure 4.6

$C_{2v}$ level	$G_{36}$ sublevels
$A_1(28)$	$A_1(6)+E_1(4)+E_3(2)+G(16)$
$A_2(28)$	$A_3(6)+E_2(4)+E_3(2)+G(16)$
$B_1(36)$	$A_2(10)+E_1(4)+E_4(6)+G(16)$
$B_2(28)$	$A_4(10)+E_2(4)+E_4(6)+G(16)$

**Table 4.3:** Correlations of rovibrational levels of acetone. Spin statistical weights are given in parentheses.

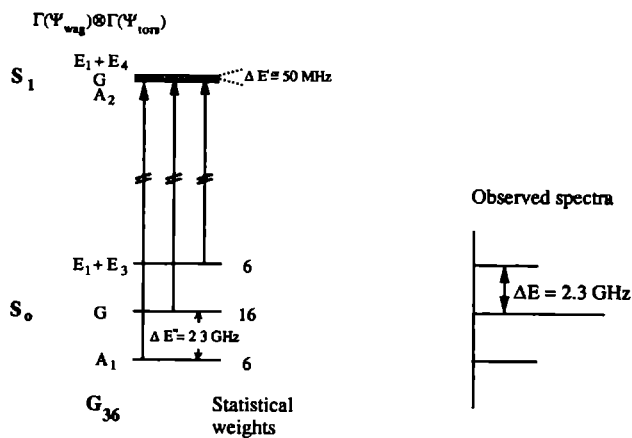


**Figure 4.5:** Diagram showing the possible  $S_1 \leftarrow S_0$  transitions between torsional tunnel components of each rotational level for the case where the splitting in the excited state is small. Only three lines can be experimentally observed in this case. The structure of each triplet is shown on the right side.

shows our calculation of the expected energy splitting,  $\Delta E''$ , as a function of the barrier height. It is found that 2.3 GHz is compatible with a barrier of about  $250 \text{ cm}^{-1}$ , as observed by microwave spectroscopy. Assuming that the splitting in the excited state is smaller than our accuracy of 50 MHz, we estimate a lower limit for the barrier height ( $V_3$ ) to internal rotation in the  $S_1$  state to be around  $600 \text{ cm}^{-1}$ . A more precise estimate is deferred to the analysis of the torsional energy levels.

The observed triplet intensities obey the ratio 3:8:3, within the experimental uncertainty, which is in agreement with predictions based upon spin statistics, see Figure 4.5.

### 4.3.2 Refined analysis of the $0_0^0$ band

The torsional energy levels and wavefunctions are well-known for the case of two-top molecules [21, 25]. The product of single-top wavefunctions serves as the basis for the total two-top Hamiltonian using the Principal-Axis-Method (PAM):

$$U_{\sigma_1 \sigma_2}^{v_1 v_2}(\alpha_1, \alpha_2) = U_{\sigma_1}^{v_1}(\alpha_1) U_{\sigma_2}^{v_2}(\alpha_2) \quad (4.5)$$

where

$$U_{\sigma}^v(\alpha) = \sum_{k=-\infty}^{\infty} A_k^{(v)} \exp[i(3k + \sigma)\alpha] \quad (4.6)$$

The label  $v$  is called the principal torsional quantum number since it becomes the quantum number for the limiting harmonic oscillator state ( $V_3 \rightarrow \infty$ ). The index  $\sigma=0, \pm 1$  gives the symmetries of the wavefunctions and thus distinguishes between the tunnelling sublevels. Each eigenstate of the two-top torsional Hamiltonian is characterized by the four quantum numbers  $v_1, \sigma_1, v_2, \sigma_2$ . In a

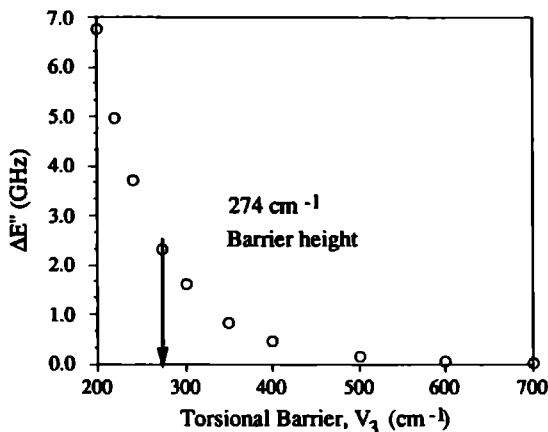


Figure 4.6: Tunnel splitting as a function of torsional barrier height in the ground state.

somewhat simplified picture,  $v_1$  and  $v_2$  denote the number of torsional quanta present in each top while the various combinations of  $\sigma_1, \sigma_2$  provide the overall nine-fold degeneracy of the torsional level.

The out-of-plane wagging mode,  $\nu'_{23}$ , of  $b_1$  symmetry can be viewed as the motion of the central C-atom with respect to the plane spanned by the two methyl groups and the O-atom. Considering first the C=O out-of-plane wagging we have calculated the double-well potential by fitting our observed spectra to the tables of Coon *et al.* [26]. The results are shown in Figure 4.7. In  $C_{2v}$ , the symmetry of the vibrational levels alternates between  $A_1$  and  $B_1$ , and thus only half of the levels will be observed in the excitation spectrum. For a reasonable potential model the barrier height,  $1350\text{ cm}^{-1}$ , was made to fit the transition at  $333\text{ cm}^{-1}$ , see Table 4.2. It leads to a splitting of about 1 GHz, due to tunneling, between the two levels  $23^2$  and  $23^3$ . The splitting between the lowest two vibrational levels is  $\ll 1$  GHz.

Since the  $23^0$  and  $23^1$  levels of the C=O out-of-plane wagging are very close in energy we propose to consider its coupling with the torsional motion. In turn, this coupling will allow transitions to some of the forbidden levels, as required by the appearance of quintets in higher members of the torsional progression. The wagging motion will be described by the distance coordinate,  $q_w$ . As follows from the character table of  $G_{36}$ , a translation along this direction belongs to the  $A_2$  irreducible representation, as does the gearing motion of the two  $\text{CH}_3$  groups. In order to couple the two kinds of motion we look for a potential term of  $A_1$  symmetry that contains naturally the coordinates of both. The operator, to be added to our Hamiltonian, equation (4.4)

$$V_{\text{coupl}} = C_{\text{coupl}} q_w \sin(3\alpha_1 - 3\alpha_2) \quad (4.7)$$

offers itself since both factors are of  $A_2$  symmetry with  $A_2 \otimes A_2 = A_1$ . Note that positive torsional angles  $\alpha_1$  and  $\alpha_2$  are defined as clockwise rotation looked from the central C-atom, i.e. the minus sign in the argument of the sine-factor corresponds to the gearing operation of  $A_2$  symmetry. Having thus established the simplest potential coupling term between wagging and torsion, we next consider qualitatively its influence on the possible transitions between energy levels. Without



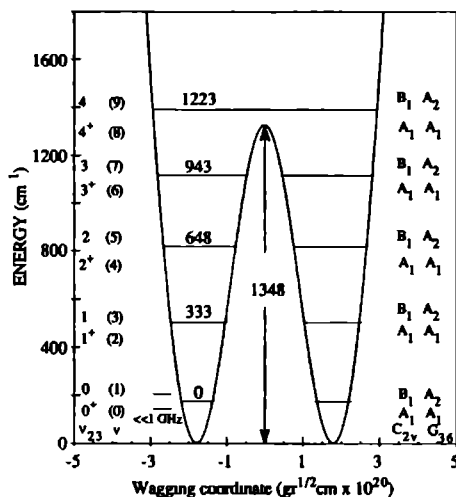


**Figure 4.7:** The calculated out-of-plane wagging potential of  $S_1$ . The parameters used in the calculation are  $\rho=1.20$ ,  $B=6.0$ ,  $\nu_0=224.6 \text{ cm}^{-1}$ , see reference [26]. Only odd vibrational levels having  $B_1$  symmetry in  $C_{2v}$ ,  $A_2$  in  $G_{30}$ , can be accessed for zero-torsion, the forbidden ones are shown in dashed lines. The splitting of the lowest level is much smaller than 1 GHz and amounts to 1, 17 and 270 GHz, respectively for the next higher ones. The position of the levels is given in wavenumbers.

this coupling the excitation from the  $S_0$  ground state yields for the  $0_1^0$  band an electronically excited state with one vibrational quantum in the wagging mode,  $23^1$ . The initial quadruplet of states ( $A_1, E_1, E_3, G$ ) is excited to the quadruplet ( $A_2, E_1, E_4, G$ ) =  $A_2 \otimes (A_1, E_1, E_3, G)$ . This would apply to the  $0_1$  as well as to the excited torsional levels  $2_1$  and  $2_3$ .

With the coupling term given by equation (4.7) the members of the quadruplet of the excited states just discussed, ( $A_2, E_1, E_4, G$ ), appear to be coupled to two members of the slightly lower quadruplet of states, ( $A_1, E_1, E_3, G$ ) of  $23^0$ , i.e.  $E_1$  with  $E_1$  and  $G$  with  $G$ . Note that this coupling leads to five energetically distinct transitions,  $A_1 \rightarrow A_2(23^1)$ ,  $E_1 \rightarrow E_1(23^1)$  and  $E_3 \rightarrow E_4(23^1)$ ,  $G \rightarrow G(23^1)$ ,  $E_1 \rightarrow E_1(23^0)$ , and  $G \rightarrow G(23^0)$ . The resulting pattern is thus a quintet, as it is observed for most bands but *not* for the  $0_0^0$  band.

In the following we will show why the proposed coupling vanishes for the  $0_0^0$  transition so that the spectrum possesses a triplet structure while the "direct" and "coupled" transitions in the spectra of bands 2, 4 and 6 display quintet structure, whose components are of similar intensity. A transition is called "direct", if the final level (with torsional splitting being neglected) has  $B_1$  symmetry, in  $C_{2v}$ , and can thus be reached through a  $B_2$  transition dipole moment, see equation (4.2). "Coupled" transition needs equation (4.7) to become allowed. The matrix element of the coupling may be expressed as:

$$\langle \Psi_{v=0}(q_w) U_{\sigma_1 \sigma_2}^{v_1 v_2}(\alpha_1, \alpha_2) | q_w \sin(3\alpha_1 - 3\alpha_2) | \Psi_{v=1}(q_w) U_{\sigma_1 \sigma_2}^{v_1' v_2'}(\alpha_1 \alpha_2) \rangle \quad (4.8)$$

where  $\langle \Psi_{v=0}(q_w) |$  and  $|\Psi_{v=1}(q_w) \rangle$  are the part of the bra and ket that describe the lowest and first excited wagging states split by the tunneling motion and  $U(\alpha_1, \alpha_2)$  the part that describes the torsional motion, see equation (4.5). The coupling between  $v=0$  and  $v=1$  wagging levels,  $23^0$  and  $23^1$ , is realized by the factor  $q_w$  in  $V_{\text{coupl}}$ . The torsional coupling takes place through the sine term of  $A_2$  symmetry. If the sine term is written as a difference of two exponentials, it becomes evident that raising the degree of torsional excitation of one internal top is accompanied by lowering the torsional excitation of the other one. For the torsional ground state, this operation necessarily yields zero, i.e. the observed triplet structure of the  $0_0^0$  band agrees with our analysis even after introduction of  $V_{\text{coupl}}$ , equation (4.7).

### 4.3.3 Analysis of the torsional progression

Table 4.4 lists the lowest torsional states with their tunneling symmetries in  $G_{36}$ . The progression bands at 0, 172.5, 314.5, 346.3, 474.3, 510 and 640.8  $\text{cm}^{-1}$  are assigned to the anti-gearing and gearing torsional modes  $\nu'_{12}$  and  $\nu'_{24}$ , see Table 4.5. The torsional energy levels calculated by diagonalizing the Hamiltonian, equation (4.4), are depicted in Figure 4.8 together with the experimental energies. The kinetic energy coefficient  $F'$  was taken as a parameter along with the potential parameters  $V_3, V_6, V_4$  and  $V_-$ , since only qualitative information is available on the excited state geometry. The best calculation resulted in an agreement within 2  $\text{cm}^{-1}$  between the experimental and calculated frequencies of the lines 2, 4 and 6. Each of the lines 2, 4 and 6 has a quintet fine structure which is constant for all the rotational lines within a given band. The remaining discrepancy and the fact that the bands display quintet fine structure, rather than triplet like in the  $0_0^0$  band, may be accounted for by introducing a coupling between the torsional motion and

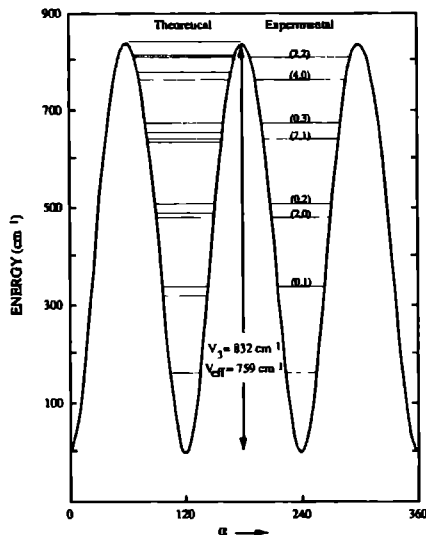


Figure 4.8: The calculated torsional potential, with  $V_{\text{eff}} = V_3 - V_{33}$  for the excited state and the associated energy levels. Unobserved levels are not shown on the right side.

$N_k$ <sup>a)</sup>	$\nu^+$	$\nu^-$	$\Gamma(C_{2v})$	selection rules based on $C_{2v}$	$\Gamma(G_{36})$ <sup>b)</sup>	
					$\Gamma_{tors} \otimes A_1(\text{wag})$	$\Gamma_{tors} \otimes A_2(\text{wag})$
0 <sub>1</sub>	0	0	A <sub>1</sub>		A <sub>1</sub> +E <sub>1</sub> +E <sub>3</sub> +G	A <sub>2</sub> +E <sub>1</sub> +E <sub>4</sub> +G
1 <sub>1</sub>	1	0	A <sub>2</sub>	forbidden	A <sub>3</sub> +E <sub>2</sub> +E <sub>3</sub> +G	A <sub>4</sub> +E <sub>2</sub> +E <sub>4</sub> +G
1 <sub>2</sub>	0	1	B <sub>1</sub>		A <sub>2</sub> +E <sub>1</sub> +E <sub>4</sub> +G	A <sub>1</sub> +E <sub>1</sub> +E <sub>3</sub> +G
2 <sub>1</sub>	(2	0)	A <sub>1</sub>		A <sub>1</sub> +E <sub>1</sub> +E <sub>3</sub> +G	A <sub>2</sub> +E <sub>1</sub> +E <sub>4</sub> +G
2 <sub>2</sub>	(1	1)	B <sub>2</sub>	forbidden	A <sub>4</sub> +E <sub>2</sub> +E <sub>4</sub> +G	A <sub>3</sub> +E <sub>2</sub> +E <sub>3</sub> +G
2 <sub>3</sub>	(0	2)	A <sub>1</sub>		A <sub>1</sub> +E <sub>1</sub> +E <sub>3</sub> +G	A <sub>2</sub> +E <sub>1</sub> +E <sub>4</sub> +G
3 <sub>1</sub>	(3	0)	A <sub>2</sub>	forbidden	A <sub>3</sub> +E <sub>2</sub> +E <sub>3</sub> +G	A <sub>4</sub> +E <sub>2</sub> +E <sub>4</sub> +G
3 <sub>2</sub>	(2	1)	B <sub>1</sub>		A <sub>2</sub> +E <sub>1</sub> +E <sub>4</sub> +G	A <sub>1</sub> +E <sub>1</sub> +E <sub>3</sub> +G
3 <sub>3</sub>	(1	2)	A <sub>2</sub>	forbidden	A <sub>3</sub> +E <sub>2</sub> +E <sub>3</sub> +G	A <sub>4</sub> +E <sub>2</sub> +E <sub>4</sub> +G
3 <sub>4</sub>	(0	3)	B <sub>1</sub>		A <sub>2</sub> +E <sub>1</sub> +E <sub>4</sub> +G	A <sub>1</sub> +E <sub>1</sub> +E <sub>3</sub> +G
4 <sub>1</sub>	(4	0)	A <sub>1</sub>		A <sub>1</sub> +E <sub>1</sub> +E <sub>3</sub> +G	A <sub>2</sub> +E <sub>1</sub> +E <sub>4</sub> +G
4 <sub>2</sub>	(3	1)	B <sub>2</sub>	forbidden	A <sub>4</sub> +E <sub>2</sub> +E <sub>4</sub> +G	A <sub>3</sub> +E <sub>2</sub> +E <sub>3</sub> +G
4 <sub>3</sub>	(2	2)	A <sub>1</sub>		A <sub>1</sub> +E <sub>1</sub> +E <sub>3</sub> +G	A <sub>2</sub> +E <sub>1</sub> +E <sub>4</sub> +G
4 <sub>4</sub>	(1	3)	B <sub>2</sub>	forbidden	A <sub>4</sub> +E <sub>2</sub> +E <sub>4</sub> +G	A <sub>3</sub> +E <sub>2</sub> +E <sub>3</sub> +G
4 <sub>5</sub>	(0	4)	A <sub>1</sub>		A <sub>1</sub> +E <sub>1</sub> +E <sub>3</sub> +G	A <sub>2</sub> +E <sub>1</sub> +E <sub>4</sub> +G

<sup>a)</sup>  $N = \nu^+ + \nu^-$  (number of torsional quanta). The group of levels having the same  $N$  is defined as a torsional polyad. Polyad  $N$  consists of  $N + 1$  levels labeled by  $k$ . The  $\nu^+$ ,  $\nu^-$  designation here refers to the gearing and anti-gearing torsional fundamentals but not to the actual distribution of energy between the two tops. Starting from the second polyad onward the  $\nu^+$ ,  $\nu^-$  designation is put into parentheses since the actual motion described by the eigenfunctions has a more complicated character.

<sup>b)</sup> The left term is the representation of the torsional states coupled to the  $A_1$  component of the out-of-plane wagging vibration, the right hand term is the representation of the same torsional state coupled to the  $A_2$  component.

**Table 4.4:** Symmetries of the lower vibrational states of acetone in the  $S_1$  excited state with there tunneling sublevels.

other vibrational modes. Thus, to the torsional Hamiltonian, equation (4.4), the coupling term,  $V_{coupl}$ , equation (4.7), will be added.

For instance, we have  $(A_1, E_1, E_3, G) = A_2 \otimes (A_2, E_1, E_4, G)$  yielding an additional doublet of  $E_1$  and  $G$  symmetry as final levels if the excitation of the  $1_2$  torsional level is accompanied by excitation of the wagging mode, see Figure 4.9 and Table 4.4. The effect of the very small splitting,  $\ll 1$  GHz, between the two lowest wagging levels is that torsional sublevels of the same symmetry, i.e.  $G$  and  $G$  and  $E_1$  and  $E_1$ , are coupled by the  $V_{coupl}$  term. The resulting pattern is a quintet, instead of a triplet. In our assignments we were guided by the nearly constant, 3.2 GHz, distance between the two strongest lines within the quintets. Our analysis implies then that the strength of the interaction caused by the  $V_{coupl}$  term is on the order of 1.6 GHz.

Linear combinations of equation (4.5) form the eigenfunctions of our torsional Hamiltonian. The same basis functions have been used and are discussed in reference [27]. As an example of an excited state, the  $1_2$  torsional level may be described with a high accuracy by the eigenfunction  $\frac{1}{\sqrt{2}}(|1, 0\rangle - |0, 1\rangle)$  where  $|v_1, v_2\rangle$  indicates  $v_1$  and  $v_2$  torsional quanta in top 1 and top 2, respectively.

$N_k$	Observed (line #)	Calculated <sup>a)</sup>	$\Delta A-G$ <sup>b)</sup>	$\Delta E-G$ <sup>b)</sup>
1 <sub>1</sub>	not observed	155.5	0.255	0.255
1 <sub>2</sub>	172.5 (2)	173.9	0.328	0.328
2 <sub>1</sub>	314.5 (4)	314.7	2.3	2.3
2 <sub>2</sub>	not observed	324.0	5.0	5.0
2 <sub>3</sub>	346.3 (6)	344.7	2.417	2.390
3 <sub>1</sub>	not observed	471.2	54.1	10.4
3 <sub>2</sub>	474.3 (8)	474.0	21.7	64.5
3 <sub>3</sub>	not observed	489.0	16.9	17.7
3 <sub>4</sub>	510 (10)	511.9	5.28	5.44
4 <sub>1</sub>	598 (12, 12a)	597.0	0.796	510.0
4 <sub>2</sub>	not observed	614.0	509.0	0.07
4 <sub>3</sub>	640.8 (14a)	641	13.0	9.9
4 <sub>4</sub>	not observed	646	26.3	28.8
4 <sub>5</sub>	not measured	673	-	-

<sup>a)</sup> Parameters ( $\text{cm}^{-1}$ ) used in the calculation:  $F=5.726$ ,  $F'=-0.2813$ ,  $V_3=832.0$ ,  $V_6=-60.3$ ,  $V_+=13.46$ ,  $V_-=-86.63$ . The frequencies are given with respect to the  $0_0^0$  transition at  $30\,439.915\text{ cm}^{-1}$ . The  $0_1$  level is calculated to be at  $164.4\text{ cm}^{-1}$  above the potential minimum.

<sup>b)</sup> Calculated maximum splitting (GHz) between the A,E and G sublevels. It is noted that the degeneracy between the pairs of E levels for a given  $N_k$  level prevails and is lifted to 15 MHz only for the  $4_5$  level.

Table 4.5: Comparison of experimental and calculated frequencies and splittings ( $\text{cm}^{-1}$ ) of low-lying torsional levels.

Substitution of this expression into the matrix element of equation (4.8) results in a non-vanishing torsional coupling: the  $\sin(3\alpha_1-3\alpha_2)$  operator working upon  $(|1,0\rangle-|0,1\rangle)$  yields *e.g.*  $(|0,1\rangle-|1,0\rangle)$  and thus a non-vanishing coupling matrix element is obtained. Within the torsional multiplet we find a wagging mixture ( $23^0$  and  $23^1$ ) through  $V_{\text{coupt}}$ , equation (4.7), yielding transitions which were forbidden before. In an analogous way the "coupled" transitions in the bands at  $314.5$  and  $346.3\text{ cm}^{-1}$  become allowed. The intensities of the "direct" and "coupled" transitions are nearly equal. This fact implies that the unperturbed eigenfunctions mix with nearly equal weights. It is the near degeneracy of the  $23^0$  and  $23^1$  levels that makes such a mixing possible. It can easily be shown [28] that if the unperturbed wagging levels are tunnel-split much less than 1 GHz, a coupling strength on the order of 1.6 GHz brings the intensity of a "coupled" transition to 50% of the "direct" one. A full treatment of the problem must be based on a Hamiltonian including the  $V_{\text{coupt}}$  term.

For the third and fourth polyads only a preliminary analysis can be presented. The band around  $474\text{ cm}^{-1}$  (line 8) spreads over  $\approx 12\text{ cm}^{-1}$ , compared to  $\approx 8\text{ cm}^{-1}$  for the nearby lying lines 7 and 9. The prediction of an exceptionally large ( $\approx 2\text{ cm}^{-1}$ ) torsional splitting within the  $3_2$  torsional level, see Table 4.5, agrees with the large shifts ( $\approx 4\text{ cm}^{-1}$ ) between various components found in a preliminary analysis of line 8. The band at  $510\text{ cm}^{-1}$  (line 10) is assigned to the  $3_4$  torsional level.

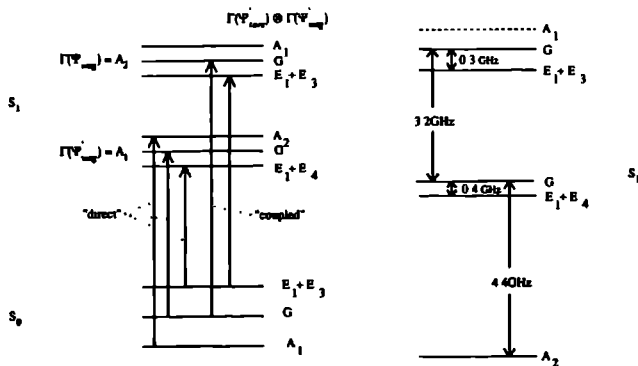


**Figure 4.9:** Level scheme for the  $S_1 (1_2) \leftarrow S_0 (0_1)$  transition in acetone. Indicated are the "direct" transitions to the lowest wagging components and the "coupled" transitions to the higher wagging component. Also indicated are the energy splittings in the  $S_1 (1_2)$  level as deduced from the observed spectrum.

Both  $3_2$  and  $3_4$  bands are expected to have a quintet fine structure. Line 10 exhibits higher than a triplet fine structure, whereas line 8 is much more complicated. The rotational analysis of line 8 and all other higher energy lines is complicated by the fact that different components within the same band have, at times, different rotational constants. We assign lines 12 and 12a to the  $4_1$  level. Line 12a was measured with  $0.2 \text{ cm}^{-1}$  resolution only [6]. It is a relatively broad band, similar to line 8 and can, therefore, accommodate the calculated  $\approx 17 \text{ cm}^{-1}$  splitting  $\Delta E$ -G, see Table 4.5. Line 14a, at  $641 \text{ cm}^{-1}$ , fits well to the assignment  $2^1 + 4_3$ . In Table 4.6 it is remarked that the nature of the eigenfunctions has the symmetry of ( $2^*$ anti-gearing +  $2^*$ gearing). Note that the eigenfunction may differ from the mixture belonging to ( $n^*$ anti-gearing +  $n^*$ gearing) in case that a parenthesis occurs in the last column of Table 4.6. Up to the second polyad, however, such a characterization is rather accurate. It is evident that the analysis of these and higher levels may require introduction of more coupling terms.

#### 4.4 Other low energy modes

In the ground state, three other low energy modes are known (Table 4.1);  $\nu_8''$ , the C-C-C bending,  $385 \text{ cm}^{-1}$ ;  $\nu_{23}''$ , the C=O out-of-plane wagging,  $484 \text{ cm}^{-1}$  and  $\nu_{19}''$ , the C=O in-plane-wagging,  $530 \text{ cm}^{-1}$ . For the  $S_1$  state we offer two possible assignments below, to explain our spectra, see Table 4.7. The band at  $373 \text{ cm}^{-1}$  (line 7) is assigned to the C-C-C bending,  $8^1$ , for both possibilities. The  $A_1$  symmetry of the  $\nu_8'$  vibration is expected to yield a triplet fine structure, just as the  $0_0^0$  band. The observed spectrum of line 7 has indeed a triplet fine structure as shown in Figure 4.4(d) with a consistent 2.1 GHz splitting of each rotational line and approximately 3:8:3 relative intensities. The 200 MHz decrease from the 2.3 GHz triplet splitting in the  $0_0^0$  band is four times our experimental accuracy. We argue that since the  $373 \text{ cm}^{-1}$  band serves as a pseudo- origin

Line	Energy <sup>a)</sup>	Assignment		
		First possibility	Second possibility	Ref. [5]
1	0 <sup>b)</sup>	23 <sup>1</sup>	23 <sup>1</sup>	23 <sup>0</sup>
2	172.5	1 <sub>2</sub>	1 <sub>2</sub>	1 <sub>1</sub>
3	hot band	not observed	not observed	
4	314.5	23 <sup>1</sup> +2 <sub>1</sub>	23 <sup>1</sup> +2 <sub>1</sub>	2 <sub>1</sub>
5	333.6	19 <sup>1</sup> +1 <sub>1</sub>	23 <sup>3</sup>	2 <sub>1</sub>
6	346.3	23 <sup>1</sup> +2 <sub>3</sub>	23 <sup>1</sup> +2 <sub>3</sub>	2 <sub>2</sub>
7	373	8 <sup>1</sup>	8 <sup>1</sup>	23 <sup>2</sup>
8	474	3 <sub>2</sub>	3 <sub>2</sub>	3 <sub>1</sub>
9	487	19 <sup>1</sup> +2 <sub>2</sub>	23 <sup>2</sup> +1 <sub>2</sub>	3 <sub>2</sub>
10	510	3 <sub>4</sub>	3 <sub>4</sub>	3 <sub>2</sub>
11	544	8 <sup>1</sup> +1 <sub>2</sub>	8 <sup>1</sup> +1 <sub>2</sub>	23 <sup>2</sup> +1 <sub>1</sub>
12	578	23 <sup>1</sup> +4 <sub>1</sub>	23 <sup>1</sup> +4 <sub>1</sub>	23 <sup>3</sup>
12a	598	23 <sup>1</sup> +4 <sub>1</sub>	23 <sup>1</sup> +4 <sub>1</sub>	c)
13a	621	19 <sup>1</sup> +3 <sub>1</sub>	19 <sup>1</sup> +1 <sub>1</sub>	
13b	624	19 <sup>1</sup> +3 <sub>1</sub>	23 <sup>3</sup> +2 <sub>1</sub>	4 <sub>1</sub>
14a	641	4 <sub>3</sub>	4 <sub>3</sub>	
14b	645	19 <sup>1</sup> +3 <sub>3</sub>	23 <sup>3</sup> +2 <sub>1</sub>	4 <sub>2</sub>

<sup>a)</sup> Energy above the origin of S<sub>1</sub> at 30 439.915 cm<sup>-1</sup>.

<sup>b)</sup> Transitions from the S<sub>0</sub> vibrationless level to the real zero-point energy level of the C=O out-of-plane wagging (23<sup>0</sup>) are electric dipole forbidden. The first overtone (23<sup>1</sup>) is calculated to be some MHz above the 23<sup>0</sup> and is the pseudo-origin of the observed spectrum.

<sup>c)</sup> Not mentioned in reference [5]. Was measured with 0.2 cm<sup>-1</sup> resolution in reference [6] and belongs to the 4<sub>1</sub> level.

**Table 4.6:** Assignment of the bands observed in the fluorescence excitation spectrum of acetone. For line 8 onward, assignments and analysis are less certain.

for the progression of 8<sup>1</sup>+torsion combination bands, the torsional barrier used in the torsional energy-levels calculations for the excited state must be lowered. Figure 4.6 shows that a 200 MHz zero-tunnel-splitting is obtained for  $V_3=450$  cm<sup>-1</sup> i.e the torsional barrier is effectively lowered by nearly the amount of vibrational excitation. The physical reason for such an effect might be that a somewhat different equilibrium geometry of acetone in the 8<sup>1</sup> vibrationally excited state lowers the hindrance of the two CH<sub>3</sub> groups.

#### 4.4.1 First possibility

The bands at 333.5, 487, 621, 624 and 645 cm<sup>-1</sup> (lines 5, 9, 13a, 13b and 14b, respectively) are assigned to the 19<sup>1</sup>+torsion progression. The C=O in-plane-wagging,  $\nu'_{19}$  (B<sub>2</sub>), can have an a-type spectrum only if coupled with the anti-gearing torsion,  $\nu'_{12}$  (A<sub>2</sub>), and is expected to have a quintet fine structure. Line 5 at 333 cm<sup>-1</sup> is assigned to 19<sup>1</sup>+1<sub>1</sub> and displays a quintet, see Figure 4.4(b). This assignment suggests a very large change in the frequency of the C=O in-plane wagging, i.e.

177  $\text{cm}^{-1}$  in  $S_1$ , compared to 530  $\text{cm}^{-1}$  in  $S_0$ , see Table 4.1. Lines 9, 13a+13b, and 14b are assigned to  $19^1 + 2_2$ ,  $19^1 + 3_1$  and  $19^1 + 3_3$  respectively. It follows from this assignment that the torsional anti-gearing motion possesses an intermode anharmonicity of about 20  $\text{cm}^{-1}$  between  $\nu'_{19}$  and  $\nu'_{12}$ .

#### 4.4.2 Second possibility

The lines 5, 9, 13b and 14b are assigned to a progression of the  $\nu'_{23}$ , C=O out-of-plane wagging. Line 5 at 333  $\text{cm}^{-1}$  is assigned to  $23^3$ , the upper tunnel-split level of the second dyade of the wagging mode. The quintet fine structure of the band with 3.2 GHz distance between the two strongest components implies that the two levels,  $23^2$  and  $23^3$  are almost degenerate (split by less than 1 GHz). The "coupled" transition to the  $23^2$  level, however, is actually not coupled by equation (4.7), because we deal here with the torsional ground state. We were not able to individuate an alternative coupling mechanism so far to explain the observed quintet (and therefore prefer the first possibility). For line 9, 13b and 14b the assignment becomes  $23^2 + 1_2$  at 484  $\text{cm}^{-1}$ ,  $23^3 + 2_1$  at 624  $\text{cm}^{-1}$  and  $23^3 + 2_3$  at 645  $\text{cm}^{-1}$ . In all cases, quintets are expected and are found for the first two in our preliminary analysis. The band at 621  $\text{cm}^{-1}$  (line 13a) is in this case assigned to a combination band of the C=O in plane wagging and the  $1_1$  torsion,  $19^1 + 1_1$ .

#### 4.5 Discussion

The high resolution spectra reported in this work led to the proposal of an effective barrier height for torsion of 759  $\text{cm}^{-1}$  in the  $S_1$  state. The torsional barrier is much larger than that in the ground state, and leads to a much smaller frequency difference between the torsional fundamentals. The calculated separation between the  $1_1$  and  $1_2$  levels is 18.4  $\text{cm}^{-1}$ , compared to 63  $\text{cm}^{-1}$  in the ground state. The high barrier may be related to the fact that the two rotors are somewhat closer to each other due to the bent configuration of the excited state. Internal rotational barriers are believed to reflect electronic densities in the bands adjacent to the rotor [29, 30]. The  $\pi^* \leftarrow n$  transition involves an increase in the electronic density of the C=O bond which could increase also the density in the C-C bond, making the bond stiffer and rising the barrier. These speculations should be checked by electronic density calculations.

The inversion barrier in the  $S_1$  state of 1348  $\text{cm}^{-1}$  is much larger than that of formaldehyde (350  $\text{cm}^{-1}$ ) and acetaldehyde (541  $\text{cm}^{-1}$ ), probably reflecting the increased stabilization of the pyramidal form upon exchange of a hydrogen atom by a methyl group.

Our analysis of the low energy torsional bands makes it compulsory to include an additional potential coupling term,  $V_{\text{coupl}}$ , into the Hamiltonian. Doing that we, nevertheless, interpret the spectra using the  $G_{36}$  molecular symmetry group for acetone in the  $S_1$  electronic state. Durig and co-workers developed a general theory for molecules with two internal rotors of  $C_{3v}$  symmetry and showed how it may be utilized for several different models [31, 32]. They recognized the difference of the torsional Hamiltonians between the models of  $C_{2v}$  and  $C_s$  molecules with two equivalent tops ( $C_{2v}(e)$  and  $C_s(e)$  in their notation) but also pointed out their formal identity. In particular, this difference manifested itself by inclusion of more potential terms into the Hamiltonian describing the torsional motion of a molecule having  $C_s$  ( $G_{18}$ ) symmetry. One of them, of  $A_1$  symmetry in  $G_{18}$ , is  $V''_{33} \sin(3\alpha_1 - 3\alpha_2)$ , compare to equation (4.7). Acetone in the ground  $S_0$  state corresponds to the  $C_{2v}(e)$  model. According to the classification of Durig *et al.*, in case the wagging tunnelling is frozen acetone in the excited  $S_1$  state should be treated within the  $C_s(e)$  model since it attains a pyramidal equilibrium geometry. That is, if we assume for a moment an infinite inversion barrier,

	S <sub>0</sub>	S <sub>1</sub>	
		first possibility	second possibility
$\nu_{12}$ torsion (anti-gearing)	77	155.5	155.5
$\nu_{24}$ torsion (gearing)	124	172.5	172.5
$\nu_8$ C-C-C bend	385	373	373
$\nu_{23}$ C=O out-of-plane wagging	484	-	333
$\nu_{19}$ C=O in-plane-wagging	530	177.5	465.4
wagging barrier	-	1350	1350
effective torsional barrier	270	759	759

Table 4.7: Barrier heights ( $\text{cm}^{-1}$ ) and low energy modes ( $\text{cm}^{-1}$ ) of acetone.

there are two equivalent potential minima corresponding to two bent (rigid) conformations of C, ( $G_{18}$ ) symmetry. These minima are distinguished by a simultaneous change of the signs of the two coordinates:  $q_w$  for the wagging and  $3\alpha_1 - 3\alpha_2$  for the gearing torsion. The term, equation (4.7), must be included in the torsional Hamiltonian. The  $C_s(e)$  model was applied to the analysis of the Raman spectra of dimethylamine where the tunnelling of the H-atom through the C-N-C plane was thought to be frozen [22]. If we lower now the inversion barrier the tunneling motion becomes feasible and the levels split. Performing a tunnelling through the barrier is equivalent to adding a new symmetry operation, *i.e.* reflection through the C-C-C plane, which is absent in the  $G_{18}$  symmetry group and belongs to the  $A_2$  irrep in  $G_{36}$ . The wavefunctions describing the wagging motion are written as symmetric and antisymmetric linear combinations of  $\Psi(+q_w)$  and  $\Psi(-q_w)$ . A feasible tunnelling through the inversion barrier rises the symmetry of the molecule and, in our case, allows to treat the internal rotation of acetone in the  $S_1$  state within  $G_{36}$ .

Thus, in our analysis we introduce a coupling between the C=O out-of-plane wagging ( $\nu'_{23}$ ) and torsional modes. The physical origin lies in the fact that for certain  $(\alpha_1, \alpha_2)$  configurations the inversion motion brings the molecule to a nonequivalent configuration if a simultaneous adjustment of  $(\alpha_1, \alpha_2)$  is not allowed. The proposed coupling term of equation (4.7) leaves the Hamiltonian invariant under the operations of the  $G_{36}$  symmetry group, being a product of two terms, both antisymmetric with respect to inversion through the C-C-C plane.

The fact that the transitions observed are *a*-type, as well as the observed splitting patterns led to some re-assignment of the vibrational bands observed in the excitation spectrum. Table 4.6 summarizes the situation. In contrast to reference [1] we assign the first band to the upper fine structure component of the tunnel split wagging motion. Thus, it is not necessary to invoke second order perturbation theory in order to account for intensity borrowing that makes the transition allowed. As in formaldehyde, this  $b_1$  type vibration mixes the  $\pi^*$  ( $A_2$ ) state with the  $\sigma^*$  ( $B_2$ ) state.

The occurrence of *b*-type transitions in the spectra cannot be entirely ruled out, since a full analysis is yet to be completed. *B*-type transitions are expected for vibrations having  $A_2(C_{2v})$  symmetry. However, up to line 7, at  $373 \text{ cm}^{-1}$ , all lines exhibit pure *a*-type rotational transitions.

The  $\pi^* \leftarrow n$  excitation leads to considerable changes in the frequencies of some low energy mode frequencies of acetone, see Table 4.7. Though, for the torsional-vibrational combination bands we prefer the "first possibility" of Table 4.7, the change  $\nu''_{19}=530 \text{ cm}^{-1} \rightarrow \nu'_{19}=177 \text{ cm}^{-1}$



is extremely large and should fill us with caution. Remember, however, that acetone changes its geometry for the transition  $S_1 \leftarrow S_0$  which permits relatively big changes of mode frequencies. In addition, for the related acetaldehyde molecule the corresponding shift is also very large,  $\nu''_{10}=509 \text{ cm}^{-1} \rightarrow \nu'_{10}=370 \text{ cm}^{-1}$  [33]. In conclusion, the first possible assignment is the favored but still tentative one.

### Acknowledgements

This work was financially supported by the Dutch organization for Fundamental Research of Matter (FOM).

## References

1. J.A. Pople and J.W. Sidman, *J. Chem. Phys.* **27**, 1270 (1957)
2. V.A. Job, V. Sethuraman and K.K. Innes, *J. mol. Spectrosc.* **30**, 365 (1969)
3. E.F. Worden, Jr., *Spectrochem. Acta*, **22**, 21 (1966)
4. D.J. Clouthier and D.A. Ramsey, *Ann. Rev. Phys. Chem.* **34**, 31 (1983)
5. M. Baba, I. Hanazaki and U. Nagashima, *J. Chem. Phys.* **82**, 3938 (1985)
6. H. Zuckermann, B. Schmitz and Y. Haas, *J. Chem. Phys.* **93**, 4083 (1989)
7. H. Zuckermann and Y. Haas, Unpublished
8. J.M. Berman and L. Goodman, *Chem. Phys. Lett.* **167**, 16 (1990)
9. P. Groner, G.A. Guirgis and J.R. Durig, *J. Chem. Phys.* **86**, 565 (1987)
10. T. Shimanouchi, "*Tables of Molecular Vibrational Frequencies*", NSRDS-NBS **39** (1987)
11. P. Cossee and J.H. Schachtschneider, *J. Chem. Phys.* **44**, 97 (1966)
12. W.C. Harris and I.W. Levin, *J. Mol. Spectrosc.* **43**, 117 (1972)
13. R. McDiarmid and A. Sabljic, *J. Chem. Phys.* **89**, 6086 (1988)
14. A.G. Ozkabak, J.G. Philis and L. Goodman, *J. Am. Chem. Soc.* **112**, 7854 (1990)  
Note that these authors use a different coordinate system than the one used in this paper.  
Their  $\nu''_{17}$  ( $b_2$ ) corresponds to our  $\nu''_{24}$  ( $b_1$ ).
15. J.D. Swalen and C.C. Costain, *J. Chem. Phys.* **31**, 1562 (1959)
16. R. Nelson and L. Pierce, *J. Mol. Spectrosc.* **18**, 344 (1965)
17. R. Peter and H. Dreizler, *Z. Naturforsch. A* **20**, 301 (1965)
18. J.M. Vacherand, B.P. Van Eijck, J. Burie and J. Demaison, *J. Mol. Spectrosc.* **118**, 355 (1986)
19. E. Cromwell, T. Trickle, Y.T. Lee and A.H. Kung, *Rev. Sci. Instrum.* **60**, 2888 (1989)
20. S. Gerstenkorn and P. Luc, "*Atlas du spectroscopie d'absorption de la molécule d'iode*", CNRS, Paris (1978)
21. C.C. Lin, J.D. Swalen, *Rev. Mod. Phys.* **31**, 841 (1959)
22. R. Engeln, J. Reuss, D. Consalvo, J.W.I. van Bladel and A. van der Avoird, *Chem. Phys. Lett.* **170**, 206 (1990)
23. P.R. Bunker, "*Molecular Symmetry and Spectroscopy*", Academic Press, New York (1979)
24. P.R. Bunker, in "*Vibrational Spectra and Structure, Vol. 3*", Ed. J.R. Durig, Marcel Dekker, New York (1975)

25. R.J. Myers and E.B Wilson, Jr., *J. Chem. Phys.* **33**, 186 (1960)
26. J.B. Coon, N.W. Naugle and R.D. McKenzie, *J. Mol. Spectrosc.* **20**, 107 (1966)
27. R. Engeln, J. Reuss, D. Consalvo, J.W.I. van Bladel, A.van der Avoird and V. Pavlov-Verevkin, *Chem. Phys.* **144**, 81 (1990)
28. C.H. Townes, A.L. Shawlow, *"Microwave Spectroscopy"*, McGraw-Hill, New York (1955)
29. X.Q. Tan, W.A. Majewski, D.F Plusquellic, D.W. Pratt, *J. Chem. Phys.* **94**, 7721 (1991)
30. X.Q. Tan, D.J. Clouthier, R.H. Judge, D.F Plusquellic, J.L. Tomer and D.W. Pratt, *J. Chem. Phys.* **95**, 7862 (1991)
31. P. Groner and J.R. Durig, *J. Chem. Phys.* **66**, 1855 (1977)
32. P.Groner, J.F. Sullivan and J.R Durig, in *"Vibrational Spectra and Structure, Vol. 9"*, Ed. J.R. Durig, Elsevier, Amsterdam (1981)
33. M. Noble, E.K.C. Lee, *J. Chem. Phys.* **81**, 1632 (1984)

### High Resolution Laser-Induced Fluorescence Study Of A Cage Molecule, 1,4-Diazabicyclo[2,2,2]octane, DABCO.

*D. Consalvo, M. Drabbels, G. Berden, W. L. Meerts, D.H. Parker and J. Reuss  
Department of Molecular and Laser Physics, University of Nijmegen,  
Toernooiveld, 6525 ED Nijmegen, The Netherlands*

#### Abstract

Rotationally resolved laser-induced fluorescence spectra of the caged amine 1,4-diazabicyclo[2,2,2]-octane, DABCO, are recorded using a Fourier limited pulsed dye laser system. Both one-photon and two-photon spectra of the  $S_1(A'_1) \leftarrow S_0(A'_1)$  transition are measured. In the one-photon spectra not only vibrationally induced electric dipole transitions to  $a''_2$  and  $e'$  vibrational levels are observed, but also electric quadrupole transitions to the  $S_1$  origin and to  $a'_1$  vibrational levels. For the first time the rotational structure of the electronic transitions has been resolved. Rotational constants are extracted from both the two-photon and one-photon spectra. Despite the presence of long progressions of several vibrational modes for the  $S_1(A'_1) \leftarrow S_0(A'_1)$  transition, the difference in  $S_0$  and  $S_1$  rotational constants are remarkably small, suggesting that compensating geometry changes take place upon excitation to  $S_1$ .

## 5.1 Introduction

In the past much effort has been devoted to the investigation of the vibrational structure of the 1,4-diazabicyclo[2,2,2]octane molecule, DABCO, a highly symmetric amine which belongs to the molecular point group  $D_{3h}$  [1, 2]. No high resolution excitation spectra of the  $S_1 \leftarrow S_0$  transition have been reported up to now which could clarify ambiguous assignments and/or confirm previous findings based upon low resolution electronic spectra [1, 2]. In the present work high resolution laser-induced fluorescence (LIF) spectroscopy is applied to study the vibrational and rotational structure of the DABCO molecule. From the observed rotational structure conclusions can be drawn with respect to the symmetry of the vibrational levels involved. In addition information concerning the change in geometrical structure upon electronic excitation is obtained.

The electronic structure and the orbital ordering have been investigated previously [3, 4, 5]. All of the electronically excited states of DABCO are Rydberg states in nature, with  $S_1(A'_1)$  (3s) at  $35\,783\text{ cm}^{-1}$  and  $S_2(E')$  ( $3p_{xy}$ ) at  $39\,814\text{ cm}^{-1}$ . Transitions from the totally symmetric electronic ground state,  $S_0$ , to the first electronically excited state,  $S_1$ , are one-photon forbidden for electric dipole transitions but two-photon allowed. The forbidden one-photon transition becomes partially allowed through an admixture of the nearby lying  $S_2$  state, of  $E'$ -symmetry, and a yet unidentified state of  $A''_2$ -symmetry, to the  $S_1$  state. Due to the high spectral brightness of the laser system used the one-photon allowed electric quadrupole transitions can be also observed. Therefore both one- and two-photon spectroscopy are useful to gain insight into the symmetry of different vibrational states.

## 5.2 Experimental

A molecular beam is formed by expanding DABCO, vapor pressure 0.4 Torr, seeded in 1.5 atm He or  $N_2$  through a pulsed valve with an orifice of 1 mm diameter. An unfocussed laser beam, 5 mm diameter, crosses the molecular beam perpendicularly 40 mm downstream of the nozzle and induces, via one- or two-photon absorption, the  $S_1 \leftarrow S_0$  transition in DABCO.

To rotationally resolve the LIF excitation spectrum of DABCO a laser source with high peak power and narrow bandwidth is used. Narrow bandwidth radiation of a cw ring dye laser (Spectra Physics 380D) operating on Rhodamine 110 dye is amplified by a pulsed dye amplifier (PDA) system operating on Fluorescein 27 dye. The PDA system is pumped by a frequency doubled Q-switched Nd:YAG laser (Quantel YG 681C-10). In this way radiation with a pulse energy of 100 mJ and a bandwidth of 135 MHz is obtained. For one-photon experiments this radiation is frequency doubled in a KDP crystal yielding 20 mJ of tunable UV light. For absolute frequency calibration the  $I_2$  absorption spectrum is recorded simultaneously with the excitation spectrum [6]. For relative frequency calibration the transmission peaks of a temperature and pressure stabilized interferometer with a free spectral range of 299.41 MHz are recorded.

The fluorescence is collected by a quartz lens system and imaged onto a photomultiplier. In order to reduce the scattered light in the two-photon experiments a Schott UG 11 glass filter is placed in front of the photomultiplier. The signals are processed by a digital oscilloscope (LeCroy 7400) and a boxcar averager (SRS 250) interfaced with a Personal Computer. The linewidth observed in the experiments is almost completely determined by the residual Doppler broadening in the molecular beam and amounts to 400 MHz and 700 MHz for  $N_2$  and He as seeding gas, respectively. The rotational temperature is found to be 1 K for He and 7 K for  $N_2$ . When argon is used as seeding gas no LIF spectra of DABCO could be observed, probably due to massive cluster formation [7].

### 5.3 Theoretical aspects

Transitions to the first electronically excited state of DABCO can be induced by one- and two-photon processes obeying different selection rules [8]. An overview is given in Table 5.1 where the possible transitions from the totally symmetric ground state to the  $S_1$  state are summarized according to the multiplication rules of  $D_{3h}$ . By one-photon excitation only levels of  $e'$  and  $a_1''$  symmetry can be probed, whereas by two-photon excitation only final states of  $a_1'$  symmetry can be probed. In case of an electric quadrupole transition the two-photon selection rules hold.

The study of Bruesch [4] on solid state DABCO has shown that DABCO is a prolate symmetric top in the electronic ground state. The excitation energy for a parallel ( $\Delta K=0$ ) transition, i.e. from a non-degenerate level in the ground state to a non-degenerate level in the electronically excited state, is for a prolate symmetric top given by [9].

$$\Delta E = \nu_0 + B'J'(J' + 1) - B''J''(J'' + 1) + [(A' - B') - (A'' - B'')]K^2 \quad (5.1)$$

Here  $J'', K, A'', B''$  and  $J', A', K'$  are the rotational quantum numbers and rotational constants for the ground state and the electronically excited state, respectively. For the electric dipole transitions the selection rule  $\Delta J=0, \pm 1$  holds, whereas for the electric quadrupole and two-photon transitions the selection rule  $\Delta J=0, \pm 1, \pm 2$  holds. The excitation energy for a perpendicular ( $\Delta K=\pm 1$ ) transition i.e. from a non-degenerate level in the ground state to a degenerate level in the excited state, is given by [9]:

$$\Delta E = \nu_0 + B'J'(J' + 1) - B''J''(J'' + 1) + [A'(1 - 2\zeta) - B'] \pm 2[A'(1 - \zeta) - B']K + [(A' - B') - (A'' - B'')]K^2 \quad (5.2)$$

Here the upper (lower) sign has to be taken for  $\Delta K=+1$  ( $-1$ ) transitions. Since the transition takes place to a degenerate level Coriolis coupling ( $\zeta$ ) has been included in the expression for the excitation energy. The  $l$ -doubling is neglected here because in the measured spectra no irregularities for the  $K'=1$  levels have been found which normally are taken as evidence of  $l$ -doubling [9].

Not all the molecular constants given in the expressions above can be determined from the observed spectra. For a parallel transition only the molecular constants  $\nu_0, B'', \Delta B = B' - B''$  and  $\Delta A = A' - A''$  can be determined. For a perpendicular transition in principle all the molecular constants can be obtained from the observed spectrum. However, if there is a Coriolis coupling present in the excited state only the molecular constants  $B'', \Delta B$  and  $\Delta A$  and the effective constants  $A'(1 - \zeta)$  and  $\nu_0 + A(1 - \zeta) + B''$  can be determined.

Type of transition		Vibrational	Rotational	
1 $h\nu$	electric dipole	$e' \leftarrow a_1'$	$\Delta J = 0, \pm 1$	$\Delta K = \pm 1$
	electric dipole	$a_2'' \leftarrow a_1'$	$\Delta J = 0, \pm 1$	$\Delta K = 0$
	electric quadrupole	$a_1'' \leftarrow a_1'$	$\Delta J = 0, \pm 1, \pm 2$	$\Delta K = 0$
2 $h\nu$	2*electric dipole	$a_1' \leftarrow a_1'$	$\Delta J = 0, \pm 1, \pm 2$	$\Delta K = 0$

**Table 5.1:** Vibrational and rotational selection rules for different type of  $S_1 \leftarrow S_0$  transitions starting from the vibrational ground state in DABCO.

The intensity of an individual rotational transition in the excitation spectrum is proportional to:

$$I \propto g_{KJ} A_{KJ} e^{-E_{rot}/kT} \quad (5.3)$$

Here  $g_{KJ}$  is the spin statistical weight, which in the case of DABCO is almost equal for all rotational levels,  $E_{rot}$  is the rotational energy,  $k$  the Boltzmann constant and  $T$  the rotational temperature. For electric dipole transitions the term  $A_{KJ}$  equals the well-known Hönl-London factor [9]. For a two-photon transition the term  $A_{KJ}$  has been evaluated by Chen and Yeung [8]. It was shown that for  $\Delta J = \Delta K = 0$  transitions  $A_{KJ}$  is given by the sum of two terms. One of these terms is only present for  $\Delta J = 0$  transitions and can give rise to extra intensity for  $\Delta J = 0$  transitions with respect to  $\Delta J \neq 0$  transitions. For electric quadrupole transitions the term  $A_{KJ}$  is equal to that of two-photon transitions except for the  $\Delta J = 0$  transitions. For quadrupole transitions the extra term giving rise to a strong Q-branch in two-photon transitions is missing.

Next we want to discuss the shift of the band origin arising from isotopic substitution. For the  $0_0^0$  band this shift represents the cumulative zero-point effect of isotopic replacement on the 36 vibrational modes. For each mode the amplitude of the motion changes upon isotopic substitution;

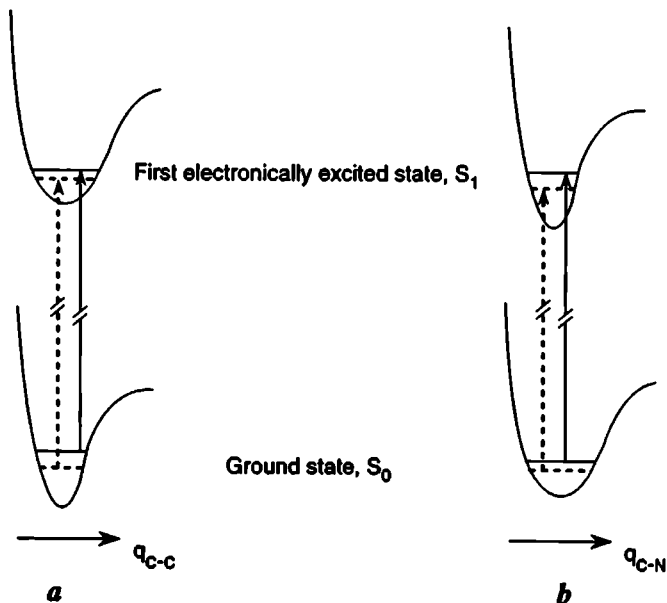


**Figure 5.1:** A qualitative potential for a dominant C–C stretching mode is shown in a). The potential well in the  $S_1$  state is more shallow, in agreement with previous observations [1, 2]. The full line correspond to DABCO with six  $^{12}\text{C}$ -atoms, the dashed one to the molecule with one  $^{12}\text{C}$  atom substituted by a  $^{13}\text{C}$ . The resulting isotopic shift is to the blue (vertical dashed line) with respect to the most abundant isotopomer. The situation depicted in b), corresponding to a potential for a dominant C–N stretch, is reversed with respect to case a). Therefore a red shift results from a  $^{15}\text{N}$  substitution.

moreover the motion itself will be modified by symmetry breaking. Both these two effect give rise to a shift in energy upon isotopic substitution. For illustration we restrict the discussion to a situation where either the  $q_{C-C}$  or  $q_{C-N}$  stretch dominates. Upon electronic excitation a softening of the C-C stretch and a stiffening of the C-N stretch has been observed [2, 10]. The situation is depicted in Figure 5.1a and 5.1b respectively. The vertical dashed lines represent transitions for a molecule where one of the  $^{12}\text{C}$  (or  $^{14}\text{N}$ ) is replaced by the heavier isotope. It's clear from this figure that in case a) the result will be a blue shift and in case b) a red shift.

In case a single vibrational mode is excited an isotopic shift with respect to the zero-point isotopic shift results characteristic for that specific vibrational mode.

## 5.4 Analysis

In Table 5.2 the measured rovibronic transitions and their assignments are reported. The band origins are listed with respect to the  $0_0^0$  transition and the type of transition is indicated.

Figure 5.2 displays the experimental result for the  $0_0^0$  band. The two-photon  $0_0^0$  spectrum is displayed in Figure 5.2a whereas the the  $0_0^0$  quadrupole transition is shown in Figure 5.2b. The most intense feature in the two-photon spectrum represents the unresolved Q-branch. The strong intensity of this band with respect to other transitions has been discussed in section 5.3. The low rotational temperature of 1 K allows the observation of rotational levels up to  $J=5$ . The observed intensity alternation in both the one- and two-photon spectrum is due to an overlap of  $\Delta J = \pm 2$  with every second  $\Delta J = \pm 1$  transition. From the rotational structure the molecular constants  $B''$ ,  $\Delta B$  and  $\nu_0$  are derived, see Table 5.3. The value for  $\Delta A$  can not be determined because the  $K$ -structure for a single  $J$ -level is not resolved with the present resolution of 700 MHz. Since no broadening of the transitions to high rotational levels is observed a maximum value of 5 MHz can be estimated for  $\Delta A$ .

In the two-photon spectrum, Figure 5.2a, the Q-branches of two different isotopomers are visible. The Q-branch shifted by  $2.535\text{ cm}^{-1}$  and with an intensity of 6.6% is attributed to the

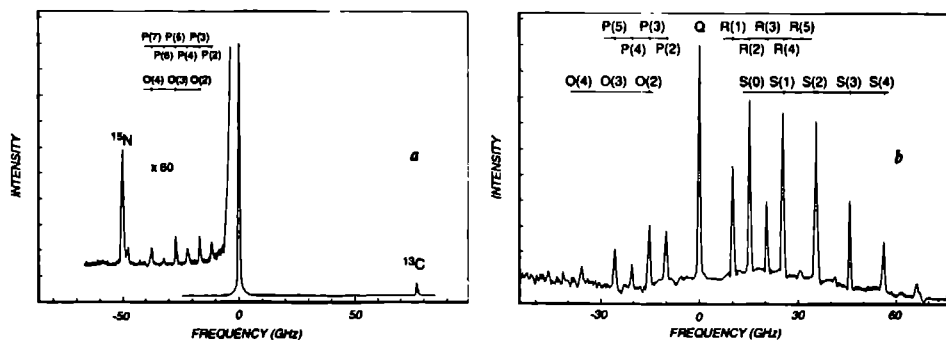


Figure 5.2: a) Two-photon LIF spectrum of the  $0_0^0$  transition. The two weak blue and red shifted Q-branches are due to different isotopomers. b) One-photon LIF spectrum of the electric quadrupole  $0_0^0$  transition.



Frequency	1-phot.	2-phot.	Symm.	Assign.	Remarks
0	Q		$a'_1$	$0_0^0$	$\Delta^{15}\text{N}=-1.571$ , $\Delta^{13}\text{C}=+2.535$ <sup>a)</sup> , Fig. 5.2
203.762	?		$?+a'_1$	$13_0^0$	one-photon weak and structureless
205.56	?	-	?	?	weak and structureless
449.113	$\perp$	-	$e'$	$27_0^1$	Fig. 5.3a
670.844	-		$a'_1$	$6_0^1$	$\Delta^{15}\text{N}=-1.632$ , $\Delta^{13}\text{C}=-1.489$
671.479		-	$a''_2$	$27_0^1+36_0^1$	weak
689.506		-	$a''_2$	$18_0^1$	hot band, see Table 5.3
691.152	-		$a'_1$	$36_0^0$	weak
777.605	Q		$a'_1$	$5_0^1$	
825.162	$\perp$	-	$e'$	$26_0^1$	Fig. 5.3b
882.189	Q		$a'_1$	$4_0^1$	
883.080		-	$a''_2$	$9_0^1+13_0^1$	weak
897.391	$\perp$		$e'+a'_1$	$27_0^2$	two-photon weak
900.51	$\perp$	-	$e'$	$25_0^1$	weak
901.070	-		$a'_1$	$35_0^1+36_0^1$	
919.467		-	$a''_2$	$17_0^1$	$\Delta^{15}\text{N}=-0.945$ , $\Delta^{13}\text{C}=-1.891$ , Fig. 5.4
1011.267	$\perp$	-	$e'$	$24_0^1$	

<sup>a)</sup> Two additional isotopomers are observed shifted by  $\Delta(^{13}\text{C}^{15}\text{N})=+1.605$   $\text{cm}^{-1}$  and  $\Delta(^{13}\text{C})^2=+1.893$   $\text{cm}^{-1}$ .

**Table 5.2:** Observed rovibronic  $S_1 \leftarrow S_0$  transitions in DABCO. Rotationally resolved parallel and perpendicular transitions are indicated by || and  $\perp$ , respectively. Quadrupole transitions are labelled by Q. The band origins ( $\text{cm}^{-1}$ ) are given with respect to the  $0_0^0$  transition at  $35\,783.234$   $\text{cm}^{-1}$ . Isotope shifts ( $\text{cm}^{-1}$ ) are indicated by  $\Delta^{13}\text{C}$  and  $\Delta^{15}\text{N}$ . The error in the observed frequencies is  $0.005$   $\text{cm}^{-1}$ .

$^{13}\text{C}$  isotopomer. The other one shifted by  $-1.571$   $\text{cm}^{-1}$  and with an intensity of 0.8% is due to the  $^{15}\text{N}$  isotopomer. In addition to these Q-branches also two very weak Q-branches are observed shifted by  $1.605$   $\text{cm}^{-1}$  and  $1.893$   $\text{cm}^{-1}$  and with intensities of 0.06% and 0.18%, respectively. The weakest of the two can be assigned to the  $^{13}\text{C}^{15}\text{N}$  isotopomer whereas the other can be assigned to the isotopomer with two  $^{12}\text{C}$ -atoms replaced by  $^{13}\text{C}$  atoms. The shift of the isotopomers band origins point to a softening (stiffening) of the C-C (C-N) stretch upon electronic excitation, as discussed in section 5.3.

In Table 5.2 three two-photon transitions to fundamentals of  $a'_1$  symmetry can be found, the  $6_0^1$  band at  $671$   $\text{cm}^{-1}$ ,  $5_0^1$  band at  $778$   $\text{cm}^{-1}$  and the  $4_0^1$  band at  $882$   $\text{cm}^{-1}$ . The latter two are also observed as one-photon quadrupole transitions. These assignments are new for what concerns the  $5_0^1$  and  $6_0^1$  bands, and are based on the assumption that the order of increasing vibrational energy does not change upon electronic excitation, taking the  $4_0^1$  band as listed in reference [1, 2].

In addition four two-photon transitions are listed which are assigned to overtone and combi-

	$0_0^0$	$9_0^1 13_1^0$	$26_0^1$	$27_0^1$
$B''$	2 509.8(2.8)	2 464.5(5.8)	2 509.8(2.8)	2 509.8(2.8)
$\Delta B$	0.6(0.6)	1.4(0.6)	0.2(2.6)	0.3(2.9)
$\Delta A$	<5	<5	12.7(1.1)	17.6(0.7)
$A'(1-\zeta)$	-	-	3 065.9(1.3)	4 030.7(1.2)
$\nu_0$	0	689.506	825.162	449.113

**Table 5.3:** Molecular constants (MHz) of some of the observed transitions. The band origins ( $\text{cm}^{-1}$ ) are given with respect to the  $0_0^0$  transition at  $35\,783.234\text{ cm}^{-1}$ . The error in the reported values is  $0.005\text{ cm}^{-1}$ . For the perpendicular transitions,  $26_0^1$  and  $28_0^1$ , the effective band origins are given.

nation bands of  $a_1'$ -symmetry. Their assignments are rather uncertain, especially if they are close in energy, like the bands at  $897\text{ cm}^{-1}$  and  $901\text{ cm}^{-1}$ .

Four one-photon transitions to excited fundamentals of  $e'$ -symmetry are observed, the  $27_0^1$  band at  $449\text{ cm}^{-1}$ , the  $26_0^1$  band at  $825\text{ cm}^{-1}$ , the  $25_0^1$  band at  $900.5\text{ cm}^{-1}$  and the  $24_0^1$  band at  $1\,011\text{ cm}^{-1}$ . Except for the  $25_0^1$  band, these assignments are in agreement with previous ones [1, 2]. If one compares the two perpendicular bands,  $27_0^1$  (Figure 5.3a) and  $26_0^1$  (Figure 5.3b) one notices that the rotational structure of the two bands looks very dissimilar. In the figure three lines are indicated which have the same rotational assignment. Since one deals with transitions taking place between a non-degenerate ground state level and a degenerate level in the excited state the Coriolis coupling has to be taken into account. Based on the fit of the experimental data it is concluded that the Coriolis coupling  $\zeta$  undergoes a 30% variation, see Table 5.3, resulting in two spectra with

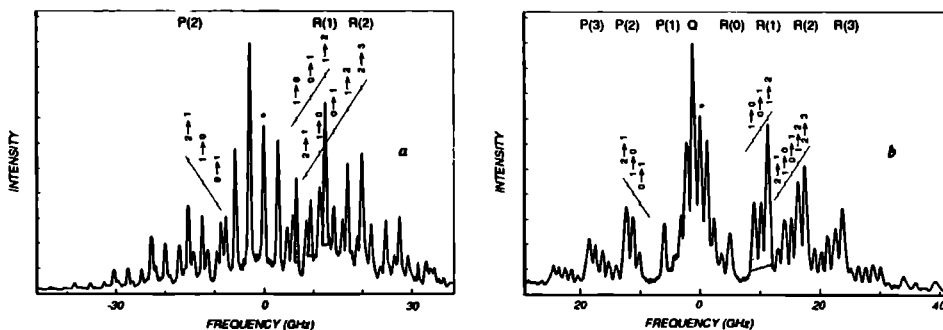


**Figure 5.3:** a) Excitation spectrum of the one-photon  $27_0^1$  transition b) Excitation spectrum of the one-photon  $26_0^1$  transition. The starred lines are assigned as a  $\Delta J=0$ ,  $K=1\leftarrow 0$  transitions. The gray shaded lines correspond to  $J=2\leftarrow 1$  with, from left to right,  $K=0\leftarrow 1$ ,  $K=1\leftarrow 0$ ,  $K=2\leftarrow 1$ .

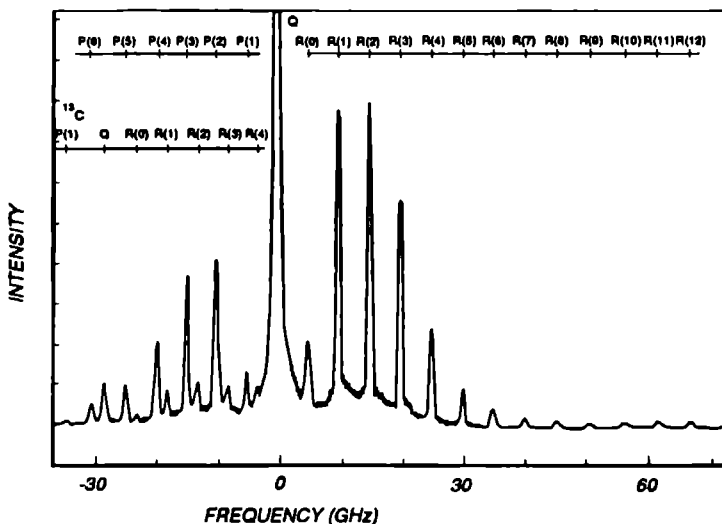


Figure 5.4: Excitation spectrum of the  $17_0^1$  one-photon parallel transition. Note the assigned transitions of the  $^{13}\text{C}$  isotopomer.

completely different rotational structures.

For a twofold excited vibration of  $e'$  or  $e''$  symmetry the resulting levels have two possible symmetries,  $a_1'$  and  $e'$ . Therefore, both one- and two-photon spectra contain correlated information: the level of  $a_1'$  symmetry can be reached by two-photon and the  $e'$  component by one-photon excitation. The relative energies are slightly different, in general. In Table 5.2 we encounter an example for such a behavior. The band at  $897\text{ cm}^{-1}$ ,  $27_0^2$ , behaves regularly having a parallel two-photon spectrum and a perpendicular one-photon spectrum. The two origins are shifted by less than our accuracy of  $0.005\text{ cm}^{-1}$ .

The observation of parallel transitions, i.e. observation of transitions to fundamental vibrations of  $a_2''$  symmetry, see Figure 5.4, makes it necessary to reassign the bands at  $690\text{ cm}^{-1}$  and  $919\text{ cm}^{-1}$ . The band at  $919\text{ cm}^{-1}$ , which was previously assigned as  $25_0^1$  is now assigned as  $17_0^1$ . The band at  $690\text{ cm}^{-1}$  has to be assigned to a hot band transition since the  $B''$  rotational constant found for this band differs by about 40 MHz from the value found for the other bands, see Table 5.3. We suggest that it involves the lowest energy mode,  $\nu_{13}'$ . A possible combination band with final  $a_2''$  symmetry is  $9_0^1 13_0^0$ , yielding a value for  $\nu_9'$  of about  $750\text{ cm}^{-1}$ . In addition there are two weak parallel one-photon transitions observed at  $671\text{ cm}^{-1}$  and  $883\text{ cm}^{-1}$ . The suggested assignment of these bands is given in Table 5.2.

The two bands at  $204\text{ cm}^{-1}$  and  $206\text{ cm}^{-1}$  are difficult to assign. We propose for the two-photon transition at  $204\text{ cm}^{-1}$  the torsional overtone  $13_0^2$ . The one-photon transitions remain unexplained so far.

## 5.5 Discussion

In the analysis of the low resolution excitation spectra of DABCO it was assumed that the one-photon transitions become allowed by an admixture of the  $S_2(E')$  state to the  $S_1(A'_1)$  state [1, 2]. As a result only vibrational levels in the electronically excited state of  $e'$  symmetry should be observable in the one-photon excitation spectrum. The observation of parallel one-photon transitions in the present high resolution study on DABCO, *i.e.* transitions to states of  $a''_2$  symmetry, leads to the question of position and identity of the electronic state of  $A''_2$  electronic symmetry, by which these transitions become allowed.

There are two approaches in the literature to the electronically excited states of DABCO. Most often [11, 12, 13] the symmetric and antisymmetric combination of the lone pair orbitals in the ground state  $n(+)$  and  $n(-)$  is simply extended to the excited state Rydberg orbitals, yielding for  $n=3$  the  $3s(+)(A'_1)$ ,  $3s(-)(A''_2)$ ,  $3p_{xy}(+)(E')$ ,  $3p_{xy}(-)(E'')$ ,  $3p_z(+)(A'_1)$  and  $3p_z(-)(A''_2)$  excited states. As pointed out by Robin [14], however, this always yields more excited state orbitals than can be accounted for spectroscopically. These observations are based on a wide series of "double" molecules, especially the diones. Robin suggests that Rydberg states even of double (two identical chromophore) molecules should be molecule-centered, yielding for DABCO only the  $3s(A'_1)$ ,  $3p_{xy}(E')$ ,  $3p_z(A''_2)$   $n=3$  states. This single center approach appears to be nicely confirmed in DABCO (diazabicyclo[3,3,3]undecane) [5], the next larger caged amine, where transitions from  $n(-) \rightarrow 3s$ ,  $3p_{xy}$  and  $3p_z$  are assigned by comparing the one- and two-photon spectra.

The  $3s$  and  $3p_{xy}$  states of DABCO have been assigned as  $S_1(A'_1)$  at  $35\,783\text{ cm}^{-1}$  and  $S_2(E')$  at  $39\,814\text{ cm}^{-1}$ , respectively. Thus far there is no direct evidence for the  $3p_z$  state which, by analogy with  $\text{NH}_3$  [15] and ABCO [16], and by *ab initio* MO theory [11], is expected to lie slightly higher than the  $3p_{xy}$  state. Ito and co-workers [1] have observed only three optically active Rydberg series in DABCO with quantum defects  $\delta=0.05$ ,  $\delta=0.19$  and  $\delta=0.45$  which can be assigned to  $d$ ,  $p_z$  and  $p_{xy}$ , respectively [14]. The  $p_z$  series is extrapolated to have its lowest ( $n=3$ ) component, lying  $2\,000\text{ cm}^{-1}$  higher than the  $3p_{xy}$  component. Avouris and Rossi [11] calculated that the oscillator strength for  $3p_z$  is lower than for the  $3p_{xy}$  for the corresponding states in ABCO. Based on these qualitative facts we suggest that the electronic state responsible for the  $a''_2$  vibrational coupling in DABCO is the  $3p_z$  component which underlies stronger and unresolved vibrational bands of the  $3p_{xy}$  transition.

The long progression seen for the  $\nu'_5$  and  $\nu'_3$  vibrational modes in the  $S_1 \leftarrow S_0$  transition indicates that geometry changes take place. On excitation to the ion-like ( $3s$ )  $S_1$  Rydberg state electron density is seen to move out of the C-C bonds and into the C-N (and N-N) bonds, just as predicted by Heilbronner and Muskat [17] for  $n(+)$   $\rightarrow$  ion transitions. Overall, these changes have little effect on the rotational constants,  $\Delta A \approx 0$  and  $\Delta B \approx 0$ , suggesting that the C-N-C angle opens up enough to compensate for longer C-C distances, yielding almost the same rotational constants for  $S_1$  as for  $S_0$ .

From the isotope shifts measured for the  $0_0^0$  band the tightening of C-N bonds and weakening of C-C bonds is confirmed by the blue shift of the  $^{13}\text{C}$  isotope and red shift of the  $^{15}\text{N}$  isotope. The observed isotope shifts in the two excited vibrational levels,  $\nu'_6$  and  $\nu'_{17}$ , are in the order of  $4\text{ cm}^{-1}$  with respect to the shift of the vibrational ground state for  $^{13}\text{C}$  substitution, see Table 5.2. For  $^{15}\text{N}$  substitution the observed shifts are much smaller. A cautious conclusion may be that for both fundamentals,  $\nu'_6$  and  $\nu'_{17}$ , the C-N stretch motion is important, with little displacement of the N-atoms.

### 5.6 Conclusion

Analysis of rotational structure of electronic transitions is well-known to yield a wealth of information on molecular properties, particularly on vibrational mode symmetry and molecular geometry. It is shown in this paper that this is also possible for a 20-atom molecule such as DABCO, provided a sufficiently low rotational temperature and a narrow laser bandwidth. The observation of parallel transitions, *i.e.* transitions to states of  $a_2''$  symmetry indicates that coupling through an  $A_2''$  electronic state, possibly the unassigned  $3p_z$  Rydberg state is also significant in DABCO.

### Acknowledgements

This research has been financially supported by the Dutch Foundation for Fundamental Research of Materials (FOM).

## References

1. N. Gonohe, N. Yatsuda, N. Mikami and M. Ito, Bull. Chem. Soc. Japan **55**, 2796 (1982)
2. D. Consalvo, J. Oomens, D.H. Parker and J. Reuss, Chem. Phys. **163**, 223 (1992)
3. P. Bishof, J.A. Hashmal, E. Heilbronner and V. Hornung, Tetrahedron Lett. **46**,4025 (1969)
4. P. Bruesch, Spectrochimica Acta **22**, 861 (1966)
5. K. Ray, M.A. Quesada, D.H. Parker, J. Phys. Chem. **92**, 5436 (1988)
6. S. Gerstenkorn and P. Luc, "*Atlas du spectroscopie d'absorption de la molecule d'iode*", CNRS, Paris (1978)
7. G. van den Hoek, D. Consalvo, D.H. Parker and J. Reuss, Z. Phys. D **27**, 73 (1993)
8. K.M. Chen and E.S. Yeung, J. Chem. Phys. **69**, 43 (1978)
9. G. Herzberg, "*Molecular Spectra and Molecular Structure, Volume III*", Van Nostrand Reinhold Company, New York (1966)
10. D. Consalvo, D.H. Parker and J. Reuss, Chem. Phys. **165**, 397 (1992)
11. P. Avouris and A.R. Rossi, J. Phys. Chem. **85**, 2340 (1981)
12. M.A. Smith, J.W. Hager and S.C. Wallace, J. Phys. Chem. **88**, 2250 (1984)
13. G.J. Fisanick, T.S. Eichelberger, M.B. Robin and N.A. Kuebler, J. Phys. Chem. **87**, 2240 (1983)
14. M.B. Robin, "*Higher Excited States of Polyatomic Molecules, Vol. I,II*", Academic Press, New York, (1974)  
M.B. Robin, "*Higher Excited States of Polyatomic Molecules, Vol. III*", Academic Press, New York, (1985)
15. J.H. Glowia, S.J. Riley, S.D. Colson and G.C. Nieman, J. Chem. Phys. **73**, 4296 (1980)
16. A.M. Weber A. Acharya and D.H. Parker, J. Phys. Chem. **88**, 6087 (1984)
17. E. Heilbronner and K.A. Muskat, J. Am. Chem. Soc. **92**, 3818 (1970)



### Production Of An Intense Pulsed Beam Of Oriented Metastable CO a $^3\Pi$

*M. Drabbels*

*Department of Molecular and Laser Physics, University of Nijmegen,  
Toernooiveld, 6525 ED Nijmegen, The Netherlands*

*S. Stolte and G. Meijer*

*Laser Center, Free University,  
De Boelelaan 1083, 1081 HV Amsterdam, The Netherlands*

#### **Abstract**

Carbon monoxide molecules in a supersonic molecular beam are resonantly excited from the  $X\ ^1\Sigma^+(v'' = 0)$  ground state to the  $a\ ^3\Pi(v' = 0)$  metastable state using pulsed laser radiation at 206 nm. In the excitation region a static electric field is applied to split individual  $M$ -components of a given rotational line of this electronic transition. The splitting can be made larger than the Fourier limited bandwidth of the pulsed radiation source and specific  $M$ -levels in the  $a\ ^3\Pi$  state can be populated. Peak fluxes of  $10^{17}$  ( $10^{15}$ ) oriented CO  $a\ ^3\Pi_1, v'=0, J'=1, M'=1$  ( $a\ ^3\Pi_2, v'=0, J'=2, M'=2$ ) molecules per second are obtained.



## 6.1 Introduction

For many years there has been a great interest in producing molecular beams of oriented molecules for the study of steric effects in reactive molecular scattering and orientation effects in molecule-surface interactions [1, 2]. Two main techniques are used for the production of these beams. In the first technique electric hexapole fields are used to focus molecules in a specific  $|JKM\rangle$  level, while molecules in other  $|JKM\rangle$  levels are blocked or deflected out of the beam [3, 4]. Here  $J$  is the total rotational angular momentum with projections  $K$  and  $M$  on the molecular symmetry axis and on the laboratory fixed direction of the electric field, respectively. This technique is only applicable to effective symmetric top molecules which have a first-order Stark effect and it requires a relatively large molecular beam apparatus. In the second method, called the brute force technique, high static electric fields are used to physically twist polar molecules in low  $J$ -states into orientation. Very cold beams of highly polar molecules with small rotational constants are needed. This latter technique has recently been developed by Loesch and Remscheid [5] in Bielefeld and, independently, by Friedrich and Herschbach [6] in Harvard and can be used even for diatomic  $\Sigma$  state molecules possessing an electric dipole moment. A disadvantage of the latter technique is, however, that the average orientation that can be obtained is relatively small.

Here we describe a technique for the production of an intense pulsed beam of fully state-selected and oriented electronically excited molecules. A pulsed laser with a Fourier limited bandwidth is used to induce an electronic transition to a metastable state that has a largely different Stark splitting from the electronic ground state. In a static electric field the individual  $M$ -components of a specific  $J' \leftarrow J''$  transition are split far enough apart that a single  $|J', K', M'\rangle$  level in the metastable state can be populated with a pulsed laser. This technique has the simplicity of the brute force method, but no brute-force field strengths are required.

It should be noted that vibrationally excited molecules have been produced in a similar way [7, 8, 9]. Because the dipole moment of the vibrationally excited state and the vibrationless state are usually very similar, higher electric fields are needed to sufficiently split the  $M$ -components. Narrow bandwidth cw lasers are then used to populate specific  $|J', K', M'\rangle$  levels in the vibrationally excited state. Sufficient excitation efficiency is only obtained when the Stark transition of the molecule under investigation can be tuned into resonance with an intense fixed frequency IR laser.

## 6.2 Method of production

A pulsed beam of oriented CO (a  $^3\Pi$ ) is produced by pumping jet-cooled CO via the spin-forbidden a  $^3\Pi(v' = 0) \leftarrow X^1\Sigma^+(v'' = 0)$  transition (Cameron band) at 206 nm. The  $^1\Sigma^+$  electronic ground state of CO has no first-order Stark effect and with a relatively small electric dipole moment of 0.10 D the splitting of the various  $M$ -levels is of the order of a MHz in electric fields of up to 4 kV/cm. The lowest energy electronically excited state of CO is the metastable a  $^3\Pi$  state which *does* show a first-order Stark effect. The a  $^3\Pi$  state of CO has an electric dipole moment of 1.37 D, enough to cause  $M$ -level splittings of several GHz in the aforementioned fields [10]. Individual  $M$ -components of rotational lines of the spin-forbidden a  $^3\Pi(v' = 0) \leftarrow X^1\Sigma^+(v'' = 0)$  transition will therefore be separated by several GHz in easily obtainable electric fields. Fully state-selected and oriented metastable CO molecules can then be produced by excitation on a single  $M$ -component in the CO Cameron band. A radiation source with a high spectral brightness is required for an efficient excitation of  $M$ -component resolved rotational lines in the weak Cameron transition. The

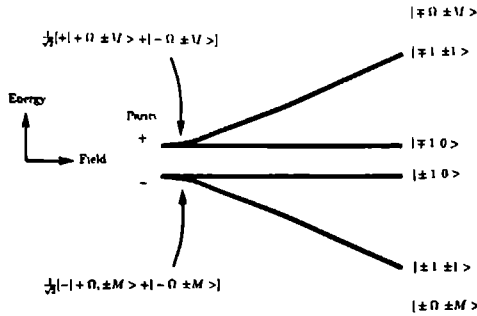


**Figure 6.1:** Schematic view of the Stark splitting for the  $J'=1$  level in a  $^3\Pi_1(v'=0)$  as a function of the applied electric field.

spin-forbidden  $^3\Pi \leftarrow X^1\Sigma^+$  transition becomes weakly allowed because the  $A^1\Pi$  state interacts with the  $a^3\Pi$  state. This interaction gives oscillator strength to transitions to the  $a^3\Pi_1$  multiplet only. For low  $J$ -values the  $a^3\Pi_1$  multiplet can therefore be reached much more easily than the other multiplets. The individual rotational levels in the  $a^3\Pi(v'=0)$  state of CO have radiative lifetimes of several ms [11], long enough to perform molecular beam experiments. An advantage of using CO is that neither the C-atom nor the O-atom have a nuclear spin which would couple to the total angular momentum and destroy the orientation of the molecules at low electric fields.

The  $a^3\Pi$  state of CO is best described as an intermediate case between Hund's case (a) and (b). For low values of  $J$ , the total angular momentum vector, the three different  $\Omega$  multiplets ( $\Omega=0,1,2$ ),  $\Omega$  being the sum of the projection of the electron spin and the electron angular momentum on the internuclear C-O axis, are only weakly interacting and can be treated separately. The first-order Stark effect is proportional to  $M\Omega$ , and therefore only the  $\Omega=1$  and  $\Omega=2$  multiplets will show an appreciable Stark splitting. In Figure 6.1 the Stark splitting for the  $J=1$  level in the  $a^3\Pi_1$  multiplet is schematically indicated. At zero electric field the two  $\Lambda$ -doublet components with opposite parity are split by 394 MHz [10]. If an electric field is applied the  $M$ -degeneracy is lifted and parity is no longer a good quantum number thus levels with different parity start to mix. There is no interaction between  $M=0$  states with different parity, however. In the high-field limit four separate levels corresponding to  $M\Omega=+1$  (down-shifted),  $M\Omega=-1$  (up-shifted) and the two unaffected  $M=0$  levels are seen. Due to the relatively large  $\Lambda$ -doublet splitting in a  $^3\Pi_1$ ,  $J'=1$  the mixing of  $+$  and  $-$  parity levels is not complete at the applied electric fields. At the maximum applied field of 4 kV/cm the up-shifted (down-shifted) level consists of 99.5% of  $M\Omega=-1$  (+1) character and of 0.5% of  $M\Omega=+1$  (-1) character.

The angular probability distribution of the CO axis for a specific  $|J\Omega M\rangle$  level, indicated by  $P_{J\Omega M}(\Theta) d\cos\Theta$  where  $\Theta$  is the angle between the molecular axis and the electric field vector, is a function of the product  $M\Omega$ . The mean orientation for CO in an electric field is given by:

$$\langle \cos \Theta \rangle = [1 + (\frac{E_{\Delta}}{2E_{Stark}})^2]^{-\frac{1}{2}} \frac{M\Omega}{J(J+1)} \quad (6.1)$$

where  $E_\Lambda$  is the  $\Lambda$ -doublet splitting and  $E_{Stark}$  is the Stark shift given by:

$$E_{Stark} = \mu E \frac{M\Omega}{J(J+1)} \quad (6.2)$$

Here  $\mu$  is the permanent electric dipole moment and  $E$  the applied static electric field. For CO (a  $^3\Pi$ ) a maximum average orientation of 1/2 and 2/3 can be reached for a  $^3\Pi_1$ ,  $J'=1$ ,  $M'=1$  and a  $^3\Pi_2$ ,  $J'=2$ ,  $M'=2$ , respectively. Due to the  $\Lambda$ -doublet splitting the mean average orientation at the maximum applied field of 4 kV/cm is 0.49 and 0.66 respectively, very close to the high-field limit. The angular probability distributions in this limit are proportional to  $P_{111}(\Theta) d\cos\Theta \sim (1 + \cos\Theta)^2$  and  $P_{222}(\Theta) d\cos\Theta \sim (1 + \cos\Theta)^4$ .

### 6.3 Experimental

The experiment is carried out with a molecular beam of CO, formed by expanding a 10:1 He:CO mixture at 2.5 atm stagnation pressure through a pulsed valve with an orifice of 1 mm. During operation the background pressure in the vacuum chamber is below  $1 \cdot 10^{-5}$  Torr. Two 40 mm diameter brass electrodes spaced 20 mm apart are used to apply an electric field of up to 4 kV/cm perpendicular to the molecular beam axis, a few cm downstream from the beam orifice. A 4 mm diameter laser beam crosses the molecular beam between the electrodes, 50 mm away from the nozzle. Here the jet cooled CO X  $^1\Sigma^+(v''=0)$  molecules are resonantly excited to the a  $^3\Pi(v'=0)$  state by the radiation of a home-built pulsed dye amplifier (PDA) system. Narrow bandwidth radiation (0.5 MHz) from a cw ring dye laser (Spectra Physics 380D) operating on DCM dye seeds the PDA system, which is pumped by a frequency doubled Q-switched Nd:YAG (Quantel YG 681C-10) laser. The output of the PDA is frequency doubled in a KDP crystal and the frequency doubled and fundamental beam are then mixed in a BBO crystal to produce radiation at 206 nm with an energy of 1 mJ per pulse and a Fourier limited bandwidth of 290 MHz. The polarization vector of the laser beam makes an angle  $\phi$  with the electric field vector of the applied Stark field. Most times  $\phi$  is set close to the magic angle  $\phi_m$  of  $54.7^\circ$  [12] such that the transition strengths to separate  $M$ -levels of a given  $J$ -level are all equal. The excited metastable CO molecules have 6.0 eV internal energy and a radiative lifetime of several ms. The metastable CO molecules collide onto the cathode of a particle multiplier, and are detected via the electrons that are created in the direct Auger de-excitation process [13]. The particle multiplier is placed about 15 cm downstream from the excitation region to diminish the effects of residual Doppler broadening in the molecular beam on the observed spectral linewidth. The signal from the particle multiplier is processed by a digital oscilloscope (LeCroy 9400) and a boxcar integrator (SRS 250) interfaced with a PDP 11/23 computer. Neither fluorescence nor ionization were observed, which suggests that the CO a  $^3\Pi$  molecules are not excited to still higher electronic states by absorption of additional photons.

### 6.4 Results

In Figure 6.2 the measured rotational transition from X  $^1\Sigma^+(v''=0)$ ,  $J''=0$  to a  $^3\Pi_1(v'=0)$ ,  $J'=1$  (the  $R_2(0)$  transition [14] around  $48\,478.48\text{ cm}^{-1}$ ) is shown in different electric fields. At the maximum applied field of 4 kV/cm three components corresponding to  $M\Omega=+1$ , 0 and  $-1$  are completely separated. When the polarization vector of the laser beam is set parallel or perpendicular to the direction of the applied electric field, only the  $\Delta M=0$  or the  $\Delta M=\pm 1$  transitions are observed, respectively, as expected. The parity of the  $J''=0$  level in the electronic ground state

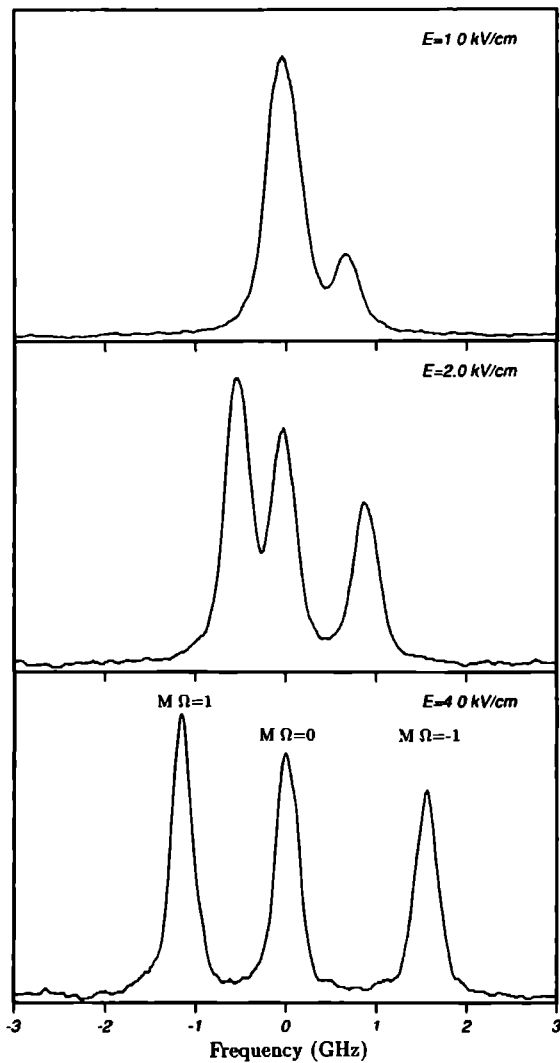


**Figure 6.2:** Observed splitting of the  $R_2(0)$  transition of CO around  $48\,478.48\text{ cm}^{-1}$  as a function of the electric field in the excitation region. The polarization vector of the excitation laser is chosen such that all  $\Delta M$  transitions appear equally strong. Due to the fact that  $M=0$  states with different parity do not interact, only the transition to the  $M=0$  state with  $-$  parity is observed.

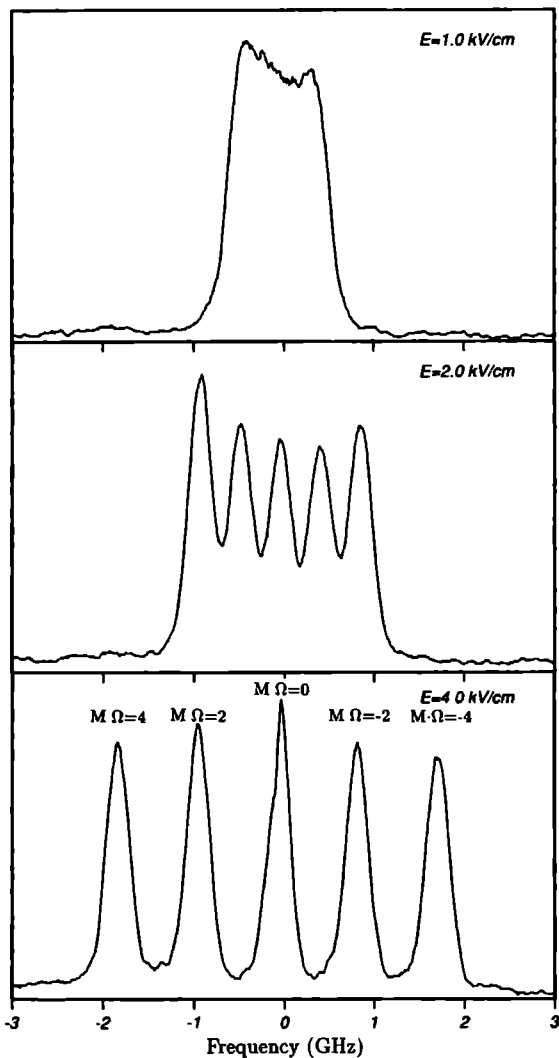


**Figure 6.3:** Observed  $R_3(1)$  transition of CO as a function of the electric field in the excitation region, again with an angle between the polarization vector of the laser and the applied electric field close to the magic angle of  $54.7^\circ$ .

of CO is positive, and therefore only levels with negative parity in the a  $^3\Pi_1$  multiplet can be reached. From the observed splitting pattern it can be concluded unambiguously that the lowest  $\Lambda$ -doublet component of a  $^3\Pi_1(v' = 0)$ ,  $J'=1$  has negative parity, in agreement with the results found in reference [10].

Although the transition moment for the  $R_3(1)$  transition is a factor 50 smaller than for the  $R_2(0)$  transition, it is still very well possible to excite to a  $^3\Pi_2(v' = 0)$ ,  $J'=2$  via the  $R_3(1)$  transition as shown in Figure 6.3. The outermost two peaks of the observed quintet are due to CO a  $^3\Pi$  molecules with an average orientation of  $\langle \cos\Theta \rangle = 2/3$ .

Unfortunately, it is not possible to determine the absolute number of oriented CO a  $^3\Pi$  molecules from the measured signals because the detection efficiency of the metastables depends strongly on the work-function, and thereby the cleanliness, of the cathode of the particle multiplier. The number of excited molecules can be calculated using the measured laser intensity, the estimated density of CO molecules in the molecular beam, and the calculated absorption cross section for the a  $^3\Pi \leftarrow X \ ^1\Sigma^+$  transition. James [11] calculated the lifetime for individual rotational levels in the a  $^3\Pi(v' = 0)$  state and from these calculated lifetimes absorption cross-sections for the  $R_2(0)$  and  $R_3(1)$  transitions of  $7.2 \cdot 10^{-20} \text{ cm}^2\text{cm}^{-1}$  and of  $1.3 \cdot 10^{-21} \text{ cm}^2\text{cm}^{-1}$  are estimated, respectively. The laser fluence at the excitation zone is  $3.3 \cdot 10^{15} \text{ photons/cm}^2$  whereas the CO density at the excitation zone is estimated to be  $1.2 \cdot 10^{15} \text{ molecules/cm}^3$ . Due to rotational cooling 50% of the CO molecules are in the  $J''=0$  level of the vibrational and electronic ground state while roughly 40% are in the  $J''=1$  level. The number of molecules excited to one specific  $M$ -sublevel of the a  $^3\Pi_1(v' = 0)$ ,  $J'=1$  state is estimated to be  $5 \cdot 10^{11}$ . For the excitation to the a  $^3\Pi_2(v' = 0)$ ,  $J'=2$  level this number is a factor 200 lower. The laser interacts with the CO molecules over a length of 4 mm, corresponding to a time interval of 3  $\mu\text{s}$ , taking 1300 m/s as the velocity for molecules in the molecular beam. The peak flux of oriented molecules is then  $2 \cdot 10^{17} \text{ molecules/sec}$ . for a  $^3\Pi_1$ ,  $J'=1$  and  $1 \cdot 10^{15} \text{ molecules/sec}$ . for a  $^3\Pi_2$ ,  $J'=2$ . This peak flux is orders of magnitude higher than the fluxes reported up to now for hexapole oriented beams, and this flux can still be increased by focusing of the 206 nm radiation.

## 6.5 Conclusion

A technique to produce an intense pulsed beam of state-selected and oriented metastable CO molecules is presented. Carbon monoxide molecules in a supersonic molecular beam are resonantly excited from the  $X \ ^1\Sigma^+(v'' = 0)$  ground state to the a  $^3\Pi(v' = 0)$  metastable state using pulsed laser radiation of 206 nm. In the excitation region a static electric field of a few kV/cm is applied, enough to split individual  $M$ -components of a given rotational line of this electronic transition by several GHz. This splitting is larger than the Fourier limited bandwidth of the pulsed radiation source and specific  $M$ -levels in the a  $^3\Pi$  state can be populated. Fluxes of over  $10^{11}$  oriented CO a  $^3\Pi_1(v' = 0)$ ,  $J'=1$ ,  $M'=1$  molecules per  $\mu\text{sec}$ . are obtained.

## Acknowledgments

G. Meijer gratefully acknowledges the support of the Dutch Royal Academy of Science (KNAW). This research was made possible by financial support of the Dutch Organization for Fundamental Research of Matter (FOM). We thank Prof. D.H. Parker for fruitful discussions and valuable suggestions.

### References

1. R.D. Levine and R.B. Bernstein, *"Molecular Reaction Dynamics and Chemical Reactivity"*, Oxford University Press, New York (1987)
2. J. Reuss, in *"Atomic and Molecular Beam Methods"*, Ed. G. Scoles, Oxford University Press, New York (1989)
3. F. Harren, D.H. Parker and S. Stolte, *Comments. At. Mol. Phys.* **26**, 109 (1991)
4. D.H. Parker and R.B. Bernstein, *Ann. Rev. Phys. Chem.* **40**, 561 (1989)
5. H.J. Loesch and A. Remscheid, *J. Chem. Phys.* **93**, 4779 (1990)  
H.J. Loesch and A. Remscheid, *J. Phys. Chem.* **95**, 8194 (1991)
6. B. Friedrich and D.R. Herschbach, *Z. Phys. D* **18**, 153 (1991)  
B. Friedrich and D.R. Herschbach, *Nature* **353**, 512 (1991)  
B. Friedrich, D.P. Pullman and D.R. Herschbach, *J. Phys. Chem.* **95**, 8118 (1991)
7. C. Doukelis, T.E. Gough, G. Scoles and H. Wang, *J. Phys. Chem.* **88**, 4484 (1984)
8. H. Jalink, M. Janssen, F. Harren, D. van den Ende, K.H. Meiwes-Broer, D.H. Parker and S. Stolte, in *"Recent Advances in Molecular Reaction Dynamics"*, Eds. R. Vetter and J. Vigue, CNRS, Paris (1986)
9. H.J. Loesch, E. Stenzel and B. Wüstenbecker, *J. Chem. Phys.* **95**, 3841 (1991)
10. B.G. Wicke, R.W. Field and W. Klemperer, *J. Chem. Phys.* **56**, 5758 (1972)
11. T.C. James, *J. Chem. Phys.* **55**, 4118 (1971)
12. R.N. Zare, *"Angular Momentum"*, John Wiley & Sons, New York (1988)
13. J.M. Price, A. Ludviksson, N. Nooney, M. Xu, R.M. Martin and A.M. Wodtke, *J. Chem. Phys.* **96**, 1854 (1992)
14. R.W. Field, S.G. Tilford, R.A. Howard and J.D. Simmons, *J. Mol. Spectrosc.* **44**, 347 (1972)

# Determination Of Electric Dipole Moments And Transitions Probabilities Of Low-Lying Singlet States Of CO

*M. Drabbels, W.L. Meerts and J.J. ter Meulen  
Department of Molecular and Laser Physics, University of Nijmegen,  
Toernooiveld, 6525 ED Nijmegen, The Netherlands*

### Abstract

Transitions from the X  $^1\Sigma^+(v = 0)$  ground state of the carbon monoxide molecule to the electronically excited A  $^1\Pi(v = 0)$ , B  $^1\Sigma^+(v = 0)$  and C  $^1\Sigma^+(v = 0)$  states have been studied by two-photon laser-induced fluorescence spectroscopy. Accurate molecular constants for the B and C state have been determined. The electric dipole moments for all three electronically excited states have been deduced from the observed Stark effects. The dipole moments for the A, B and C state are found to be  $0.335 \pm 0.013$  D,  $1.95 \pm 0.03$  D and  $4.50 \pm 0.07$  D, respectively. From the observed radiative lifetimes the transition probabilities of the B-A, B-X and C-B, C-A and C-X transitions have been determined.



## 7.1 Introduction

Although spectroscopic studies of the CO molecule began more than a century ago it still is one of the most extensively studied diatomic molecules. Transitions between the  $X^1\Sigma^+$  ground state and electronically excited singlet states have been observed in absorption [1, 2] and recently in emission [3, 4]. Transitions between electronically excited singlet states were observed in emission many years ago [5]. In recent years these transitions have been studied under high resolution by Fourier transform spectroscopy [6, 7]. Many different laser excitation and detection schemes have also been applied to study the electronically excited states of the CO molecule [8, 9, 10, 11, 12, 13].

Despite these extensive studies only little information is available on the electronic dipole moments of electronically excited singlet states. The only study up to now is by Fisher and Dalby [14] who observed the  $B^1\Sigma^+(v' = 0) \rightarrow A^1\Pi(v'' = 0)$  and  $C^1\Sigma^+(v' = 0) \rightarrow A^1\Pi(v'' = 3)$  emission spectra in the presence of high electric fields. From the observed lineshifts the electric dipole moments for the three states involved could be determined. However, the lineshifts could only be observed at the maximum applied field and therefore the authors could not unambiguously conclude that the observed lineshifts were caused by the Stark effect, or as the authors state themselves: "*Calculations would be valuable in order to rule out the possibility that the experimental results observed here were due to some malevolent field induced perturbation rather than straightforward Stark effects.*" Recently Cooper and Kirby [15] performed *ab initio* calculations for the lowest lying singlet states of CO and obtained values for the electric dipole moments of the A, B and C state which agree to a reasonable extent with the experimental values of Fisher and Dalby [14].

In the present experiment transitions from the electronic ground state  $X^1\Sigma^+(v'' = 0)$  to the  $A^1\Pi(v' = 0)$ ,  $B^1\Sigma^+(v' = 0)$  and  $C^1\Sigma^+(v' = 0)$  states are studied in the presence of electric fields up to 30 kV/cm. To be able to observe the relatively small shifts and splittings of the rotational levels caused by the Stark effect a narrow bandwidth Fourier limited pulsed laser system is used.

The radiative lifetimes of the  $B^1\Sigma^+$  and  $C^1\Sigma^+$  states have been determined by many different techniques. The values reported for the radiative lifetimes disagree seriously with each other, especially for the C state, see for example the summary in reference [16]. In the present study the radiative lifetime of the  $B^1\Sigma^+$  state is determined directly from the decay of the the observed laser-induced fluorescence whereas the lifetime for the  $C^1\Sigma^+$  state is determined from the width of the observed transitions. By making use of fluorescence trapping the transition probabilities from the B and C states to lower lying states are determined.

## 7.2 Experimental

A molecular beam is formed by expanding 3 atm neat CO through a pulsed valve, operated at 10 Hz, with an orifice of 0.5 mm. The molecular beam is collimated 25 mm downstream of the nozzle by a skimmer with an opening of 5 mm. During operation the background pressure in the vacuum chamber is well below  $1 \cdot 10^{-5}$  Torr. Two 45 mm diameter stainless steel electrodes spaced 9.7 mm apart are used to apply a static electric field up to 30 kV/cm perpendicular to the molecular beam axis. The center part of the electrodes consist of a 15 mm diameter honeycomb structured grid, through which the laser-induced fluorescence can be observed. Calculations have shown that the inhomogeneity of the electric field between the two electrodes due to the presence of the grids is less than 0.2%. Ground state  $X^1\Sigma^+(v'' = 0)$  carbon monoxide is two-photon excited to the  $A^1\Pi(v' = 0)$ ,  $B^1\Sigma^+(v' = 0)$  or  $C^1\Sigma^+(v' = 0)$  state by a softly focussed ( $f=500$  mm)

laser beam that crosses the molecular beam between the two electrodes 80 mm downstream of the nozzle. The laser-induced fluorescence in the visible and UV region of the spectrum is collected through the grids of the electrodes by a quartz lens system and imaged onto a photomultiplier tube (EMI 9893B). An F/3.7 monochromator with a bandwidth of 1.8 nm can be placed in front of the photomultiplier to disperse this fluorescence. The VUV fluorescence is detected by a solar blind type photomultiplier (EMI 9413) placed in the vacuum chamber. The signals from the photomultipliers are processed by a digital oscilloscope (LeCroy 7400) and two boxcar integrators (SRS 250) interfaced with a Personal Computer.

In order to be able to observe the relatively small shifts and splittings of rotational lines caused by the Stark effect a Fourier limited pulsed dye laser system is used to excite the CO molecules. Narrow bandwidth radiation of a cw single-frequency ring dye laser (Spectra Physics 380D) operating on Stilbene 3 dye is amplified by a home-built pulsed dye amplifier (PDA) system which is pumped by a frequency tripled Q-switched Nd:YAG laser (Quantel YG681-10C). The output of the PDA system is frequency doubled in a BBO crystal yielding 2.5 mJ UV radiation with an estimated bandwidth of 400 MHz. For relative frequency calibration the transmission fringes of a pressure and temperature stabilized Fabry-Perot interferometer with a free spectral range of  $149.72 \pm 0.05$  MHz are recorded. For absolute frequency calibration the absorption spectrum of the  $\text{Te}_2$  molecule [17] is simultaneously recorded with the excitation spectrum.

## 7.3 Results

### 7.3.1 Spectroscopic

The B  $^1\Sigma^+(v=0)$  state at  $86\,916\text{ cm}^{-1}$ , which is the first member of the ( $n\sigma$ ) Rydberg series, was the subject of a former study [13] where only the lowest five rotational levels in the ground state were populated due to the strong rotational cooling in the molecular beam. In the present experiment the rotational temperature is increased to 10 K due to collisions of the CO molecules with the skimmer and as a result higher rotational levels are populated. The molecules are two-photon excited from the X  $^1\Sigma^+(v''=0)$  ground state to the B  $^1\Sigma^+(v'=0)$  state via  $\Delta J=0$  and  $\Delta J=\pm 2$  transitions which are, however, 2 to 3 orders of magnitude weaker than the  $\Delta J=0$  transitions. As a result only  $\Delta J=2$  transitions from the lowest two rotational levels are observed. The B  $^1\Sigma^+(v'=0) \leftarrow$  X  $^1\Sigma^+(v''=0)$  transition is recorded by detecting the strong fluorescence from the B state to the lower lying A  $^1\Pi$  state. The linewidth of the individual rotational transitions is 760 MHz and is largely determined by the bandwidth of the laser system. The observed line frequencies for the B  $^1\Sigma^+(v'=0) \leftarrow$  X  $^1\Sigma^+(v''=0)$  transitions together with their assignments are listed in Table 7.1. The observed transitions are fit to the following expression for a  $^1\Sigma^+ \leftrightarrow ^1\Sigma^+$  transition:

$$\nu = T_0 + B'_0 J'(J'+1) - D'_0 J'^2(J'+1)^2 - [B''_0 J''(J''+1) - D''_0 J''^2(J''+1)^2] \quad (7.1)$$

Here  $B'_0$ ,  $D'_0$ ,  $J'$  and  $B''_0$ ,  $D''_0$ ,  $J''$  refer to the upper state and the ground state, respectively. The rotational constants for the ground state are kept fixed in the least squares fit at the accurate values obtained by Guelachvili *et al.* [18]. From the work of Amiot *et al.* [6], who performed a high resolution Fourier transform spectroscopy study on the C  $\rightarrow$  B and E  $\rightarrow$  B transitions, it is known that the  $J=4$  and  $J=6$  levels in the B state are weakly perturbed. Transitions to these levels have therefore not been included in the least squares fit. The molecular constants resulting from the fit are given in Table 7.2. For comparison the constants determined by Amiot *et al.* [6]

Transition	$B^1\Sigma^+(v=0)$		$C^1\Sigma^+(v=0)$	
	Obs. Freq.	Obs.-Calc.	Obs. Freq.	Obs.-Calc.
Q(0)	86916.149(3)	-0.001	91919.066(3)	0.003
Q(1)	86916.203(3)	0.001	91919.105(3)	0.000
Q(2)	86916.304(3)	0.000	91919.188(3)	-0.001
Q(3)	86916.456(3)	-0.002	91919.312(3)	-0.002
Q(4)	86916.646(3) <sup>a)</sup>	-0.017	91919.482(3)	0.001
Q(5)	86916.918(3)	-0.001	91919.693(10)	0.003
Q(6)	86917.239(3) <sup>a)</sup>	0.013	91919.951(30)	0.010
Q(7)	86917.588(3)	0.004		
Q(8)	86917.993(3)	0.000		
Q(9)	86918.453(3)	0.001		
Q(10)	86918.961(3)	-0.001		
Q(11)	86919.519(3)	-0.003		
Q(12)	86920.130(3)	-0.002		
Q(13)	86920.794(3)	0.002		
Q(14)	86921.504(10)	0.003		
S(0)	86927.839(3)	0.000	91930.723(3)	-0.001
S(1)	86935.682(3)	0.000	91938.541(3)	0.001

<sup>a)</sup> Not included in the least squares fit.

Table 7.1: Observed and calculated transition frequencies ( $\text{cm}^{-1}$ ) of the  $B^1\Sigma^+(v'=0) \leftarrow X^1\Sigma^+(v''=0)$  and the  $C^1\Sigma^+(v'=0) \leftarrow X^1\Sigma^+(v''=0)$  transitions in CO.

are also included in this table. The agreement between our results and those of Amiot *et al.* [6] is satisfactory.

From the fit it can be concluded that the  $J=4$  level of the B state is  $0.017 \text{ cm}^{-1}$  downshifted in energy and that the  $J=6$  level is  $0.013 \text{ cm}^{-1}$  upshifted in energy. These observed perturbations are in excellent agreement with the experiments of Amiot *et al.* [6]. From the work of Tilford and Simmons [1] it is known that the three states  $A^1\Pi(v=19)$ ,  $a'^3\Sigma^+(v=37)$  and  $e^3\Sigma^-(v=28)$  lie within  $20 \text{ cm}^{-1}$  of the B state. It is therefore highly probable that at least one of these states is responsible for the observed perturbations. The  $a'^3\Sigma^+(v=37)$  can be ruled out as perturbing state since an interaction between the  $B^1\Sigma^+$  state and the  $a'^3\Sigma^+$  is in first-order forbidden by spin-orbit selection rules. The absence of a line shift for the  $J=5$  level implies that the perturbations of the  $J=4$  and  $J=6$  levels result from two independent level-crossings. Since the  $A^1\Pi(v=19)$  state could produce only one accidental level-crossing this state can not be responsible for both observed perturbations. The  $e^3\Sigma^-(v=28)$  state, however, has two  $e$  parity components which both will perturb the  $B^1\Sigma^+(v=0)$  state at different  $J$ -values. Although the observed perturbations can not be fully analyzed, the directions of the level shifts indicate that the  $F_1$ ,  $N=3$ , component of the  $e^3\Sigma^-(v=28)$  state lies just above the  $J=4$  level of the  $B^1\Sigma^+(v=0)$  state and that the  $F_3$ ,  $N=7$ , component lies just below the  $J=6$  level. So it seems most probable that the  $e^3\Sigma^-(v=28)$  state is the perturbing state although it cannot be excluded that also the  $A^1\Pi(v=19)$  state is involved in one of the two perturbations.

		This work	Ref. [6]
B $^1\Sigma^+(v=0)$	$T_0$	86 916.1501(16)	86 916.20(4)
	$B_0$	1.948173(28)	1.94811(2)
	$D_0$	6.90(27)·10 <sup>-6</sup>	6.71(2)·10 <sup>-6</sup>
C $^1\Sigma^+(v=0)$	$T_0$	91 919.0639(20)	91 919.11(4)
	$B_0$	1.943425(97)	1.943381(4)
	$D_0$	6.172·10 <sup>-6</sup> <sup>a)</sup>	6.172(5)·10 <sup>-6</sup>
	$\nu_{BC}$	5 002.9138(26)	5 002.9094(6)

<sup>a)</sup> Kept fixed in the least squares fit at the value determined by Amiot *et al.* [6].

**Table 7.2:** Molecular constants (cm<sup>-1</sup>) of the B  $^1\Sigma^+(v=0)$  and C  $^1\Sigma^+(v=0)$  state of carbon monoxide.

The C  $^1\Sigma^+$  state, which is the first member of the ( $n\rho\sigma$ ) Rydberg series converging to the ground state of the ion, lies only 5 000 cm<sup>-1</sup> higher in energy than the B  $^1\Sigma^+$  state and can therefore be observed with the same experimental setup as the B state. The C  $^1\Sigma^+(v'=0) \leftarrow X^1\Sigma^+(v''=0)$  transition is recorded by detecting the fluorescence from the C state down to the A state in the region from 365 to 550 nm. The linewidths of the transitions to the C state are considerably larger than those of transitions to the B state, 1 000 MHz instead of 760 MHz. The observed excitation frequencies and their assignments are listed in Table 7.1. The highest observable rotational level in the C state is  $J=6$ . The difference with the B state, where the  $J=14$  level could still be observed, is mainly due to the difference in branching ratio for fluorescence from both states down to the A state, see section 7.3.3. The observed excitation frequencies have been fit to the expression (7.1) for a  $^1\Sigma^+ \leftrightarrow ^1\Sigma^+$  transition. The molecular constants resulting from the least squares fit are listed in Table 7.2 together with the constants obtained by Amiot *et al.* [6]. There is a rather good agreement between the values for the rotational  $B_0$  constant found in both experiments. The energy difference between the B and C state is determined from the term values of both states. The agreement with the value obtained by Amiot *et al.* [6], who observed the direct transitions between these two states, is satisfactory.

The E  $^1\Pi(v=0)$  state, the first member of the ( $n\rho\pi$ ) Rydberg series, lies only 1 000 cm<sup>-1</sup> higher in energy than the C  $^1\Sigma^+(v=0)$  state. Transitions to this state should therefore be observable with the present experimental setup. However, these transitions have not been observed. From the work of Letzelter *et al.* [19] it is known that the  $v=0$  level of the E  $^1\Pi$  state predissociates. Most probably due to the extra loss channel introduced by the predissociation the transitions to the E  $^1\Pi(v=0)$  state have not been observed.

### 7.3.2 Dipole moments

The electric dipole moments for the A  $^1\Pi(v=0)$ , B  $^1\Sigma^+(v=0)$  and C  $^1\Sigma^+(v=0)$  states are determined from the shifts and splittings of rotational levels in an electric field due to the Stark effect. The energy shift of a rotational level in an electric field in the presence of  $\Lambda$ -doubling is in

first-order given by:

$$\Delta W = \sqrt{\left(\frac{E_{\Lambda}}{2}\right)^2 + (\mu E)^2 \left(\frac{M\Omega}{J(J+1)}\right)^2} - \frac{E_{\Lambda}}{2} \quad (7.2)$$

Here  $E_{\Lambda}$  is the energy difference between the two  $\Lambda$ -doublet components,  $\mu$  the permanent electric dipole moment,  $E$  the applied static electric field,  $M$  the projection of the total angular momentum  $J$  on the electric field vector and  $\Omega$  the projection of  $J$  on the internuclear axis. The first-order contribution is, however, zero for electronic states with  $\Omega=0$ , such as  $^1\Sigma^+$  states. These states are described by the second-order Stark effect. The energy shift of a rotational level is then given by:

$$\Delta W = \frac{(\mu E)^2}{2hB} \frac{J(J+1) - 3M^2}{J(J+1)(2J-1)(2J+3)} \quad (7.3)$$

Here  $h$  is Planck's constant and  $B$  is the rotational constant of the electronic state involved. For states having  $\Omega \neq 0$  the second-order contribution is usually much smaller than the first-order contribution and can therefore be neglected.

In the present experiment transitions are induced from the electronic ground state  $X^1\Sigma^+(v=0)$  to electronically excited states. The electronic ground state of CO has no first-order Stark effect and with a relatively small electric dipole moment of 0.1098 D the splitting of the various  $J$ -levels is in the order of a few MHz in electric fields up to 30 kV/cm [20]. The observed Stark patterns are thus completely determined by the Stark splittings in the electronically excited states.

For the determination of the electric dipole moment of the  $A^1\Pi(v=0)$  state, which exhibits a first-order Stark effect, the  $A^1\Pi(v'=0) \leftarrow X^1\Sigma^+(v''=0)$  Q(1) transition is studied in the presence of an electric field. The molecules are two-photon excited to the A state by a weakly focussed laser beam polarized perpendicular to the electric field. The VUV fluorescence down to the ground state is then detected by a solar blind photomultiplier. The dipole moment of the  $A^1\Pi(v=0)$  state can directly be determined from the observed line splitting using equation (7.2) and taking into account the  $\Lambda$ -doubling of 180 MHz for the  $J=1$  level of the A state [21]. Figure 7.1 shows the Q(1) transition in zero field and in an electric field of 15 kV/cm. At this field strength the  $M\Omega=+1$  and  $M\Omega=-1$  components are almost completely separated. The  $M\Omega=0$  component is not observed due to selection rules. Unfortunately, the solar blind photomultiplier failed before measurements at higher electric fields and other rotational levels could be performed, which would yield a more accurate value for the dipole moment. The error in the electric dipole moment is now determined by the uncertainty in the observed splitting of the two  $M$ -components. The electric dipole moment for the  $A^1\Pi^+(v=0)$  state was found to be  $0.335 \pm 0.013$  D. This value is a factor of two larger than the upper limit which was given by Fisher and Dalby [14] and is also considerably larger than the value calculated by Cooper and Kirby [15], see Table 7.3. It is, however, smaller than the value of 0.58 D calculated by Cooper and Langhoff [22].

The  $B^1\Sigma^+$  and  $C^1\Sigma^+$  states both exhibit a second-order Stark effect. In the presence of an electric field the  $J=0$  level will shift in energy by an amount of  $\Delta W = -(\mu E)^2/6hB$ . The  $J=1$  level will split into two components,  $|M|=1$  and  $M=0$ , which are separated by  $3(\mu E)^2/20hB$ . In the present experiment the electric dipole moments for the B and C states are determined by measuring these shifts and splittings as a function of the electric field. Figure 7.2 shows a part of the Q-branch of the  $B^1\Sigma^+(v'=0) \leftarrow X^1\Sigma^+(v''=0)$  transition. The shift and splitting become observable at electric fields of 15 kV/cm and higher. At the maximum applied field of 30 kV/cm the splitting of the  $J=2$  level becomes observable. In Figure 7.3 the observed shift for the  $J=0$  level

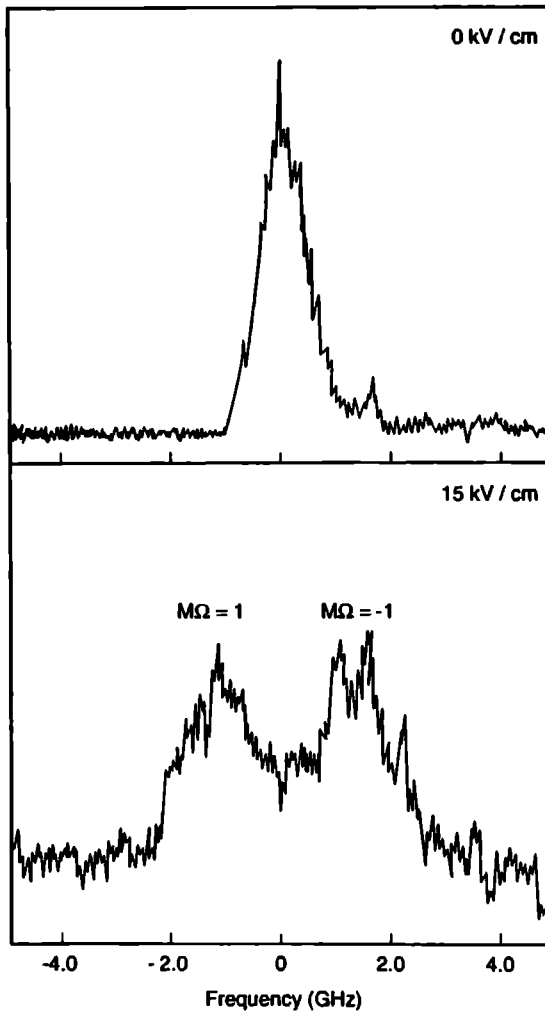


**Figure 7.1:** Recording of the  $A\ ^1\Pi(v'=0) \leftarrow X\ ^1\Sigma^+(v''=0)$   $Q(1)$  transition at zero field and at an electric field of 15 kV/cm.

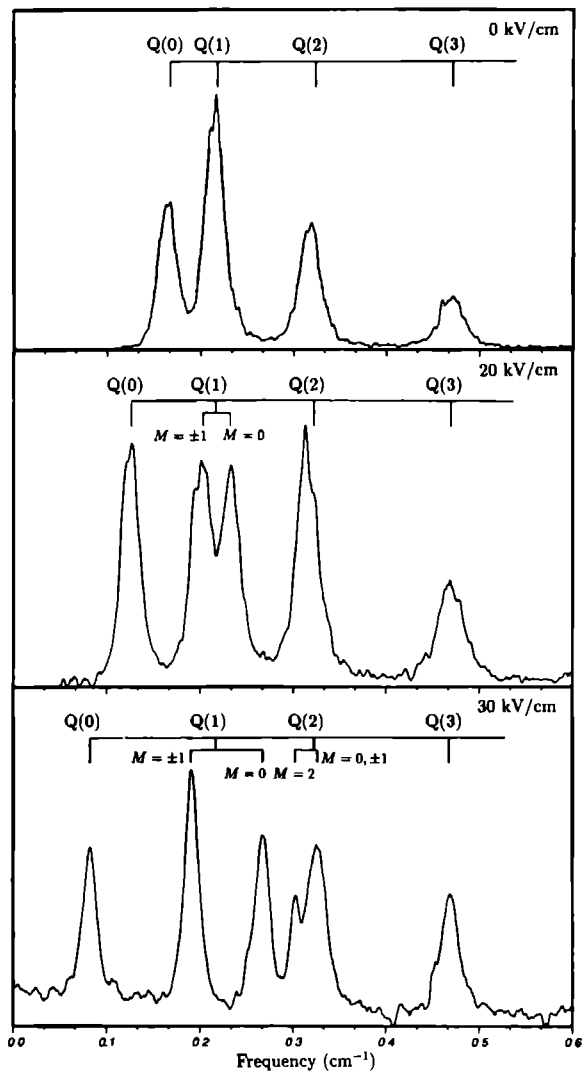


**Figure 7.2:** Part of the observed Q-branch of the  $B^1\Sigma^+(v'=0) \leftarrow X^1\Sigma^+(v''=0)$  transition as a function of the electric field in the excitation region.

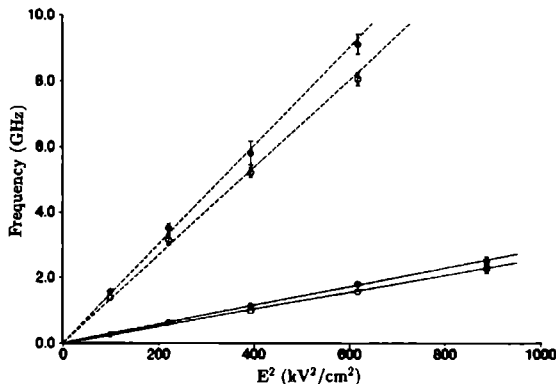


**Figure 7.3:** Observed shift of the  $J=0$  level (filled dots) and splitting of the  $J=1$  level (open dots) for the  $B\ ^1\Sigma^+(v=0)$  state (solid line) and for the  $C\ ^1\Sigma^+(v=0)$  state (dashed line) as a function of the square of the electric field.

and the splitting for the  $J=1$  level are plotted as a function of the square of the electric field. As can be seen the observed Stark patterns are very well described by the second-order Stark effect, equation (7.3). From these measurements an electric dipole moment of  $1.95 \pm 0.03$  D is obtained for the  $B\ ^1\Sigma^+(v=0)$  state. For the  $C\ ^1\Sigma^+(v=0)$  state a much larger value of  $4.50 \pm 0.07$  D is found. In these cases the error is determined by the uncertainty in the distance between the two electrodes. The value found for the electric dipole moment of the B state is considerably larger than the value found by Fisher and Dalby [14] but smaller than the value calculated by Cooper and Kirby [15], see Table 7.3. For the C state the agreement with the result of Fisher and Dalby is excellent. The value for the electric dipole moment calculated by Cooper and Kirby for the C state is also slightly too large.

It's not possible to determine the sign of the dipole moment from the Stark measurements. Since the values of the electric dipole moment calculated by Cooper and Kirby are relatively close to the experimentally determined values it can be assumed that the signs of the electric dipole moments are equal to those calculated by Cooper and Kirby.

	This work	Ref. [14]	Ref. [15]
A $1\Pi(v=0)$	0.335(13)	< 0.15(5)	0.19
B $1\Sigma^+(v=0)$	1.95(3)	1.60(15)	2.79
C $1\Sigma^+(v=0)$	-4.50(7)	-4.52(35)	-5.34

**Table 7.3:** Electric dipole moments (Debye) of electronically excited states of CO. The signs of the dipole moments are taken from the work of Cooper and Kirby [15]. A positive value indicates polarity  $C^+O^-$ .



### 7.3.3 Transition probabilities

The transition probabilities from the B and C state to the lower lying A state and the ground state can be deduced from the observed radiative lifetimes. The radiative lifetime for the B state is related to the transition probabilities by:

$$\frac{1}{\tau} = A_{B \rightarrow X} + A_{B \rightarrow A} \quad (7.4)$$

Here  $A_{B \rightarrow X}$  and  $A_{B \rightarrow A}$  are the transition probabilities from the B  $^1\Sigma^+(v=0)$  to all the vibrational levels in the ground state and the A  $^1\Pi$  state, respectively. At relatively high CO densities fluorescence trapping between the B and the ground state can occur. The observed lifetime,  $\tau_{obs}$ , which is in this case larger than the actual radiative lifetime is related to the transition probabilities by:

$$\frac{1}{\tau_{obs}} = (1-g)A_{B \rightarrow X} + A_{B \rightarrow A} \quad (7.5)$$

Here  $g$  is the fraction of the B  $\rightarrow$  X fluorescence that is reabsorbed by ground state molecules. At high densities this fraction becomes equal to the relative vibrational transition probability for the B  $^1\Sigma^+(v'=0) \rightarrow$  X  $^1\Sigma^+(v''=0)$  transition and the observed lifetime approaches a constant value,  $\tau_{trap}$ . By measuring the lifetime of the B state at low and high densities the transition probabilities from the B state to the ground state and the A state can be determined.

The radiative lifetime of the B state is measured for several rotational levels. In order to make sure that fluorescence trapping does not occur, a mixture of 2% CO in Argon is used. The observed laser-induced fluorescence has been fit to a single exponential decay. The radiative lifetime for the B  $^1\Sigma^+(v=0)$  state was found to be  $29.8 \pm 1.2$  ns, independent of the rotational level. This value is in agreement with most of the published results, see for example the summary in reference [16].

In order to measure the lifetime of the B state at high CO densities the skimmer is removed and the molecules are excited closer to the nozzle. To make sure that fluorescence trapping occurs the lifetime was measured as a function of the distance between the excitation region and the nozzle. For a distance smaller than 4 cm, a constant lifetime,  $\tau_{trap}$ , of  $68.0 \pm 2.3$  ns was found. In order to calculate the transition probabilities the relative vibrational transition probability of the B  $^1\Sigma^+(v'=0) \rightarrow$  X  $^1\Sigma^+(v''=0)$  transition has to be known. Since the relative vibrational transition probabilities for this transition have not been determined experimentally we have calculated these probabilities. In a first step the RKR potential energy curves for both electronic states are calculated from their molecular constants. In a second step the Schrödinger equation is solved numerically for these potentials and the overlap integral for the vibrational wavefunctions is calculated using the R-dependent transition moment function for the B  $\leftrightarrow$  X transition given by Kirby and Cooper [16]. As a result we find that 0.990 of the fluorescence to the ground state is emitted to the  $v''=0$  level. The transition probabilities for the B  $^1\Sigma^+(v'=0)$  to the X  $^1\Sigma^+(v'')$  and to the A  $^1\Pi(v'')$  states can now be determined. The results are listed in Table 7.4. For comparison the values obtained by Dotchin *et al.* [23], who performed lifetime measurements on electronically excited states using a proton beam as excitation source, and the calculated values of Kirby and Cooper [16] are also included in this table. The agreement with these experimentally and calculated values is quite satisfactory.

The values found for the radiative lifetime of the C  $^1\Sigma^+(v=0)$  state vary strongly, from  $<1.5$  to 50 ns [16]. This large discrepancy between the different measurements may be due to several experimental factors such as cascading effects and fluorescence trapping which tend to increase the

		This work	Ref. [23]	Ref. [16]
$B \ ^1\Sigma^+(v=0)$	$\tau$	29.8(12)	23(3)	33.5
	$\tau_{\text{trap}}$	68.0(27)	72(3)	-
	$A_{B \rightarrow X}$	1.90(10)	3.0(6)	1.052
	$A_{B \rightarrow A}$	1.45(6)	1.39(6)	1.935
$C \ ^1\Sigma^+(v=0)$	$\tau$	0.48(12)	2.2(8)	1.47
	$\tau_{\text{trap}}$	58.8(23)	36(2)	-
	$A_{C \rightarrow X}$	207(52)	42(17)	67.13
	$A_{C \rightarrow A}$	0.55(15)	2.8(1)	0.514
	$A_{C \rightarrow B}$	0.12(5)	-	0.391

**Table 7.4:** Radiative lifetimes (ns) and transition probabilities ( $10^7 \text{ s}^{-1}$ ) of the  $B \ ^1\Sigma^+(v=0)$  and  $C \ ^1\Sigma^+(v=0)$  states.

apparent lifetime or due to unreliable extrapolations to zero pressure in cell experiments due to the absence of data at sufficiently low pressures. In the present experiment all these effects can be avoided. The radiative lifetime was at first instance determined by monitoring the laser-induced fluorescence from the  $C \ ^1\Sigma^+(v=0)$  state to the A state. From this measurement it is concluded that the radiative lifetime of the C state is considerably shorter than the 5 ns response time of our electronics.

If the lifetime of the C state is shorter than 1 ns it will result in an observable broadening of the lines in the excitation spectrum. As mentioned in section 7.3.1 the linewidth of the transitions to the C state is substantially broader than that of the transitions to the B state. In order to obtain the lifetime of the C state, the extra line broadening is determined. In a first step the isolated S(0) and S(1) transitions to the B state are fit to a Voigt profile in order to determine the contribution of instrumental effects to the Lorentzian part of the linewidth. Next the S(0) and S(1) transitions of the  $C \leftarrow X$  system are fit to a Voigt profile. The Lorentzian contribution to the linewidth is 330 MHz larger for the transitions to the C state, whereas the Gaussian contribution is the same as for the transitions to the B state. To make sure that the observed line broadening is not due to saturation of the  $C \leftarrow X$  transition or due to fast ionization the laser power has been varied. Since no power dependence of the linewidth has been observed it is concluded that the line broadening is due to the short radiative lifetime of the C state. The extra contribution of  $330 \pm 80$  MHz to the linewidth corresponds to a radiative lifetime for the  $C \ ^1\Sigma^+(v=0)$  state of  $0.48 \pm 0.12$  ns. This value for the lifetime of the C state is considerably shorter than the previously determined values for the lifetime.

The  $C \ ^1\Sigma^+(v=0)$  state can fluoresce to the  $X \ ^1\Sigma^+$ ,  $A \ ^1\Pi$  and  $B \ ^1\Sigma^+$  states. The *ab initio* calculations by Kirby and Cooper [16] show that although the transition frequency for the  $C \rightarrow B$  transition is much smaller than that of the  $C \rightarrow A$  transition the probabilities for both transitions are almost equal. Since the potential energy curves of the B and C states are almost identical, nearly all the  $C \rightarrow B$  fluorescence will be to the  $v=0$  level of the  $B \ ^1\Sigma^+$  state. The fluorescence from this level to the ground state and the electronically excited A state can then be detected.

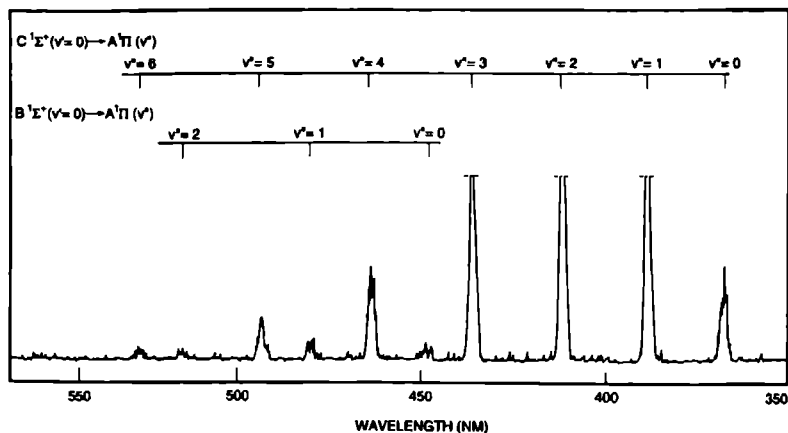


**Figure 7.4:** Dispersed fluorescence spectrum after excitation to the  $J=0$  level of the  $C\ ^1\Sigma^+(v=0)$  state.

In order to determine the branching ratio for the  $C \rightarrow A$  and  $C \rightarrow B$  transitions the dispersed fluorescence spectrum is recorded. Figure 7.4 shows the dispersed fluorescence spectrum after populating the  $J=0$  level of the  $C\ ^1\Sigma^+(v=0)$  state. Clearly two distinct branches are observed, one due to transitions from the  $C\ ^1\Sigma^+(v=0)$  state to the vibrational levels of the A state and the other due to transitions from the  $B\ ^1\Sigma^+(v=0)$  state to the A state. The branching ratio for the  $C \rightarrow A$  and the  $C \rightarrow B$  transitions can be determined from the observed intensity ratio of the two branches, after correction for the wavelength dependence of the detection system. Taking into account the branching ratio for the  $B \rightarrow X$  and the  $B \rightarrow A$  transitions, see Table 7.4, we find a branching ratio for the transitions from the  $C\ ^1\Sigma^+(v=0)$  to the A state of  $0.82 \pm 0.06$  and to the B state of  $0.18 \pm 0.06$ .

To be able to determine the absolute transition probabilities, the lifetime of the C state is determined at CO densities at which fluorescence trapping occurs. The apparent lifetime is found to be  $\tau_{trap} = 58.8 \pm 2.3$  ns. In order to derive the transition probabilities from the observed lifetimes, the relative vibrational transition probabilities for the  $C \leftrightarrow X$  transition are calculated, since no experimental values for the relative vibrational transition probabilities are available for this transition. In these calculations a R-dependent transition moment for the  $C \leftrightarrow X$  transition is assumed as given by Kirby and Cooper [16]. As a result we find that the relative vibrational transition probability for the  $C\ ^1\Sigma^+(v'=0) \leftrightarrow X\ ^1\Sigma^+(v''=0)$  transition is equal to 0.995. Using the previously determined branching ratios for the transitions to the A and B states the transition probabilities can be determined. The results are given in Table 7.4. It has to be noticed that these values for the transition moments of the  $C \rightarrow A$  and  $C \rightarrow B$  transitions depend strongly on the calculated value of  $g$ , and can thus easily change if experimentally a different value for the relative vibrational transition probability is found. There is a clear difference between the values determined in the present study and those determined by Dotchin *et al.* [23], see Table 7.4. This difference is mainly due to the difference in the radiative lifetime found for the C state. The

agreement with the calculated values of Kirby and Cooper [16] is satisfactory only for the value of the  $C \rightarrow A$  transition.

#### 7.4 Summary

Transitions from the electronic ground state of the CO molecule to the electronically excited  $A \ ^1\Pi(v = 0)$ ,  $B \ ^1\Sigma^+(v = 0)$  and  $C \ ^1\Sigma^+(v = 0)$  states have been studied at high resolution in a molecular beam employing a Fourier limited pulsed laser system. Accurate molecular constants are obtained for the excited states and weak perturbations in the B state were observed, which can be attributed to an interaction with the  $e \ ^3\Sigma^-(v = 28)$  state. The electric dipole moments of the electronically excited states have been determined from the observed Stark effects. The transition probabilities of the B and C state to lower lying states could be deduced from the observed lifetimes of these two states.

#### Acknowledgements

The authors wish to thank Dr. M. Eidelsberg for stimulating discussions and valuable suggestions and Prof. R.W. Field for valuable comments on the interpretation of the observed perturbations. The financial support from the Foundation for Fundamental Research on Matter (FOM) is gratefully acknowledged.

### References

1. S.G. Tilford and J.D. Simmons, *J. Phys. Chem. Ref. Data* **1**, 147 (1972)
2. M. Eidelsberg and F. Rostas, *Astron. Astrophys.* **235**, 472 (1990)
3. M. Eidelsberg, J.Y. Roncin, A. Le Floch, F. Launay, C. Letzelter and J. Rostas, *J. Mol. Spectrosc.* **121**, 309 (1987)
4. A.C. Le Floch, F. Launay, J. Rostas, R.W. Field, C.M. Brown and K. Yoshino, *J. Mol. Spectrosc.* **121**, 337 (1987)
5. R. Schmid and L. Gerö, *Z. Phys.* **93**, 656 (1935)
6. C. Amiot, J.Y. Roncin and J. Verges, *J. Phys. B: At. Mol. Phys.* **19**, L19 (1986)
7. J.I. Choe, D.K. Lee A.C. Le Floch and S.G.Kukolich, *J. Mol. Spectrosc.* **136**, 173 (1989)
8. G.W. Loge, J.J. Tise and F.B. Wampler, *J. Chem. Phys.* **79**, 196 (1983)
9. P. Klopotek and C.R. Vidal, *J. Opt. Soc. Am. B.* **2**, 869 (1985)
10. M.A. Hines, H.A. Michelsen and R.N. Zare, *J. Chem. Phys.* **93**, 8557 (1990)
11. N. Hosoi, T. Ebata and M. Ito, *J. Chem. Phys.* **95**, 4182 (1991)
12. P.F. Levelt, W. Ubachs and W. Hogervorst, *J. Chem. Phys.* **97**, 7160 (1992)
13. M. Drabbels, *Ph.D. Thesis, Chapter 8*, Katholieke Universiteit Nijmegen (1993)  
M. Drabbels, J. Heinze, J.J. ter Meulen and W.L. Meerts, accepted for publication in *J. Chem. Phys.*
14. N.J. Fisher and F.W. Dalby, *Can. J. Phys.* **54**, 258, (1976)
15. D.L. Cooper and K. Kirby, *J. Chem. Phys.* **87**, 424, (1987)
16. K. Kirby and D.L. Cooper, *J. Chem. Phys.* **90**, 4895 (1989)
17. J. Cariou and P. Luc, *"Atlas de spectroscopie d'absorption de la molécule tellure"*, CNRS, Paris (1980)
18. G. Guelachvili, D. de Villeneuve, R. Farrenq, W. Urban, and J. Verges, *J. Mol. Spectrosc.* **98**, 64 (1983)
19. C. Letzelter, M. Eidelsberg, F. Rostas, J. Breton and B. Thieblemont, *Chem. Phys. Lett.* **114**, 273 (1987)
20. J.S. Muentzer, *J. Mol. Spectrosc.* **55**, 490 (1975)
21. A.C. Le Floch, F. Launay, J. Rostas, R.W. Field, C.M. Brown and K. Yoshino, *J. Mol. Spectrosc.* **121**, 337 (1987)
22. D.M. Cooper and S.R. Langhoff, *J. Chem. Phys.* **74**, 1200 (1981)
23. L.W. Dotchin, E.L. Chupp and D.J. Pegg, *J. Chem. Phys.* **59**, 3960 (1973)

### High Resolution Double-Resonance Spectroscopy On Rydberg States Of CO

*M. Drabbels, J. Heinze, J.J. ter Meulen and W.L. Meerts  
Department of Molecular and Laser Physics, University of Nijmegen,  
Toernooiveld, 6525 ED Nijmegen, The Netherlands*

#### Abstract

The Rydberg states  $L^1\Pi(v=0)$ ,  $L'^1\Pi(v=1)$ ,  $K^1\Sigma^+(v=0)$ ,  $W^1\Pi(v=0)$  and  $W'^1\Pi(v=2)$  have been studied in a 2+1 double-resonance excitation scheme with a resolution of  $0.005\text{ cm}^{-1}$ . Accurate molecular constants have been derived for these states. From the observed linewidths of individual rotational transitions predissociation rates for the Rydberg states have been deduced. For the first time a clear  $J$ - and  $e/f$ -dependence for the predissociation of CO has been observed. One of the states causing the observed predissociation could be identified as the  $D'^1\Sigma^+$  state.

## 8.1 Introduction

Carbon monoxide is believed to be the most abundant interstellar molecule after  $\text{H}_2$  and its isotopic variants. It is therefore an important tracer for  $\text{H}_2$ , which in most cases can not be detected directly in interstellar clouds, circumstellar envelopes and in planetary and cometary atmospheres. The ratio abundance of CO to that of  $\text{H}_2$  is difficult to determine from observations but can be derived by complex theoretical models [1]. One of the most important but also one of the most uncertain parameters in these models is the photodissociation rate of CO in the wavelength range between 91.2 nm, the absorption continuum of atomic hydrogen, and 111.8 nm corresponding to the dissociation limit of CO [2].

Some years ago Letzelter *et al.* [3] recorded the absorption spectrum in this wavelength range and derived photoabsorption cross sections and predissociation rates. As an important result it was established that the XUV photodissociation of CO takes place rather via discrete line absorption than via continuous absorption. Since then many experiments have been performed to determine accurate photoabsorption cross sections [4, 5, 6], line positions and photodissociation rates for the electronic states in the XUV region. Employing a 10 m VUV spectrograph Eidelsberg *et al.* [7, 8, 9, 10] performed the most extensive study on CO in the region between 91.2 and 115.2 nm. Most of the observed electronic states could be assigned to members of Rydberg series converging to the  $X^2\Pi$  and  $A^2\Pi$  states in the  $\text{CO}^+$  ion and molecular constants for the four most important isotopes of CO were obtained. Recently Levelt *et al.* [11, 12] accurately determined the absolute line positions for most of the Rydberg states observed by Eidelsberg *et al.* using a laser based XUV spectrometer calibrated to the  $\text{I}_2$  standard. In addition to direct XUV absorption spectroscopy other detection schemes can be applied. Optogalvanic spectroscopy has been applied to study inter-Rydberg transitions in CO [13, 14, 15, 16]. Accurate molecular constants for the involved Rydberg states were obtained. Furthermore, different REMPI [17, 18, 19] and four-wave mixing schemes [20, 21] have been applied to study the Rydberg states of CO.

In this paper we present a high resolution study on 5 Rydberg states in the energy range between 102 300 and 103 500  $\text{cm}^{-1}$ , *i.e.* the  $L(4p\pi)^1\Pi(v=0)$ ,  $L'(3d\pi)^1\Pi(v=1)$  and  $K(4p\sigma)^1\Sigma^+(v=0)$  states all converging to the electronic ground state of  $\text{CO}^+$ , the  $W(A^2\Pi)(3s\sigma)^1\Pi(v=0)$  state converging to the first electronically excited state  $A^2\Pi$  of  $\text{CO}^+$  and the  $W'^1\Pi(v=2)$  which is most probably a valence state. Besides molecular constants also predissociation rates for the different electronic states are determined.

The method used here to study the Rydberg states of CO is similar to the method used by Klopotek and Vidal [22] who after populating a single rotational level in the  $A^1\Pi$  state of CO probed the  $E^1\Pi$  state with a second laser. The detection scheme we used to study Rydberg states in carbon monoxide is given in Figure 8.1. In a first step the CO molecules are two-photon excited from the ground state  $X^1\Sigma^+(v=0)$  to a single rotational level in the  $B^1\Sigma^+(v=0)$  state. The B state can be populated either via  $\Delta J=0$  or via  $\Delta J=\pm 2$  transitions, which are however two to three orders of magnitude weaker than the  $\Delta J=0$  transitions. The population of the B state is monitored by detecting the strong fluorescence from the  $B^1\Sigma^+$  to the  $A^1\Pi$  state. In the second step the molecules are further excited by a second (probe) laser from the B state to a higher lying Rydberg state. A transition to a Rydberg state causes a depletion of the B state and can therefore be detected by a decrease of the  $B \rightarrow A$  fluorescence. By scanning the probe laser a laser-depleted fluorescence dip spectrum of the inter-Rydberg transition is obtained. Employing a Fourier limited pulsed laser system for the second step, accurate linewidth measurements can be performed yielding precise predissociation rates for the Rydberg states.

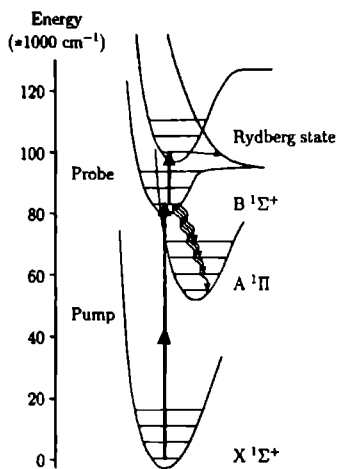


Figure 8.1: Detection scheme used to study Rydberg states of CO.

## 8.2 Experimental

A schematic overview of the experimental setup is given in Figure 8.2. Two different laser systems are used in the experiments. Either laser system can be used as pump laser or as probe laser. Both laser systems are simultaneously pumped by a Q-switched Nd:YAG laser (Quantel YG 681C-10). The third harmonic of the Nd:YAG laser with a pulse energy of 200 mJ is used to pump the laser system which induces the  $B \leftarrow X$  transition. The second harmonic of the Nd:YAG laser, pulse energy about 300 mJ, is used to pump the probe laser. One laser system is a commercial pulsed dye laser (Continuum TDL60). When used as pump laser the dye laser is operated on Coumarin 460 dye. The output of the laser is frequency doubled in a BBO crystal yielding 3 mJ of radiation at 230 nm. When used as probe laser the laser operates on DCM dye yielding 60 mJ of tunable light between 605-655 nm with a bandwidth of  $0.1 \text{ cm}^{-1}$ . The absolute frequency of the dye laser is measured with a calibrated monochromator and can be determined within  $0.5 \text{ cm}^{-1}$ . Relative frequency measurements are performed by recording the transmission fringes of a Fabry-Perot interferometer with a free spectral range of  $0.6634 \pm 0.0002 \text{ cm}^{-1}$ .

The other laser system is a pulsed dye amplifier (PDA) system. When used as pump laser the output of a single-frequency ring dye laser (Spectra Physics 380 D), operating on Stilbene 3 dye, is amplified by a home-built PDA system, operating on Coumarin 460. In this way radiation with a bandwidth of 235 MHz and a pulse energy of 10 mJ is obtained. After frequency doubling in a BBO crystal radiation around 230 nm is obtained with a pulse energy of about 1 mJ. When used as probe laser the system is operated on DCM dye. The bandwidth of the amplified laser beam is in this case 135 MHz whereas the pulse energy is typically 50 mJ. The fact that the bandwidth of the system is smaller when operated in the red than when operated in the blue is caused by the fact that the pulse length of the second harmonic of the Nd:YAG laser is somewhat longer than that of the third harmonic. For absolute frequency measurements the  $I_2$  or  $Te_2$  absorption spectrum [23, 24, 25] is recorded simultaneously with the excitation or fluorescence dip spectrum.



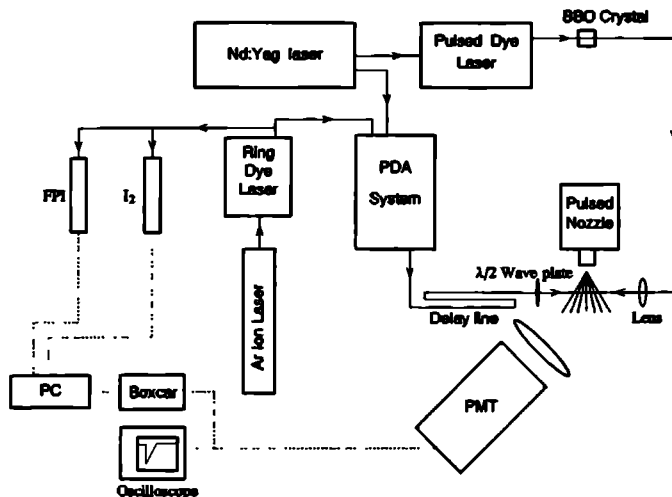


Figure 8.2: Schematic overview of the experimental setup.

For relative frequency calibration the transmission peaks of a pressure and temperature stabilized interferometer with a free spectral range of  $299.84 \pm 0.05$  MHz are recorded.

A molecular jet is formed by expanding 2 atm neat CO into a vacuum chamber through an electromagnetic pulsed valve operating at 10 Hz with an orifice of 1 mm. The molecular jet is 50 mm downstream of the nozzle crossed by the two counter-propagating laser beams. The pump laser is softly focussed by a lens ( $f=500$  mm) into the jet in order to excite the CO molecules to a single rotational level in the  $B^1\Sigma^+(v=0)$  state. The fluorescence from  $B^1\Sigma^+(v=0) \rightarrow A^1\Pi$  is collected by a quartz lens system and imaged onto a photomultiplier. In order to reduce the scattered light a Schott KV 370 glass filter is placed in front of the photomultiplier. The fluorescence signal is processed by a digital oscilloscope (LeCroy 7400) and two boxcar integrators (SRS 250) interfaced with a Personal Computer. The probe laser with a diameter of 2 mm counter-propagates the pump laser and is delayed 10 ns with respect to the pump laser by a delay line of 3 m. The fluorescence during the first few nanoseconds, which is proportional to the initial population of the B state, is used to normalize the fluorescence detected after the probe laser is fired. By introducing a delay between the pump and probe laser coherence effects such as, for example, Autler-Townes splittings [26] are avoided. When the molecules are excited to the B state only some specific  $M$ -components of a rotational level are populated, due to selection rules. The fraction of molecules in this rotational level that can be excited to a Rydberg state depends therefore strongly on the polarization of the probe laser. In order to be able to excite all the molecules the polarization of the probe laser can be adjusted by a  $\lambda/2$  wave plate.

### 8.3 Determination of predissociation rates

The predissociation rate of a Rydberg state is determined by measuring the width of the transition from the  $B^1\Sigma^+(v=0)$  to this Rydberg state. Assuming that the radiative decay rates for both the B state and the Rydberg state are much smaller than the predissociation rate of the Rydberg

state the predissociation rate is given by:

$$k_p = 2\pi\Gamma \quad (8.1)$$

where  $\Gamma$  is the linewidth (FWHM) of the transition observed. The corresponding lifetime of this state is then given by:

$$\tau = \frac{1}{k_p} = \frac{1}{2\pi\Gamma} \quad (8.2)$$

The linewidths observed in the present experiment are however not only determined by predissociation but also by the linewidth of the probe laser. The laser has a Gaussian line shape and the line profile observed will therefore be a Voigt profile. It has been shown [27] that the Lorentzian linewidth, in this case caused by the predissociation, is related to the observed linewidth by:

$$\Delta\nu_L = \Delta\nu_{obs} - \frac{(\Delta\nu_G)^2}{\Delta\nu_{obs}} \quad (8.3)$$

where  $\Delta\nu_L$ ,  $\Delta\nu_G$  and  $\Delta\nu_{obs}$  are the Lorentzian, Gaussian and observed linewidth, respectively. In our case the linewidth of the probe laser is much smaller than the observed linewidth and the Lorentzian linewidth is therefore almost equal to the observed linewidth.

In the present experiment a transition to a Rydberg state is observed by a depletion of the intermediate B  $^1\Sigma^+$  state. However, if a large fraction of the CO molecules in this intermediate state is excited to a Rydberg state the width of the transition will increase due to saturation broadening. In order to determine the effect of saturation broadening on the linewidth we performed calculations on a two-level scheme. Since in our case the predissociation rate of the upper level is much larger than the excitation rate, rate equations can be used instead of the optical Bloch equations [28]. We start with the assumption that the experiment can be described by a two-level scheme as indicated in Figure 8.3, thus neglecting the extra loss channel introduced by ionization after absorbing one more photon of the probe laser. Although the ionization rate can not be exactly determined, since

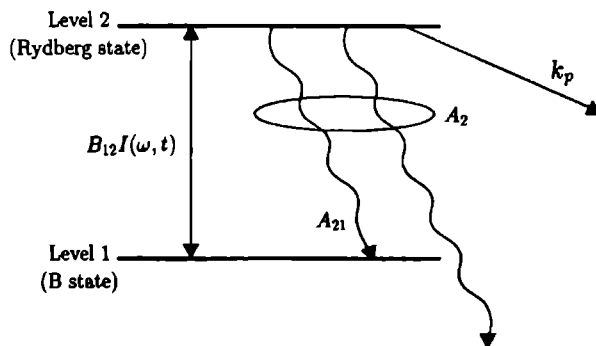


**Figure 8.3:** The two-level scheme used to calculate line broadening effects.  $A_1$  is the total radiative decay rate of the B state,  $A_2$  the total radiative decay rate of the Rydberg state,  $A_{21}$  the radiative decay rate from the Rydberg state to the B state,  $B_{12}$  the usual line integrated Einstein coefficient,  $I(t, \omega)$  the laser intensity and  $k_p$  the predissociation rate.

he ionization cross sections of the Rydberg states involved are not known, it can be estimated from the ground state ionization cross section [29] and the laser intensity used ( $5 \cdot 10^4 \text{ W/cm}^2$ ) to be several orders of magnitude smaller than the radiative decay rate and excitation rate, justifying the previously made assumption. In the calculations we furthermore assume that at time  $t=0$  the B state is instantaneously populated by the pump laser. The rate equations describing the temporal behavior of the populations in the different levels are given by:

$$\frac{dN_1}{dt} = -B_{12}I(t, \omega)G(\omega)(N_1 - \frac{g_1}{g_2}N_2) - A_1N_1 + A_{21}N_2 \quad (8.4)$$

$$\frac{dN_2}{dt} = B_{12}I(t, \omega)G(\omega)(N_1 - \frac{g_1}{g_2}N_2) - (A_2 + k_p)N_2 \quad (8.5)$$

Here  $N_1$  and  $N_2$  are the time dependent population in the  $B^1\Sigma^+$  and Rydberg state, respectively, and  $g_1$  and  $g_2$  are the degeneracy of the two states involved.  $A_1$  is the total radiative decay rate of the B state,  $A_2$  the total radiative decay rate of the Rydberg state,  $A_{21}$  the radiative decay rate from the Rydberg state to the B state and  $B_{12}$  is the usual line integrated Einstein coefficient,  $G(\omega)$  is a Lorentzian lineshape function,  $k_p$  the predissociation rate of the Rydberg state and  $I(t, \omega)$  the laser intensity of the probe laser. For the laser intensity a Gaussian time profile with a maximum intensity at  $t=10 \text{ ns}$  and a width of  $5 \text{ ns}$  is assumed. The term  $B_{12}I(t, \omega)G(\omega)$  is then given by:

$$B_{12}I(t, \omega)G(\omega) = \frac{k_p}{(\omega - \omega_0)^2 + k_p^2} B_{12}I_0 e^{-(10-t)^2 / (\frac{5}{2\sqrt{\ln 2}})^2} \quad (8.6)$$

Here  $\omega$  is the laser frequency and  $\omega_0$  is the center frequency of the transition.

These rate equations are solved numerically as a function of the laser frequency. In these calculations a value of  $3.3 \cdot 10^7 \text{ s}^{-1}$  is used for  $A_1$ , corresponding to a lifetime of  $30 \text{ ns}$  for the B

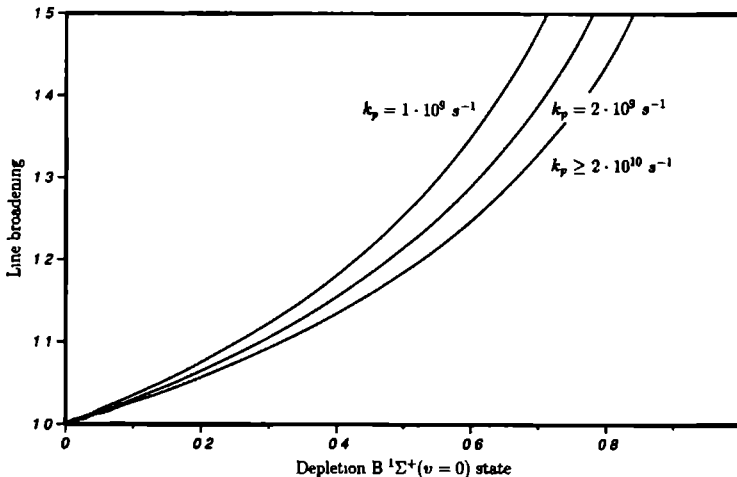


Figure 8.4: Calculated line broadening as a function of the depletion of the B state for different predissociation rates,  $k_p$ , of the upper state.

state, see section 8.4.1. The values for  $A_2$  and  $A_{21}$  are however not known. For  $A_2$  we assumed a value of  $1 \cdot 10^8 \text{ s}^{-1}$ . This value corresponds to a lifetime of 10 ns for the Rydberg state, a value common for low-lying Rydberg states in CO. For  $A_{21}$  a value of  $1 \cdot 10^6 \text{ s}^{-1}$  is assumed. To simulate the experiment where the  $B \rightarrow A$  fluorescence is monitored by a boxcar integrator with its gate set 20 ns after the pump laser the quantity describing this fluorescence,  $A_1 N_1$ , is integrated for times greater than 20 ns. From the resulting calculated line shape the width and the depth of the fluorescence dip are determined. This procedure has been performed for different laser intensities. The results obtained hardly depend on the values for  $A_{21}$  and  $A_2$  but vary strongly with the predissociation rate  $k_p$ . Figure 8.4 shows the extra broadening due to saturation of the transition as a function of the depletion of the B state for different values of the predissociation rate. The broadening due to saturation is larger for small values of  $k_p$  and becomes independent of  $k_p$  for values  $k_p \geq 2 \cdot 10^{10} \text{ s}^{-1}$ . For a depletion smaller than 40% the variation in power broadening is smaller than 5% for values of  $k_p$  greater than  $1 \cdot 10^9 \text{ s}^{-1}$ . This variation is well within the experimental error at which the linewidth can be determined, see section 8.4. In the experiment performed the laser power of the probe laser is kept low so that the depletion of the B state is always smaller than 40%. In this case the correction for the saturation broadening can be assumed to be independent of the predissociation rate  $k_p$ .

## 8.4 Results

### 8.4.1 B ( $3s\sigma$ ) $^1\Sigma^+$ state

The B  $^1\Sigma^+$  state is the first member of the ( $ns\sigma$ ) Rydberg series converging to the electronic ground state of the carbon monoxide ion. It has been studied extensively in both absorption [7, 30] and emission [7, 31]. Eidelsberg *et al.* [7] concluded that the B  $^1\Sigma^+$  state is perturbed by another nearby lying state which causes high rotational and vibrational levels in the B state to predissociate. The B  $^1\Sigma^+ \leftarrow X^1\Sigma^+$  transition has also been studied using two-photon spectroscopy [32, 33]. In this case only Q- and O- and S-branches can be observed. Due to the fact that the potential of the B state is similar to that of the ground state the difference in the rotational constants is very small. As a consequence the Q-branch, at least for low  $J$ -values, can not be resolved with a normal pulsed dye laser. The O and S transitions can easily be resolved but their intensity is two to three orders of magnitude lower than that of the Q-branch. However, with the high power laser systems now available they can be observed [33].

The two-photon excitation spectrum of the B  $^1\Sigma^+(v=0) \leftarrow X^1\Sigma^+(v=0)$  transition is shown in Figure 8.5. As can be seen in the figure the Q-branch can just be resolved with our resolution of 760 MHz, which is largely determined by the bandwidth of the laser system. Due to the low rotational temperature of 4 K only the lowest 5 rotational levels can be observed. This makes it possible to observe also transitions of the  $^{13}\text{C}^{16}\text{O}$  and  $^{12}\text{C}^{18}\text{O}$  isotopic species in natural abundance. The B  $^1\Sigma^+(v=1) \leftarrow X^1\Sigma^+(v=0)$  transition is much weaker due to the Franck-Condon factor and therefore only the Q-branch could be observed. The rotational constant in the  $v=1$  is so close to that one of the ground state that the Q-branch could not be resolved. The observed transitions together with their assignments are listed in Table 8.1.

The observed line frequencies have been fit to the following expression for a  $^1\Sigma^+ \leftrightarrow ^1\Sigma^+$  transition:

$$\nu = T_v + B'_v J'(J' + 1) - D'_v J'^2(J' + 1)^2 - [B''_0 J''(J'' + 1) - D''_0 J''^2(J'' + 1)^2] \quad (8.7)$$

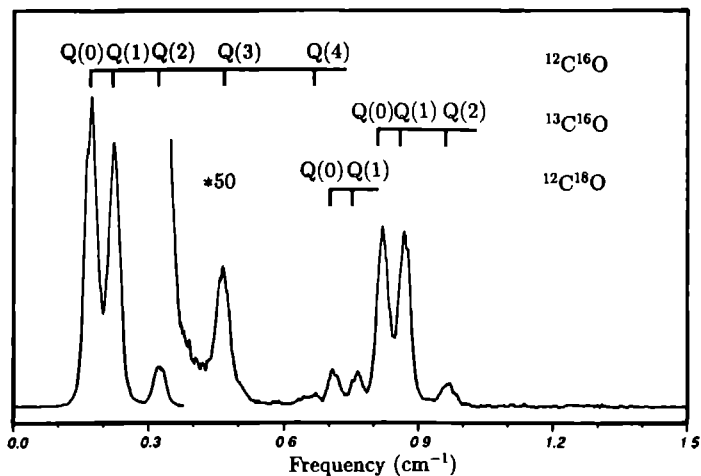


Figure 8.5: Excitation spectrum of the  $B^1\Sigma^+(v=0) \leftarrow X^1\Sigma^+(v=0)$  transition around  $86\,916\text{ cm}^{-1}$ .

Isotope	Transition	Obs. freq.	Obs.-calc.
$^{12}\text{C}^{16}\text{O}$ ( $v' = 0$ )	Q(0)	86 916.149(3)	-0.001
	Q(1)	86 916.204(3)	0.002
	Q(2)	86 916.306(3)	0.001
	Q(3)	86 916.458(3)	0.002
	Q(4)	86 916.652(9)	-0.012
	S(0)	86 927.839(3)	0.001
	S(1)	86 935.682(3)	0.001
$^{12}\text{C}^{18}\text{O}$ ( $v' = 1$ )	Q(0)	88 998 32(3)	-0.001
	Q(1)	88 998 32(3)	0 001
	Q(2)	88 998.32(3)	0.003
$^{13}\text{C}^{16}\text{O}$ ( $v' = 0$ )	Q(0)	86 916.812(3)	-0.001
	Q(1)	86 916.863(3)	0.001
	Q(2)	86 916.960(3)	-0.001
$^{12}\text{C}^{18}\text{O}$ ( $v' = 0$ )	Q(0)	86 916.706(3)	-0.001
	Q(1)	86 916.756(3)	0.001

Table 8.1: Observed and calculated line positions ( $\text{cm}^{-1}$ ) of the  $B^1\Sigma^+(v') \leftarrow X^1\Sigma^+(v''=0)$  transition for different isotopic species of CO.

Here  $B'_v, D'_v, J'$  and  $B''_0, D''_0, J''$  refer to the upper and ground state respectively. The rotational constants for the ground state were kept fixed in the least squares fit at the values obtained by Guelachvili *et al.* [34]. The centrifugal distortion constants,  $D'_v$ , for the B state were fixed at the values derived by Eidelsberg *et al.* [7]. The resulting rotational constants for the B state are given in Table 8.2. The agreement between our results and those of Eidelsberg *et al.* [7] are excellent, with one exception however, the value of  $T_0$  for the  $^{12}\text{C}^{18}\text{O}$  isotopomer.

The radiative lifetimes for the vibrational levels in the B state have been measured in many different ways. There is, however, a rather large spread in the values found for the lifetimes. This is caused by the fact that in most of the experiments fluorescence trapping and cascading effects play an important role. In our experiment no cascading effects can occur since only one rotational level in the B state is excited and only the  $B \rightarrow A$  fluorescence is detected. Fluorescence trapping can occur but by diluting the CO fraction in Ar down to 2% this effect can be avoided. The lifetimes for the different isotopes of CO have been measured on several rotational transitions. The values found are listed in Table 8.2 and are equal for the different isotopic species. The lifetime for the  $B(v=1)$  state is measured to be shorter than that for the  $B(v=0)$  state by almost a factor of 1.5. The *ab initio* calculations of Cooper and Langhof [35] and Kirby and Cooper [36] on the B state show a similar effect for the lifetimes of the two vibrational levels. They pointed out that this effect is caused by a strong dependence of the transition moment on the internuclear distance.

		$B$ (cm $^{-1}$ )	$D$ (cm $^{-1}$ )	$T_v$ (cm $^{-1}$ )	$\tau$ (ns)
$^{12}\text{C}^{16}\text{O}$	$v' = 0$	1.94816(23)	$6.8 \cdot 10^{-6}$ <sup>a)</sup>	86 916.1501(19)	29.3(1.6)
	$v' = 1$	1.921902 <sup>a)</sup>	$7.4 \cdot 10^{-6}$ <sup>a)</sup>	88 998.32(3)	19.8(1.3)
$^{13}\text{C}^{16}\text{O}$	$v' = 0$	1.86274(44)	$6.2 \cdot 10^{-6}$ <sup>a)</sup>	86 916.8110(19)	29.6(1.6)
$^{12}\text{C}^{18}\text{O}$	$v' = 0$	1.85553 <sup>a)</sup>	$6.2 \cdot 10^{-6}$ <sup>a)</sup>	86 916.7047(19)	29.2(1.6)

<sup>a)</sup> Kept fixed in the fit at the value obtained by Eidelsberg *et al.* [7].

**Table 8.2:** Molecular constants for the  $B \ ^1\Sigma^+$  state of different isotopic species of CO.

#### 8.4.2 L ( $4p\pi$ ) $^1\Pi(v=0)$ state

The L state is a member of the ( $n\pi\pi$ ) Rydberg series converging to the ionic ground state  $X \ ^2\Sigma^+$  of  $\text{CO}^+$ . It has been studied by direct XUV absorption spectroscopy [8, 10, 12] and by optogalvanic spectroscopy via the  $L \ ^1\Pi(v=0) \leftarrow B \ ^1\Sigma^+(v=0)$  transition [13, 14]. From these measurements it is known that the L state interacts with another state which causes an accidental perturbation of the  $J=7$  level of the  $f \ \Lambda$ -doublet component.

The L state is measured using the pulsed dye laser as pump laser to populate one specific rotational level in the B state via an S transition. The PDA system is then used to probe the L state. The observed line frequencies of the  $L \ ^1\Pi(v=0) \leftarrow B \ ^1\Sigma^+$  transitions together with their assignments are listed in Table 8.3. The observed line frequencies have been fit to the following expressions for a  $^1\Pi \leftarrow ^1\Sigma^+$  transition:

$$\nu_{\Pi^+} = \nu_0 + B'_e J'(J'+1) - D' J'^2 (J'+1)^2 - [B'' J''(J''+1) - D'' J''^2 (J''+1)^2] \quad (8.8)$$

$$\nu_{\Pi^-} = \nu_0 + B'_f J'(J'+1) - D' J'^2 (J'+1)^2 - [B'' J''(J''+1) - D'' J''^2 (J''+1)^2] \quad (8.9)$$

Transition	Obs freq	Obs -calc	$\Gamma$
P(2)	16347 913(6)	-0 003	0 023(2)
P(3)	16344 157(6)	0 003	0 047(6)
Q(2)	16355 712(6)	0 002	0 0096(13)
Q(3)	16355 779(6)	0 002	0 0098(11)
R(2)	16367 691(16)	-0 002	0 088(8)
R(3)	16371 884(32)	0 012	0 188(14)

**Table 8.3:** Observed and calculated line frequencies ( $\text{cm}^{-1}$ ) and observed linewidths ( $\text{cm}^{-1}$ ) of the  $L^1\Pi(v'=0) \leftarrow B^1\Sigma^+(v''=0)$  transition

Here expression (8 8) describes transitions to the  $\Pi^+$  ( $e$ )  $\Lambda$ -doublet component probed by P and R transitions and expressions (8 9) transitions to the  $\Pi^-$  ( $f$ )  $\Lambda$ -doublet component probed by Q transitions It is assumed that the centrifugal distortion constant  $D'$  is equal for both  $\Lambda$ -doublet components The rotational constants for the B state were kept fixed in the fit at the values given in Table 8 2 The resulting molecular constants for the L state are given in Table 8 4 together with the constants found in references [8, 10, 12, 13, 14] The  $\Lambda$ -doubling parameter  $q_\pi$  is given by the relation.

$$q_\pi = |B'_e - B'_f| \quad (8\ 10)$$

The constant  $T_0$  for the L state can be calculated by adding the value of  $T_0$  of the B state to that of the  $\nu_{00}$  for the  $L \leftarrow B$  transition

From the work of Letzelter *et al* [3], which is reproduced by Eidelsberg and Rostas [8], it is known that the L state predissociates and that the lifetime is of the order of 100 ps In the present work the lifetime is deduced from the widths of the transitions observed The observed line profiles are therefore fit to a Lorentzian line profile Since the homogeneous line broadening caused by the predissociation is much larger than the bandwidth of the probe laser, no large error is introduced by fitting the observed transition to a Lorentzian line profile The linewidths obtained are then corrected for saturation broadening as described in section 8 3 Figure 8 6 shows the observed Q(2) transition together with the fitted line profile Although the line profile observed is quite noisy the linewidth can still be determined with an accuracy of 10% As can be seen from Table 8 3 the linewidth depends strongly on the rotational level observed When the linewidths are plotted as a function of  $J(J+1)$ , as is done in Figure 8 7, it can be seen that for the  $f$ -component the linewidth is independent of  $J$  whereas for the  $e$ -component the linewidth is proportional to  $J(J+1)$  The observed linewidths for the  $e$ -component are therefore fit to the following expression for the linewidth

$$\Gamma_e = \Gamma_{0e} + \alpha_e J(J+1) \quad (8\ 11)$$

The observed linewidths are very well described by this expression except for  $J=4$  The calculated linewidth of  $0\ 138\ \text{cm}^{-1}$  for this level is considerable smaller than the observed width of  $0\ 181(20)\ \text{cm}^{-1}$  Probably this level is locally perturbed, like the  $J=7$  level of the  $f$ -component, by a crossing with a (pre)dissociating state The predissociation rate for the  $e$ -component is now

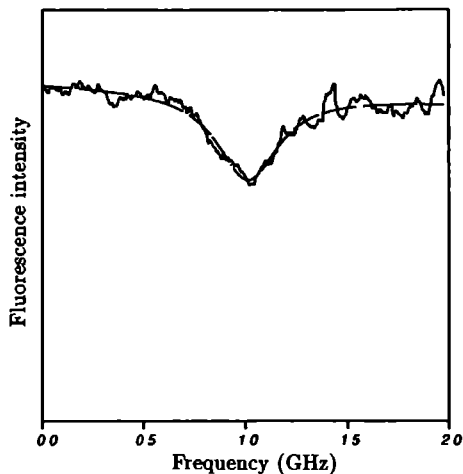


Figure 8.6: Observed line profile of the  $L^1\Pi(v'=0) \leftarrow B^1\Sigma^+(v''=0) Q(2)$  transition (solid line) and calculated Lorentzian line profile with a linewidth (FWHM) of  $0.0097 \text{ cm}^{-1}$  (dashed line).

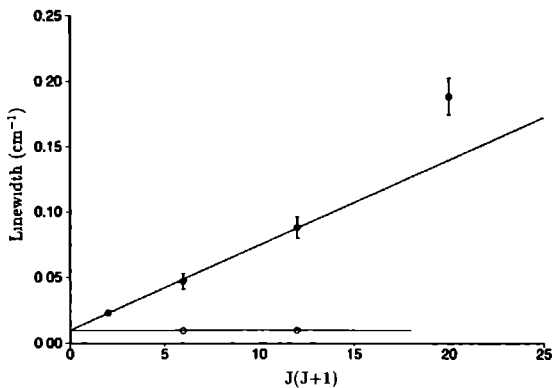


Figure 8.7: Observed linewidths ( $\text{cm}^{-1}$ ) for the  $f$ -levels (open dots) and the  $e$ -levels (filled dots) of the  $L^1\Pi(v=0)$  state as function of  $J(J+1)$ .



best described by:

$$k_{pe} = k_{0e} + k_{\alpha_e} J(J+1) \quad (8.12)$$

with  $k_{0e} = 2\pi\Gamma_{0e}$  and  $k_{\alpha_e} = 2\pi\alpha_e$ . The resulting values from the least squares fit for the parameters describing the linewidth and predissociation rate are given in Table 8.4. The obtained lifetimes for the  $f$ -levels are nearly an order of magnitude larger than the values reported by Eidelsberg and Rostas [8].

	This work	Ref. [8, 10]	Ref. [12]	Ref. [13, 14]
$B_e$	1.98173(53)	1.9796(18)	–	1.998(14)
$B_f$	1 95972(36)	–	a)	1.95968(24)
$D$	$6.7 \cdot 10^{-8}$ a)	$9(3) \cdot 10^{-8}$	a)	$6.7(1) \cdot 10^{-8}$
$q_\pi$	0.02201(40)	–	a)	0.0213(12)
$\nu_{00}$	16 355 6420(30)	–	–	16 355.660(12)
$T_0$	103 271 7921(41)	103 271.9(1)	103 271.87(2)	103 271.808(12)
$\Gamma_{0f}$	0 0097(7)	–	–	–
$\Gamma_{0e}$	0.0101(4)	–	–	–
$\alpha_e$	0.00635(10)	–	–	–
$k_{0f}$	$1.83(13) \cdot 10^9$	$1 \cdot 10^{10}$	$< 3 \cdot 10^{10}$	–
$k_{0e}$	$1.91(7) \cdot 10^9$	$1 \cdot 10^{10}$	b)	–
$k_{\alpha_e}$	$1 20(2) \cdot 10^9$	–	b)	–

a) Kept fixed in the fit at the value obtained by Sekine *et al.* [14]

b) In a recent study on the L state a  $J$ -dependent linewidth was observed for the  $e$ -levels [37]

**Table 8.4:** Molecular constants ( $\text{cm}^{-1}$ ), linewidth ( $\text{cm}^{-1}$ ) and predissociation rate ( $\text{s}^{-1}$ ) for the  $L^1\Pi(v=0)$  state of CO.

### 8.4.3 $L'(3d\pi)^1\Pi(v=1)$ state

Since the  $L^1\Pi(v=1)$  state and the  $L^1\Pi(v=0)$  state are very close in energy the two bands overlap when observed by low resolution spectroscopy. In the present experiment where we start from one rotational level in the B state these two states can easily be separated. The B state is populated by the PDA system after which the  $L'$  state is probed by the pulsed dye laser. Figure 8.8 shows a scan of the dye laser after populating the  $J=2$  level in the B state. The intensities of the different transitions directly reflect the Hönl-London factors for these transitions. The transitions frequencies together with their assignments are listed in Table 8.5. The observed frequencies have been fit to a  $^1\Pi \leftarrow ^1\Sigma^+$  transition. The resulting molecular constants are listed in Table 8.6. For comparison the molecular constants found by Eidelsberg *et al.* [8, 10], Levelt *et al.* [12] and Sekine *et al.* [15] have also been included in this table.

Transition	Obs. freq.	Obs.-calc.	$\Gamma$
P(2)	16 287 41(6)	0.01	1.13(9)
P(3)	16 282.86(6)	-0.04	1.27(14)
Q(1)	16 295.15(6)	0.01	1.27(9)
Q(2)	16 294.40(6)	0.01	1.26(9)
Q(3)	16 293.22(6)	0.05	1.24(14)
R(0)	16 299.10(6)	-0.01	1.21(7)
R(1)	16 302.38(6)	-0.01	1.21(6)
R(2)	16 305.35(6)	0.01	1.24 (8)
R(3)	16 308.02(6)	0.01	1.11(17)

**Table 8.5:** Observed and calculated line positions ( $\text{cm}^{-1}$ ) and observed linewidths ( $\text{cm}^{-1}$ ) of the  $L' \ ^1\Pi(v'=1) \leftarrow B \ ^1\Sigma^+(v''=0)$  transition. The values given in parentheses are the relative errors for the measured line positions. The absolute uncertainty in the line positions is  $0.5 \text{ cm}^{-1}$ .

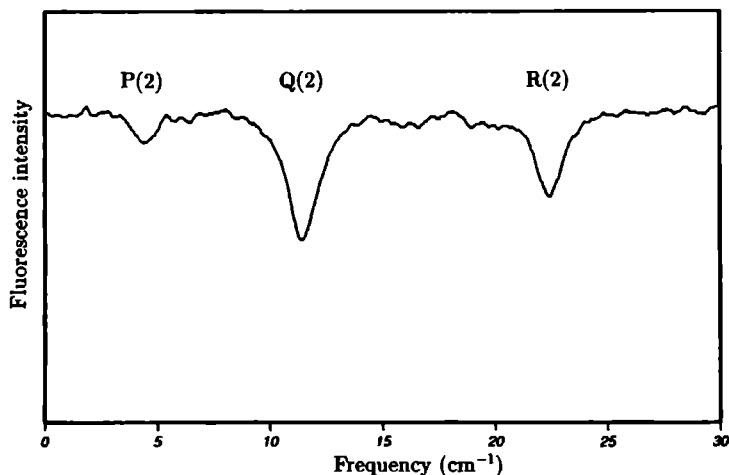


**Figure 8.8:** The laser-depleted fluorescence dip spectrum of the  $L' \ ^1\Pi(v'=1) \leftarrow B \ ^1\Sigma^+(v''=0)$  transition after populating the  $J=2$  level in the  $B$  state.

	This work	Ref. [8, 10]	Ref. [12]	Ref. [16]
$B_e$	1.7931(15)	1.7966(23)	<sup>a)</sup>	–
$B_f$	1.7603(13)	–	–	1.7535(48)
$D$	$1.0 \cdot 10^{-5}$ <sup>a)</sup>	$1.0(5) \cdot 10^{-5}$	<sup>a)</sup>	$1.0(9) \cdot 10^{-5}$
$q_\pi$	0.0328(22)	–	–	–
$\nu_{00}$	16 295.5(5)	–	–	16 295.6(4)
$T_0$	103 211.6(5)	103 211.8(1)	103 211.88(9)	103 211.8(4)
$\Gamma$	1.22(6)	–	1.4(5)	–
$k_p$	$2.26(11) \cdot 10^{11}$	–	$2.7(9) \cdot 10^{11}$	–
$\tau$	$4.42(22) \cdot 10^{-12}$	$3 \cdot 10^{-12}$	$3.7(13) \cdot 10^{-12}$	–

<sup>a)</sup> Kept fixed in the fit at the value obtained by Eidelsberg and Rostas [8].

**Table 8.6:** Molecular constants ( $\text{cm}^{-1}$ ), linewidth ( $\text{cm}^{-1}$ ), predissociation rate ( $\text{s}^{-1}$ ) and lifetime (s) for the  $L' \ ^1\Pi(v=1)$  state.

It is well-known that the  $L'$  state undergoes a fast predissociation [3, 8, 12]. This is confirmed by our results. The observed linewidth which is  $J$ -independent, this in contrast to the  $L$  state, is  $1.22 \pm 0.06 \text{ cm}^{-1}$ . This value for the linewidth corresponds to a predissociation rate of  $(2.26 \pm 0.11) \cdot 10^{11} \text{ s}^{-1}$  and a lifetime of  $4.42 \pm 0.22 \text{ ps}$ , a value in agreement with the above mentioned experiments.

#### 8.4.4 $K(4p\sigma) \ ^1\Sigma^+(v=0)$ state

The  $K$  state is the second member ( $n=4$ ) of the ( $np\sigma$ ) Rydberg series converging to the electronic ground state of  $\text{CO}^+$ . It has been studied by several different techniques. There is, however, a rather large discrepancy in the  $B$  rotational constants found, see Table 8.8.

The  $K(v=0)$  state is measured with the same experimental setup as the  $L(v=0)$  state.

Transition	Obs. freq.	Obs.-calc.	$\Gamma$
P(2)	16 130.649(10)	–0.003	0.110(13)
P(3)	16 126.630(10)	0.003	0.122(12)
R(2)	16 149.810(10)	0.001	0.125(14)
R(3)	16 153.436(10)	–0.001	0.114(11)

**Table 8.7:** Observed and calculated line positions ( $\text{cm}^{-1}$ ) and linewidths ( $\text{cm}^{-1}$ ) of the  $K \ ^1\Sigma^+(v'=0) \leftarrow B \ ^1\Sigma^+(v''=0)$  transition.

The observed line frequencies of the  $K \ ^1\Pi(v=0) \leftarrow B \ ^1\Pi(v=0)$  transition together with their assignments are listed in Table 8.7. The observed line positions have been fit to a  $^1\Sigma^+ \leftarrow ^1\Sigma^+$  transition. The resulting molecular constants for the  $K$  state are listed in Table 8.8. The value found for the  $B$  rotational constant agrees best with the value found by Eidelsberg and Rostas [8].

It is known that already the first member of the  $(n\rho\pi)$  Rydberg series, the  $E \ ^1\Pi(v=0)$  state, predissociates. Also the  $K \ ^1\Pi$  state is known to predissociate. Levelt *et al.* [12] have deduced from the observed linewidths a predissociation rate of  $(2.7\pm 1.8)\cdot 10^{10} \text{ s}^{-1}$  for this state. In the present experiment we found that the predissociation rate is independent of the rotational level and has a value of  $(2.22\pm 0.13)\cdot 10^{10} \text{ s}^{-1}$ , corresponding to a lifetime of  $45\pm 3 \text{ ps}$ .

	This work	Ref. [8, 10]	Ref. [12]	Ref. [13]
$B$	1.91653(22)	1.91664(27)	1.9159(2)	1.900(2)
$D$	$5.85\cdot 10^{-5}$ <sup>a)</sup>	$6.0(1)\cdot 10^{-5}$	$5.85(6)\cdot 10^{-5}$	$5.3\cdot 10^{-5}$
$\nu_{00}$	16 138.5037(48)	–	–	16 138.08(8)
$T_0$	103 054.6590(72)	103 054.57(2)	103 054.71(2)	103 054.23(8)
$\Gamma$	0.118(7)	–	0.14(10)	–
$k_p$	$2.22(13)\cdot 10^{10}$	–	$2.7(18)\cdot 10^{10}$	–
$\tau$	$4.50(27)\cdot 10^{-11}$	$1\cdot 10^{-10}$	$3.7(25)\cdot 10^{-11}$	–

<sup>a)</sup> Kept fixed in the fit at the value determined by Levelt *et al.* [12].

Table 8.8: Molecular constants ( $\text{cm}^{-1}$ ), linewidth ( $\text{cm}^{-1}$ ), predissociation rate ( $\text{s}^{-1}$ ) and lifetime (s) found for the  $K \ ^1\Sigma^+(v=0)$  state.

#### 8.4.5 $W (A^2\Pi) (3s\sigma) \ ^1\Pi(v=0)$ state

The  $W \ ^1\Pi$  state is the first member of the  $(1\pi)^3 (ns\sigma)$  Rydberg series converging to the first electronically excited state,  $A \ ^2\Pi$ , in the  $\text{CO}^+$  ion. The rotational and vibrational constants determined for this state are quite different from the constants found for Rydberg states converging to the ionic ground state and are close to the constants for the  $A \ ^2\Pi$  state in  $\text{CO}^+$ .

The  $W(v=0)$  state has been measured with the same experimental setup as the  $L$  and the  $K$  state. The measured line positions, see Table 8.9, have been fit to a  $^1\Pi \leftarrow ^1\Sigma^+$  transition. The resulting molecular constants for the  $W$  state are listed in Table 8.10. The  $\Lambda$ -doubling parameter  $q_\pi$  found for this state is almost equal to zero, this in contrast to the other Rydberg states converging to the ionic ground state.

From the experiments of Levelt *et al.* [12] it is known that also the  $W$  state predissociates. They obtained in their experiments a  $J$ -independent predissociation rate of  $(3.6\pm 1.9)\cdot 10^{10} \text{ s}^{-1}$ . In the present experiment we find however a  $J$ -dependent linewidth, see Table 8.10, resulting in a  $J$ -dependent predissociation rate. In Figure 8.9 the observed linewidth is plotted as a function of  $J(J+1)$ . It can directly be seen that for the  $e$ -component the linewidth is proportional to  $J(J+1)$  whereas for the  $f$ -component the linewidth is  $J$ -independent, just as is seen for the  $L$  state. The observed linewidths for the  $e$ -component have been fit to equation (8.11). The

Transition	Obs. freq.	Obs.-calc.	$\Gamma$
P(2)	15 881.923(12)	-0.008	0.065(8)
P(3)	15 876.516(24)	0.007	0.122(9)
Q(2)	15 888.219(11)	0 009	0.055(7)
Q(3)	15 885.908(11)	-0.005	0.048(6)
R(2)	15 897.584(40)	0.003	0.202(14)
R(3)	15 898.388(64)	-0.005	0.325(35)

**Table 8.9:** Observed and calculated line positions ( $\text{cm}^{-1}$ ) and observed linewidths ( $\text{cm}^{-1}$ ) of the  $W^1\Pi(v'=0) \leftarrow B^1\Sigma^+(v''=0)$  transition.

	This work	Ref. [8, 10]	Ref. [12]	Ref. [15]
$B_e$	1.5650(17)	1.56216(27)	1.5634(5)	1.5549(68)
$B_f$	1.5668(13)	-	-	-
$D$	$7.8 \cdot 10^{-5}$ <sup>a)</sup>	$7.8(9) \cdot 10^{-5}$	$8.3(2) \cdot 10^{-5}$	-
$q_\pi$	0.002(2)	-	-	-
$\nu_{00}$	15 990.500(11)	-	-	15 891.6(6)
$T_0$	102 806.650(13)	102 807 0(2)	102 806.74(2)	102 807.8(6)
$\Gamma_{0f}$	0.051(4)	-	0.19(10)	-
$\Gamma_{0e}$	0.037(2)	-	0.19(10)	-
$\alpha_e$	0.014 0(3)	-	-	-
$k_{0f}$	$9.6(8) \cdot 10^9$	$1 \cdot 10^{10}$	$3.6(19) \cdot 10^{10}$	-
$k_{0e}$	$7.0(4) \cdot 10^9$	$1 \cdot 10^{10}$	$3.6(19) \cdot 10^{10}$	-
$k_{\alpha_e}$	$2.64(6) \cdot 10^9$	-	-	-

<sup>a)</sup> Kept fixed in the fit at the value determined by Eidelsberg and Rostas [8].

**Table 8.10:** Molecular constants ( $\text{cm}^{-1}$ ), linewidth ( $\text{cm}^{-1}$ ) and predissociation rate ( $\text{s}^{-1}$ ) for the  $W^1\Pi(v=0)$  state of CO.

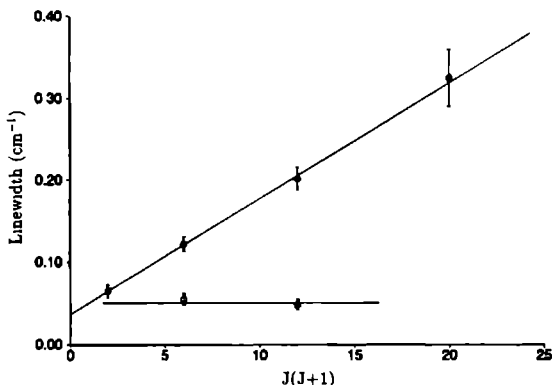


Figure 8.9: Observed linewidths ( $\text{cm}^{-1}$ ) for the  $f$ -levels (open dots) and the  $e$ -levels (filled dots) of the  $W\ ^1\Pi(v=0)$  state as function of  $J(J+1)$ .

resulting constants for the linewidths together with those for the predissociation rate are listed in Table 8.10. These results differ considerably from the results of Levelt *et al.* who obtained a  $J$ -independent predissociation for both  $\Lambda$ -doublet components. The  $J$ -dependence most probably was not observed due to the absence of high rotational  $e$ -levels in their spectra of the  $W$  state, where the extra line broadening should become observable. The fact that the higher rotational levels were not observed already indicates that the predissociation for these levels is faster than for low rotational levels.

#### 8.4.6 $W'\ ^1\Pi(v=2)$ state

The  $W'\ ^1\Pi(v=2)$  state around  $102\,310\ \text{cm}^{-1}$  has first been observed by Ogawa and Ogawa [38] in 1974. However, they were not able to assign this band to a member of a Rydberg series. Later Hammond *et al.* [39] observed this state in a threshold electron spectroscopy study on CO, but they also couldn't assign this band. Recently Eidelsberg and Rostas [8] assigned this band as the  $v=2$  level of the first member ( $n=3$ ) of the ( $A\ ^2\Pi$ ) ( $ns\sigma$ )  $^3\Pi$  Rydberg series converging to the first electronically excited state in  $\text{CO}^+$ . They based their result on the fact that the observed rotational and vibrational constants for this series are close to those of the  $A\ ^2\Pi$  state of the  $\text{CO}^+$  ion. Furthermore the observed intensity for the transition is very low as expected for a  $^3\Pi \leftarrow ^1\Sigma^+$  transition.

The  $W'(v=2)$  state has been measured with the same experimental setup as the  $L'(v=1)$  state. In order to probe higher rotational levels in the  $W'$  state the rotational temperature is increased to about 10 K by placing a skimmer between the nozzle and the detection zone. The observed line positions for the  $W'(v'=2) \leftarrow B(v''=0)$  transition are listed in Table 8.11. In a first attempt the observed line positions have been fit to a  $^3\Pi \leftarrow ^1\Sigma^+$  transition. The Hamiltonian describing a  $^3\Pi$  state is taken from reference [40]. Only the observed P and R transitions could be fit within their experimental error to this transition. The Q transitions and especially the Q transitions involving high  $J$ -levels observed by Eidelsberg *et al.* [9] could not be fit to this

Transition	Obs freq	Obs -calc	$\Gamma$
P(2)	15 387 31(10)	-0 01	2 04(15)
P(3)	15 381 48(10)	-0 01	2 30(17)
P(4)	15 374 86(10)	0 07	2 14(26)
P(5)	15 367 31(10)	0 04	2 08(44)
P(6)	15 358 94(10)	-0 03	1 89(52)
Q(1)	15 395 25(10)	-0 01	1 96(19)
Q(2)	15 393 66(10)	0 06	1 99(14)
Q(3)	15 391 13(10)	0 02	2 13(12)
Q(4)	15 387 71(10)	-0 08	2 44(28)
Q(5)	15 383 56(10)	-0 08	2 32(42)
Q(6)	15 378 74(10)	0 08	2 18(28)
R(0)	15 399 00(10)	-0 01	2 04(17)
R(1)	15 400 96(10)	-0 01	2 21(16)
R(2)	15 402 13(10)	0 07	2 13(19)
R(3)	15 402 37(10)	0 04	2 04(24)
R(4)	15 401 79(10)	-0 03	2 24(28)
R(5)	15 400 47(10)	-0 05	2 34(18)
R(6)	15 378 48(10)	0 03	2 04(50)

**Table 8.11:** Observed and calculated line positions ( $\text{cm}^{-1}$ ) and observed linewidths ( $\text{cm}^{-1}$ ) of the  $W' \ ^1\Pi(v'=2) \leftarrow B \ ^1\Sigma^+(v''=0)$  transition. The values given in parentheses are the relative errors for the measured line positions. The absolute uncertainty in the line positions is  $0.5 \text{ cm}^{-1}$ .

type of transition within their experimental error. From the fit a spin-orbit coupling constant of  $A=25 \text{ cm}^{-1}$  was obtained. For this value of the spin-orbit coupling constant the Hund's case (a) wavefunctions describing the  $^3\Pi$  state are almost completely mixed for  $J=5$ . This implies that already for relatively low  $J$ -levels transitions to the three different states,  $^3\Pi_0$ ,  $^3\Pi_1$  and  $^3\Pi_2$ , become equally probable. However, these transitions are not observed. It can therefore be concluded that the  $W'$  state is *not* a  $^3\Pi$  state. As a consequence this state can not be assigned as a member of the ( $A \ ^2\Pi$ ) ( $ns\sigma$ )  $^3\Pi$  Rydberg series. Since it can not be assigned as a member of any other Rydberg series it is most probably a high-lying valence state.

Since it is clear from combination differences that only the  $e$   $\Lambda$ -doublet components are perturbed an interaction with a  $^1\Sigma^+$  state is the most probable. The energy levels for the  $f$   $\Lambda$ -doublet components are then given by

$$E_{\Pi^-} = T_0 + B'_f J(J+1) + D'_f J(J+1) \quad (8.13)$$

The energy levels for the  $e$   $\Lambda$ -doublet components are obtained by diagonalization of the matrix describing the interaction between a  $\Pi^+$  and a  $\Sigma^+$  state [41]. On the  $|^1\Pi^+\rangle$ ,  $|^1\Sigma^+\rangle$  basis this matrix

	This work	Ref [8, 10]
$B_e$	1 53281(63)	1 5365(36)
$B_f$	1 5417(24)	—
$D$	0 8(7) $10^{-5}$	1 2(2) $10^{-5}$
$q_\pi$	0 0111(27)	—
$\nu_{00}$	15 392 5(5)	—
$T_0$	102 312 3(4)	102 311 0(2)
$B_{\Sigma^+}$	1 9 <sup>a)</sup>	—
$\eta$	0 60(5)	—
$\Delta$	16(5)	—
$\Gamma$	2 14(14)	—
$k_p$	3 86(21) $10^{11}$	—
$\tau$	2 59(14) $10^{-12}$	1 $10^{-11}$

<sup>a)</sup> Kept fixed in the least squares fit

**Table 8.12.** Molecular constants ( $\text{cm}^{-1}$ ), linewidth ( $\text{cm}^{-1}$ ), predissociation rate ( $\text{s}^{-1}$ ) and lifetime (s) for the  $W' \ ^1\Pi(v=2)$  state

is given by

$$\left( \begin{array}{l} T_0 + B'_e J(J+1) + D' J^2(J+1)^2 \\ 2\eta\sqrt{J(J+1)} \end{array} \quad \begin{array}{l} 2\eta\sqrt{J(J+1)} \\ T_0 + \Delta + B_{\Sigma^+} J(J+1) \end{array} \right) \quad (8.14)$$

Here  $B'_e$  and  $B_{\Sigma^+}$  are the rotational constants of the  $^1\Pi^+$  and  $^1\Sigma^+$  state, respectively,  $T_0$  the term value of the  $W'$  state,  $\Delta$  the energy difference and  $\eta$  the interaction strength between the two states. The transitions observed in the present experiment together with the transitions observed by Eidelsberg *et al* [9] have been fit to these expressions. Since only transitions to the  $^1\Pi$  state are observed not all the constants for the  $^1\Sigma^+$  state can be determined. The parameter  $B_{\Sigma^+}$  has therefore been fixed at  $1.9 \text{ cm}^{-1}$  a value common for Rydberg states converging to the ground state of the ion. All the observed line positions could be fit within their experimental error to this type of transition. The resulting molecular constants are listed in Table 8.12. As can be seen from Table 8.12 the perturbing  $^1\Sigma^+$  state is very close in energy,  $16 \text{ cm}^{-1}$ , to the  $W' \ ^1\Pi(v=2)$  state. The mixing between the two states is small, less than 5%, even for high  $J$ -levels, and as a consequence the transitions to the  $^1\Sigma^+$  state are too weak to be observed in the present experiment.

The linewidths observed for the  $W'(v=2)$  state are independent of the rotational level and amount to  $2.14 \pm 0.14 \text{ cm}^{-1}$ . The corresponding predissociation rate and lifetime for this state are  $(3.9 \pm 0.3) \cdot 10^{11} \text{ s}^{-1}$  and  $2.6 \pm 0.2 \text{ ps}$ , respectively.



## 8.5 Discussion

In the present experiment the term values,  $T_0$ , for three Rydberg states have been determined within  $0.01 \text{ cm}^{-1}$ . In a first step the energy levels of the  $B \ ^1\Sigma^+(v=0)$  state were accurately determined by calibrating the  $B \ ^1\Sigma^+(v'=0) \leftarrow X \ ^1\Sigma^+(v''=0)$  transition to the  $\text{Te}_2$  frequency standard [25]. In a second step the transitions from the B state to a Rydberg state were calibrated to the  $\text{I}_2$  standard [23, 24]. When our values obtained for the term values are compared with those obtained by Levelt *et al.* [12], who calibrated their transitions also to the  $\text{I}_2$  standard, a systematic difference of  $0.07 \text{ cm}^{-1}$  is observed. Although this difference is within the experimental error of  $0.13 \text{ cm}^{-1}$  given by Levelt *et al.* for the  $T_0$ , it is still significant. We therefore have checked carefully for possible lineshifts caused by saturation of the  $B \leftarrow X$  transition. The transition could, however, not be saturated by the laser power used in the present experiment and consequently no lineshifts were observed. Since we have carefully avoided saturating the transitions to the Rydberg states no lineshifts were observed for these transitions. Furthermore, lineshifts caused by the Autler-Townes effect can also be ruled out. Since there were no electric or magnetic fields present at the excitation region which can shift the energy levels we conclude that our values found for the term values of the Rydberg states are accurate within  $0.01 \text{ cm}^{-1}$ .

At an energy of about  $103\,000 \text{ cm}^{-1}$  above the ground state of CO many electronic states can be expected to interact with each other, giving rise to perturbations in the observed spectra. In section 8.4.6 it is concluded that the  $W' \ ^1\Pi(v=2)$  state is perturbed by a state of  $^1\Sigma^+$  symmetry. This  $^1\Sigma^+$  state is most probably the  $v=5$  level of the  $C(3s\sigma) \ ^1\Sigma^+$  state. The  $v=5$  level of this state is calculated to lie within  $50 \text{ cm}^{-1}$  of the  $W' \ ^1\Pi(v=2)$  state, using the values for  $\omega_e$  and  $\omega_e x_e$  given by Huber and Herzberg [42]. Direct transitions to the  $v=5$  level of the C state are, however, too weak to be observed due to the poor Franck-Condon overlap with the ground state. Although the rotational  $B$  constant for the  $C \ ^1\Sigma^+(v=5)$  could not be determined from the fit of the transitions to the  $W' \ ^1\Pi(v=2)$ , the term value for the C state could be determined as well as the interaction strength between the two states. For the term value of the C state a value of  $T_0 = 102\,328 \pm 5 \text{ cm}^{-1}$  is found. The value of  $0.6 \text{ cm}^{-1}$  for the interaction strength  $\eta$  indicates that there is a rather good Franck-Condon overlap between the two interacting states. From the observed linewidths of the  $W' \ ^1\Pi(v=2)$  state and calculated mixing between the two states limits can be given for the predissociation rate of the  $C \ ^1\Sigma^+(v=5)$  state, *i.e.*  $2 \cdot 10^{10} < k_p < 1 \cdot 10^{12} \text{ s}^{-1}$ .

Interactions of repulsive states with bound states such as the Rydberg states observed can cause predissociation of these bound states. The predissociation observed for the  $L \ ^1\Pi(v=0)$ ,  $K \ ^1\Sigma^+(v=0)$  and  $W \ ^1\Pi(v=0)$  states is most probably caused by the interaction of these states with a repulsive state of  $^1\Sigma^+$  symmetry. The interaction matrix element describing the interaction between  $^1\Pi^+$  and  $^1\Sigma^+$  states is proportional to  $\sqrt{J(J+1)}$ . This gives rise to a  $J(J+1)$ -dependent predissociation rate for the  $e$ -levels as has been observed for the  $L \ ^1\Pi(v=0)$  state and the  $W \ ^1\Pi(v=0)$  state. Since there is no interaction between a  $^1\Sigma^+$  and a  $^1\Pi^-$  state possible the  $^1\Pi^-$  state will not predissociate via the  $^1\Sigma^+$  state. The linewidths observed for the  $f$ -levels indicate, however, that these levels also predissociate, probably due to weak interactions with dissociating states of other symmetry.

The  $J$ -independent linewidth,  $\Gamma_{0e}$  found for the  $e$ -levels and the linewidths found for the  $f$ -levels of the  $L \ ^1\Pi(v=0)$  correspond to a lifetime of  $0.55 \pm 0.03 \text{ ns}$ . It can well be that this lifetime is solely determined by the radiative lifetime of the L state. A similar value for the radiative lifetime is found for the  $C \ ^1\Sigma^+(v=0)$  state [43]. The fluorescence yield experiments of Letzelter *et al.* [3] on the L state seem to indicate, however, that the observed lifetime is largely determined by

predissociation. The results of these experiments have to be interpreted with some caution since the fluorescence yield is determined after excitation to several rotational levels in the L state with a broadband light source.

The predissociation observed for the  $K \ ^1\Sigma^+(v=0)$  is most probably caused by the same  $^1\Sigma^+$  state responsible for the predissociation in the L and W state. The interaction between the two  $^1\Sigma^+$  states is  $J$ -independent and as a result the predissociation in the K state will not depend on the rotational quantum number, as has been observed.

The  $^1\Sigma^+$  state which is responsible for the predissociation in these states can on energetic grounds only correlate to the ground state atoms C ( $^3P$ ) and O ( $^3P$ ). Only two  $^1\Sigma^+$  states are expected to correlate to the ground states atoms, i.e. the X  $^1\Sigma^+$  ground state and the D'  $^1\Sigma^+$  valence state. The D' state which has only recently been observed by Wolk and Rich [44] is very weakly bound at a relatively large internuclear distance. Recent calculations performed by Tchang-Brillet *et al.* [45] on the D'  $^1\Sigma^+$  and B  $^1\Sigma^+$  states show that the predissociation observed in the B state is caused by the interaction of the D' state with the B state. The predissociation observed for the Rydberg states L  $^1\Pi$ , K  $^1\Sigma^+$  and W  $^1\Pi$  is most likely also caused by an interaction of these states with the the D' valence state, whose repulsive part of the potential is expected to cross the potential curves of the Rydberg states at the outer turning points.

The predissociation rates found for the L'  $^1\Pi(v=1)$  and W'  $^1\Pi(v=2)$  are much larger than those found for the L  $^1\Pi(v=0)$ , K  $^1\Sigma^+(v=0)$  and W  $^1\Pi(v=0)$  states. In contrast to these states the L' and the W' state show no  $J$ -dependence of the predissociation rate. The perturbing state causing this strong predissociation can therefore not be the  $^1\Sigma^+$  state which is responsible for the predissociation in the L, K and W state nor can it be a state of  $^1\Sigma^-$  or  $^1\Delta$  symmetry which would also yield  $J$ -dependent predissociation rates. It has to be concluded that the perturbing state has  $^1\Pi$  or  $^3\Pi$  symmetry. The difference in interaction strength between the L' and W' and the L, K and W states with the perturbing  $\Pi$  state is most probably due to a difference in Franck-Condon overlap between the wavefunctions of the interacting states. Since it is not clear whether the perturbing state has  $^1\Pi$  or  $^3\Pi$  symmetry it is not possible to identify the perturbing state. It can very well be that this state is the same state which is responsible for the observed predissociation in the E  $^1\Pi(v=0)$  state [3, 22].

## 8.6 Summary

In a 2+1 double-resonance experiment on CO, where the B  $^1\Sigma^+$  state is used as intermediate state, five Rydberg states around  $103\,000\text{ cm}^{-1}$  have been studied. Accurate molecular constants have been obtained. From the observed W'(v=2)  $\leftarrow$  B  $^1\Sigma^+(v=0)$  transition it is concluded that the W'(v=2) state is a  $^1\Pi$  state and that it is perturbed by the C  $^1\Sigma^+(v=5)$  state. From the observed linewidths predissociation rates for the Rydberg states could be determined. For the first time a clear  $J$ - and  $e/f$ -dependence for the predissociation rates could be observed. On ground of the observed  $J$ -dependence of the predissociation rates one of the perturbing states has been identified as the D'  $^1\Sigma^+$  state.

## Acknowledgements

The authors wish to thank Drs. Giel Berden for his help with the data acquisition program and Dr. Gerard Meijer and Prof. D.H. Parker for fruitful discussions and valuable suggestions. Prof. R.W. Field is gratefully acknowledged for his suggestions on the interpretations of the observed

predissociation rates. This research was made possible by the financial support of the Dutch Organization for Fundamental Research of Matter (FOM).

## References

1. E.F. van Dishoek and J.H. Black, in *"Physical Processes in Interstellar Clouds"*, ed. G. Morfill and M.S. Scholer Reidel, Dordrecht, (1987)
2. E.F. van Dishoek and J.H. Black, *Astroph. J.* **334**, 771 (1988)
3. C. Letzelter, M. Eidelsberg, F. Rostas, J. Breton and B. Thieblemont, *Chem. Phys. Lett.* **114**, 273 (1987)
4. G. Stark, K. Yoshino, P.L. Smith, K. Ito and W.H. Parkinson, *Astrophys. J.* **369**, 574 (1991)
5. G. Stark, K. Yoshino, P.L. Smith, K. Ito and W.H. Parkinson, *Astrophys. J.* **395**, 705 (1992)
6. G. Stark, K. Yoshino, P.L. Smith, J.R. Esmond, K. Ito and H.M. Stevens, accepted for publication in *Astrophys. J.*
7. M. Eidelsberg, J.Y. Roncin, A. Le Floch, F. Launay, C. Letzelter, and J. Rostas, *J. Mol. Spectrosc.* **121**, 309 (1987)
8. M. Eidelsberg and F. Rostas, *Astron. Astrophys.* **235**, 472 (1990)
9. M. Eidelsberg, J.J. Benayoun, Y. Viala and F. Rostas, *Astron. Astrophys. Suppl. Ser.* **90**, 231 (1990)
10. M. Eidelsberg, J.J. Benayoun, Y. Viala and F. Rostas, P.L. Smith, K. Yoshino, G. Stark and A. Shettle, *Astron. Astrophys.* **265**, 839 (1992)
11. P.F. Levelt, W. Ubachs and W. Hogervorst, *J. Phys. II France* **2**, 801, (1992)
12. P.F. Levelt, W. Ubachs and W. Hogervorst, *J. Chem. Phys.* **97**, 7160 (1992)
13. T. Masaki, Y. Adachi and C. Hirose, *Chem. Phys. Lett.* **139**, 62 (1987)
14. S. Sekine, T. Masaki, Y. Adachi and C. Hirose, *J. Chem. Phys.* **89**, 3951 (1988)
15. S. Sekine, Y. Adachi and C. Hirose, *J. Chem. Phys.* **90**, 5346 (1989)
16. S. Sekine, S. Iwata and C. Hirose, *Chem. Phys. Lett.* **180**, 173 (1991)
17. M.A. Hines, H.A. Michelsen and R.N. Zare, *J. Chem. Phys.* **93**, 8557 (1990)
18. N. Hosoi, T. Ebata and M. Ito, *J. Phys. Chem.* **95**, 4182 (1991)
19. T. Ebata, N. Hosoi and M. Ito, *J. Chem. Phys.* **97**, 3920 (1992)
20. K. Tsukiyama, M. Momose, M. Tsukakoshi and T. Kasuya, *Opt. Comm.* **79**, 88 (1990)
21. F. Merkt and T.P. Softley, *Mol. Phys.* **72**, 787 (1991)
22. P. Klopotek and C.R. Vidal, *Opt. Soc. Am.* **2**, 869 (1985)
23. S. Gerstenkorn and P. Luc, *"Atlas du spectroscopie d'absorption de la molecule d'iode"*, CNRS, Paris (1978)

24. S. Gerstenkorn and P. Luc, *Rev. Phys. Apl.* **14**, 791 (1979)
25. J. Cariou and P. Luc, *"Atlas du spectroscopie d'absorption de la molecule tellure"*, CNRS, Paris (1980)
26. M.A. Quesada, A.M.F. Lau, D.H. Parker, D.W. Chandler, *Phys. Rev. A* **36**, 4107 (1987)
27. S.N. Dobryakov and Y.S. Lebedev, *Sov. Phys. Docl* **13**, 873 (1969)
28. R. Loudon, *"The Quantum Theory of Light"*, Clarendon Press, Oxford (1973)
29. G.R. Cook, P.H. Metzger and M. Ogawa, *Can. J. Phys.* **43**, 1706 (1965)
30. Tilford and Vanderslice, *J. Mol. Spectrosc.* **26**, 419 (1968)
31. Schmid and Gerö, *Z. Phys.* **93**, 656 (1935)
32. G.W. Loge, J.J. Tiee and F.B. Wampler, *J. Chem. Phys.* **79**, 196 (1983)
33. P.J.H. Tjossem and K.C. Smyth, *J. Chem. Phys.* **91**, 2041 (1989)
34. G. Guelachvili, D. de Villeneuve, R. Farrenq, W. Urban and J. Verges, *J. Mol. Spectrosc.* **98**, 64 (1983)
35. D.M. Cooper and S.R. Langhof, *J. Chem. Phys.* **74**, 1200 (1981)
36. K. Kirby and D.L. Cooper, *J. Chem. Phys.* **90**, 4895 (1989)
37. K. Eikema, W. Ubachs and W. Hogervorst, private communication
38. S. Ogawa and M. Ogawa, *J. Mol. Spec.* **49**, 454 (1974)
39. P. Hammond, G.C. King, J. Jureta and F.H. Read, *J. Phys. B* **18**, 2057 (1985)
40. M. Ebben, M. Drabbels, J.J. ter Meulen, *J. Chem. Phys.* **95**, 2292 (1991)
41. I. Kovacs, *"Rotational Structure in the Spectra of Diatomic Molecules"*, Adam Hilger LTD, London (1969)
42. K.P. Huber and G. Herzberg, *"Molecular Spectra and Molecular Structure. IV. Constants of Diatomic Molecules"*, Van Nostrand-Reinhold, New York (1979)
43. M. Drabbels, *Ph.D Thesis, Chapter 7*, Katholieke Universiteit Nijmegen (1993)  
M. Drabbels, W.L. Meerts and J.J. ter Meulen, accepted for publication in *J. Chem. Phys.*
44. G.L. Wolk and J.W. Rich, *J. Chem. Phys.* **79**, 12 (1983)
45. W. Tchang-Brillet, P.S. Julienne, J.M. Robbe, C. Letzelter and F. Rostas, *J. Chem. Phys.* **96**, 6735 (1992)

### **Pulsed-Cw Double-Resonance Spectroscopy On The B $^1\Sigma^+(v' = 0) \leftarrow$ A $^1\Pi(v'' = 0)$ system of CO**

#### **Abstract**

A 2+1 double-resonance laser-induced fluorescence study of the B  $^1\Sigma^+(v' = 0) \leftarrow$  A  $^1\Pi(v'' = 0)$  system of CO has been performed in which the high power of a pulsed laser is combined with the narrow bandwidth of a single-mode cw ring dye laser. Using this technique the term value of the A state could be accurately be determined,  $T=64\,748.0085\pm 0.0019\text{ cm}^{-1}$ . This study has shown that with this technique it is in principle possible to perform spectroscopy on highly excited electronic states of molecules up to 20 eV with a resolution of several MHz.

## 9.1 Introduction

Spectroscopy of highly excited states of molecules has been hampered by the lack of intense and tunable light sources in the VUV and XUV region of the electromagnetic spectrum. With the rapid development of laser technology during the last decades it is now possible to generate tunable coherent VUV and XUV radiation via third-order frequency conversion in atomic or molecular gasses [1]. Because of the high powers that are required for the generation of intense VUV radiation pulsed lasers are used, although it has been shown that in some favorable cases it is possible to use cw dye lasers [2]. Due to the relatively large bandwidth of pulsed laser the resolution at which highly excited states can be studied by direct VUV or XUV spectroscopy has been limited to 200 MHz [3].

Another way to study high-lying electronically excited states is by double-resonance spectroscopy. It has been shown by Meijer *et al.* [4] that it is possible to study states at an energy of  $65\,000\text{ cm}^{-1}$  with a resolution of several MHz by using a pulsed laser to efficiently populate a high energy intermediate state and a single-mode cw dye laser to probe the highly excited state.

In this paper we report a high resolution study on the  $B\ ^1\Sigma^+(v' = 0) \leftarrow A\ ^1\Pi(v'' = 0)$  system of CO using a similar technique. The A state at an energy of  $64\,750\text{ cm}^{-1}$  is populated with a pulsed dye laser via a two-photon transition after which the  $B \leftarrow A$  transition is probed by a single-frequency ring dye laser. Since the excitation efficiency of the two-photon transition is expected to be small the experiment has not been performed on a molecular beam but on a jet where the density of molecules is several orders of magnitude higher. As a consequence the resolution is limited by the residual Doppler width of 150 MHz.

Both the  $B\ ^1\Sigma^+$  and the  $A\ ^1\Pi$  state of CO have been extensively studied. Although previous low resolution studies on the A state showed that this state undergoes numerous perturbations [5, 6, 7] the first comprehensive study of the A state was performed in 1972 by Field *et al.* [8] who established the appropriate energy matrix and fitted all the absorption and emission data involving the  $A\ ^1\Pi$  and perturbing states. This systematic analysis provided deperturbed band origins and rotational constants for the A state and the perturbing states. Recently this perturbation analysis has been extended to rotational levels up to  $J=75$  by Le Floch *et al.* [9].

Ever since the first studies of the B state it is well known that the high rotational levels of this state are subjected to a strong predissociation [10, 11, 12, 13]. Until recently it was assumed that no other perturbations are present in the B state. But high resolution studies on the B state using Fourier transform spectroscopy [14] and two-photon laser-induced fluorescence spectroscopy [15] have revealed that this state is weakly perturbed at low  $J$ -levels by the nearby lying  $e\ ^3\Sigma^-(v = 28)$  state. In the present study the perturbations in both systems are investigated by double-resonance spectroscopy with a resolution of 150 MHz.

## 9.2 Experimental

To excite the molecules from the electronic ground state to a rotational level in the electronically excited  $A\ ^1\Pi(v = 0)$  state a pulsed laser system is used consisting of a Nd:YAG (Quintel YG 681-10C) pumped dye laser (Continuum TDL60) operated with DCM dye. After frequency doubling the output of this laser in a KDP crystal 10 mJ tunable UV light is obtained with a bandwidth of  $0.2\text{ cm}^{-1}$ .

The narrow bandwidth radiation to induce the  $B\ ^1\Sigma^+(v = 0) \leftarrow A\ ^1\Pi(v = 0)$  transition is produced by a single-frequency cw ring dye laser (Spectra Physics 380D) operated on Stilbene 3

dye and pumped with 5 W of an Argon ion laser (Spectra Physics 2045-15). The output power at 440 nm is typically 200 mW. The bandwidth of this laser system, determined by the high frequency jitter is less than 1 MHz. For absolute frequency calibration the absorption spectrum of the Te<sub>2</sub> molecule is recorded along with the excitation spectrum [16]. For relative frequency calibration the transmission fringes of a pressure and temperature stabilized Fabry-Perot interferometer with a free spectral range of 149.72 MHz are recorded.

The experiments are performed with a molecular jet of CO formed by expanding 2 atm neat CO through a pulsed valve with an orifice of 1 mm. The molecular jet is crossed 50 mm downstream of the orifice by the two counter-propagating laser beams. The ground state carbon monoxide is at this point two-photon excited by the softly focussed ( $f=100$  cm) pulsed laser beam. The VUV fluorescence from the A state down to the ground state is monitored by a solar blind photomultiplier (EMI 9413) placed in the vacuum chamber. In order to efficiently excite molecules from the A state to the B state the counter-propagating cw laser beam is also focussed into the jet using an  $f=50$  cm lens. The fluorescence from the B state down to the various vibrational levels of the A state is collected by a quartz lens system and imaged onto the photocathode of a photomultiplier (EMI 9893B). In order to reduce the scattered light from both the cw and the pulsed laser a Schott GG 475 cutoff filter is placed in front of the photomultiplier. In this way only the fluorescence from the B state to the higher vibrational levels in the A state is monitored. The signals from both photomultipliers are processed by a digital oscilloscope (LeCroy 7400) and two boxcar integrators (SRS 250) interfaced with a Personal Computer.

### 9.3 Results

In a first step a rotational level in the  $A^1\Pi(v=0)$  state is populated by the frequency doubled pulsed dye laser. Figure 9.1 shows a recording of the  $A^1\Pi(v'=0) \leftarrow X^1\Sigma^+(v''=0)$  transition, detecting the VUV fluorescence from the A state to the electronic ground state. Due to the low rotational temperature, 4 K, only the lowest 3 rotational levels are populated and a relatively simple excitation spectrum is obtained. Besides the normal P, Q and R transitions the for two-photon characteristic O and S transitions are also observed. According to the selection rules for a two-photon transition the  $\Pi^+$  ( $e$ )  $\Lambda$ -doublet component in the A state is probed by  $\Delta J=0, \pm 2$  transitions and the other  $\Lambda$ -doublet component,  $\Pi^-$  ( $f$ ), is probed by  $\Delta J=\pm 1$  transitions. These selection rules also prohibit observation of the R(0) transition.

In the second step the  $B^1\Sigma^+(v'=0) \leftarrow A^1\Pi(v''=0)$  transition is induced by the cw laser. From the selection rules it follows that from  $e$ -symmetry levels in the A state only  $\Delta J=\pm 1$  transitions can be induced whereas from  $f$ -symmetry levels only  $\Delta J=0$  transitions are possible. Figure 9.2 shows the  $B \leftarrow A$  P(2) transition after the  $J=2$  rotational level in the A state is populated via an S(0) transition. The linewidth of this transition amounts to 145 MHz and is mainly determined by the residual Doppler broadening in the molecular jet. The homogeneous line broadening caused by the short lifetime of both the A state, 10 ns [17], and the B state, 30 ns [15], is negligible.

The number of transitions that can be studied at high resolution is limited by the poor signal-to-noise ratio. Only the strongest  $A \leftarrow X$  transitions provide a high enough population in the A state that a double-resonance signal can be observed. For this reason most of the observed transitions involve the  $e$ -symmetry  $\Lambda$ -doublet components in the A state which can be populated by the strong S transitions. Only one  $B \leftarrow A$  transition involving an  $f$   $\Lambda$ -doublet component in the A state is observed, i.e. the Q(2) transition. However, the frequency of this transition could



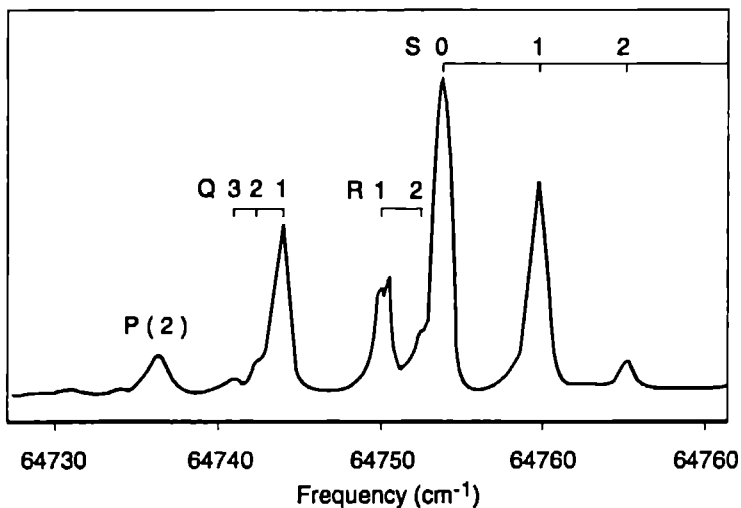


**Figure 9.1:** Laser-induced fluorescence spectrum of the  $A^1\Pi(v'=0) \leftarrow X^1\Sigma^+(v''=0)$  two-photon transition in CO.

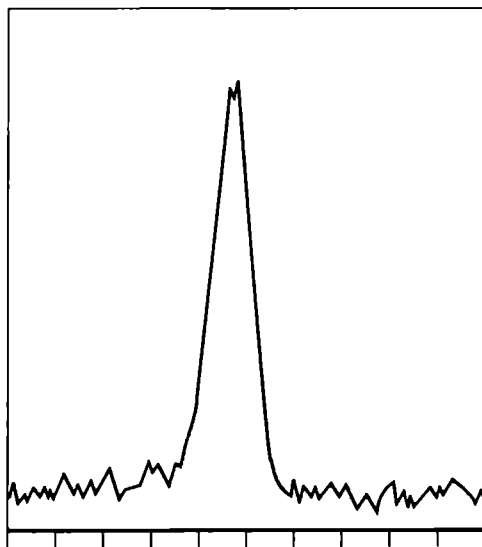


**Figure 9.2:** Recording of the  $B^1\Sigma^+(v'=0) \leftarrow A^1\Pi(v''=0)$   $P(2)$  double-resonance transition. The  $J=2$  level in the A state is populated via the  $A^1\Pi(v'=0) \leftarrow X^1\Sigma^+(v''=0)$   $S(0)$  transition. The frequency is marked every 150 MHz

Trans.	Frequency	Trans.	Frequency
P(1)	22 168 169(2)	R(1)	22 179.859(2)
P(2)	22 165.698(2)	R(2)	22 185.176(2)
P(3)	22 163.941(2)	R(3)	22 191.197(2)
P(4)	22 162.919(2)	R(4)	22 197.983(2)

**Table 9.1:** Observed line positions ( $\text{cm}^{-1}$ ) of the  $B^1\Sigma(v'=0) \leftarrow A^1\Pi(v''=0)$  transition in carbon monoxide.

not accurately be determined since the  $\text{Te}_2$  absorption spectrum is very sparse in this frequency region. The frequencies of the other observed  $B \leftarrow A$  transitions are listed in Table 9.1. The error in the listed frequencies is mainly determined by the uncertainty at which the line center of a  $\text{Te}_2$  absorption can be determined.

The  $B^1\Sigma(v=0)$  state has already been the subject of a high resolution study [15]. The positions of the rotational energy levels determined in that study are confirmed by the combination differences of the P and R transitions observed in the present experiment. The energy levels of the A state can thus be directly calculated from the observed transition frequencies and the known energy levels of the B state [15]. The results are listed in Table 9.2.

It is well known that the  $A^1\Pi(v=0)$  state is strongly perturbed due to interactions with the nearby lying states,  $D^1\Delta$ ,  $I^1\Sigma^-$ ,  $d^3\Delta$ ,  $e^3\Sigma^-$  and  $a'^3\Sigma^+$  [8]. Recently, the rotational levels in the A state, up to  $J=75$  have been studied by conventional grating spectroscopy with a resolution of  $0.02 \text{ cm}^{-1}$  [9]. The observed rotational structure was fit to an effective Hamiltonian incorporating 10 perturbing states, yielding a matrix of dimension 26. Although the perturbing states cross the A state at high rotational levels,  $J>10$ , the low  $J$ -levels are also strongly perturbed by these states due to the large interaction strengths, which are of the order of  $10 \text{ cm}^{-1}$ . The energy of the lowest rotational levels in the A state of CO can therefore not be described by the simple equation normally used to describe the rotational structure in  $^1\Pi$  states. Since the spectra obtained by the low resolution work can be perfectly described by the Hamiltonian in reference [9]

$J$	Parity	Observed	Calculated [9]	Obs.-Calc.
1	<i>e</i>	64 747.981(2)	64 748.025	-0.044
2	<i>e</i>	64 754.350(2)	64 754.394	-0.044
3	<i>e</i>	64 763.897(2)	64 763.940	-0.043
4	<i>e</i>	64 776.608(2)	64 776.651	-0.043

**Table 9.2:** Observed and calculated [9] energies ( $\text{cm}^{-1}$ ) of rotational levels of the  $A^1\Pi(v=0)$  state of CO.

it can be expected that the parameters for this Hamiltonian are accurate enough to describe the spectra obtained in the present study, even though the resolution in the present experiment is an order of magnitude higher. In Table 9.2 the calculated energies of the lowest rotational levels are listed. When the calculated values are compared with the experimentally determined values a  $J$ -independent difference of  $0.043 \text{ cm}^{-1}$  is observed. This difference is most probably caused by a difference in the absolute values of the transition frequencies determined in both experiments. It is well known that it is very difficult to determine the absolute frequency of a transition better than  $0.1 \text{ cm}^{-1}$  by conventional grating spectroscopy. Since our spectra are calibrated to the  $\text{Te}_2$  frequency standard [16] the values reported in this study are probably the most accurate ones. In order to describe the present results with the Hamiltonian of reference [9] the deperturbed term value of the  $A \ ^1\Pi(v=0)$  state has to be changed to  $T = 64\,748.0085 \pm 0.0019 \text{ cm}^{-1}$ . The model of Le Floch *et al.* [9] is thus capable to describe our high resolution spectra provided a small correction is made for the term value of the  $A$  state.

## 9.4 Discussion

In the present study it is shown that it is possible to study high-lying electronically excited states with a  $2+1$  pulsed-cw excitation scheme. The resolution in the present study has been limited by the residual Doppler broadening in the molecular jet. In order to make full use of the narrow bandwidth of the cw laser system it is necessary to perform this experiment in a molecular beam where the molecules are then excited 30 cm downstream of the nozzle [18]. The density of the CO molecules in the excitation region will in that case be a factor of 50 lower than in the present setup. In view of the poor signal-to-noise ratio in the present study it is not possible to perform a double-resonance study on the  $B \leftarrow A$  transition of CO with MHz resolution.

This does not mean that it is not possible to study electronically excited states in molecules at high resolution with a  $2+1$  excitation scheme. The number of molecules that are excited to the upper electronic state is determined by two factors, *i.e.* the number of molecules excited to the intermediate state and the number of molecules excited from the intermediate state to the upper state.

Whereas it is possible to transfer 50% of the molecules in a rotational level of the electronic ground state to an intermediate excited state via a one-photon transition this is in most cases not possible via a two-photon transition. The excitation rate for a two-photon transition, which is usually several orders of magnitude lower than that for an one-photon transition, depends quadratically on the power of the laser system. In order to excite a large fraction of the ground state molecules to the intermediate state it is necessary to use a laser system with a high spectral brightness, *e.g.* a pulsed dye amplifier (PDA) system. The spectral brightness of a PDA system is usually a factor of 10-20 higher than that of a "normal" pulsed dye laser. This implies that the number of molecules that are excited to the intermediate state can be increased by 2-3 orders of magnitude by replacing a "normal" pulsed dye laser by a PDA laser system. A study of the  $B \leftarrow A$  transition of CO at MHz resolution becomes feasible in this way.

The fraction of molecules that are excited from the intermediate state to the higher electronic state is determined by the excitation rate and the interaction time of the molecules with the laser radiation. The excitation rate depends on the transition strength and the laser intensity. With the laser powers available from narrow bandwidth cw ring dye lasers excitation rates up to  $10^9 \text{ s}^{-1}$  can easily be obtained for one-photon allowed transitions. The interaction time of the molecules with the laser light is mainly determined by the lifetime of the intermediate state. For most diatomic

molecules the radiative lifetime of electronically excited states is in the order of 10-1000 ns. In combination with the above mentioned excitation rates this implies that in most cases a very large fraction of the molecules in the intermediate state can be excited to a higher lying electronic state.

Concluding we can say that the total number of molecules excited to the upper electronic state is largely determined by the excitation efficiency of the two-photon transition to the intermediate state. From the results obtained in the present study it can be concluded that it is very well possible to perform high resolution 2+1 pulsed-cw double-resonance spectroscopy on highly excited states, provided that a laser system with a high spectral brightness, *e.g.* a pulsed dye amplifier system, is used to induce the two-photon transition to the intermediate state. The energy region in which electronically excited states can be studied by this technique is determined by the energy of the intermediate level and the wavelength range that can be covered by both laser systems. With the development of  $\beta$ -BaB<sub>2</sub>O<sub>4</sub> as a non-linear material it is possible to generate efficiently UV light with a wavelength down to 188 nm. Using radiation of this wavelength it is at least in principle possible to study electronic states up to 20 eV with a resolution of a few MHz.

### References

1. C.R. Vidal, in *"Topics in Applied Physics, Volume 59: Tunable Lasers"*, Eds. L.F. Mollenauer and J.C. White, Springer Verlag, Berlin (1987)
2. J. Nolting H. Kunze, I. Schütz and R. Wallenstein, *Appl. Phys. B* **50**, 331 (1990)  
J. Nolting and R. Wallenstein, *Opt. Comm.* **79**, 437 (1990)
3. E. Cromwell, T. Trickl, Y.T. Lee and A.H. Kung, *Rev. Sci. Instr.* **60**, 2888 (1989)
4. G. Meijer, M. Ebben and J.J. ter Meulen, *Chem. Phys. Lett.* **147**, 525 (1988)  
G. Meijer, M. Ebben and J.J. ter Meulen, *Chem. Phys.* **127**, 173 (1988)
5. L. Gerö, *Z. Phys.* **99**, 52 (1936)
6. R. Onaka, *J. Chem. Phys.* **26**, 1763 (1957)
7. J.D. Simmons, A.M. Bass and S.G. Tilford, *Astrophys. J.* **155**, 345 (1969)
8. R.W. Field, B.G. Wicke, J.D. Simmons and S.G. Tilford, *J. Mol. Spectrosc.* **44**, 383 (1972)
9. A.C. Le Floch, F. Launay, J. Rostas, R.W. Field, C.M. Brown and K. Yoshino, *J. Mol. Spectrosc.* **121**, 337 (1987)
10. R. Schmid and L. Gerö, *Z. Phys.* **93**, 656 (1935)
11. A.E. Douglas and C.K. Moller, *Can. J. Phys.* **33**, 125 (1955)
12. P. Klopotek and C.R. Vidal, *J. Opt. Soc. Am.* **2**, 869 (1985)
13. M. Eidelsberg, J.Y. Roncin, A. Le Floch, F. Launay, C. Letzelter and J.Rostas, *J. Mol. Spectrosc.* **121**, 309 (1987)
14. C. Amiot, J.Y. Rochin and J. Verges, *J. Phys. B* **19**, L19 (1986)
15. M. Drabbels, *Ph.D Thesis, Chapter 7*, Katholieke Universiteit Nijmegen (1993)  
M. Drabbels, W.L. Meerts and J.J. ter Meulen, accepted for publication in *J. Chem. Phys.*
16. J. Cariou and P. Luc, *"Atlas de spectroscopy d'absorption de la molecule tellure"*, CNRS, Paris, (1980)
17. R.W. Field, O. Nenoist d'Azy, M. Lavollée, R. Lopez-Delgado and A. Tramer, *J. Chem. Phys.* **78**, 2838 (1982)
18. W.A. Majewski and W.L. Meerts, *J. Mol. Spectrosc.* **104**, 271 (1984)

## Hoge Resolutie UV Spectroscopie Aan In Een Supersone Expansie Gekoelde Moleculen

In dit proefschrift zijn de resultaten weergegeven van experimenten aan aangeslagen electronische toestanden van moleculen. Laser spectroscopie aan deze toestanden kan zeer gedetailleerde informatie leveren over de geometrische en electronische structuur en de diverse bewegingen van de moleculen. Afhankelijk van de resolutie waarmee de moleculen worden bestudeerd kunnen de interacties tussen de verschillende type bewegingen worden waargenomen.

In het experiment beschreven in hoofdstuk 3 is een zeer smalbandige continue kleurstoflaser in combinatie met een moleculaire bundelopstelling gebruikt om de laagst gelegen singlet toestanden in acetyleen te bestuderen. Dankzij de hoge resolutie konden de interacties tussen deze singlet toestanden en isoenergetische triplet toestanden worden bestudeerd en kon bovendien het karakter van de triplet toestanden worden bepaald.

Het is echter niet altijd mogelijk aangeslagen electronische toestanden te bestuderen met een dergelijk smalbandig lasersysteem als gevolg van het relatief lage vermogen van dit type laser. Een aantrekkelijk alternatief is een PDA (pulsed dye amplifier) systeem. Bij dit systeem wordt de smalbandige straling van een continue kleurstoflaser verstrekt door een krachtige gepulste laser. Op deze wijze kan gepulste straling worden gegenereerd met een zeer hoog piekvermogen en een relatief kleine bandbreedte.

Met een dergelijk PDA systeem zijn in hoofdstuk 4 de interne beweging bestudeerd in het molecuul aceton,  $\text{CO}(\text{CH}_3)_2$ . Onderzocht is op welke wijze de rotatie van de twee methyl groepen afhangt van de interne energie en de electronische toestand van het molecuul. Gebleken is dat er niet alleen een sterke interactie bestaat tussen de bewegingen van de twee methyl groepen maar ook tussen deze bewegingen en bepaalde vibraties in het molecuul.

In hoofdstuk 5 is een experiment beschreven aan het zeer symmetrisch molecuul, DABCO. Het is gebleken dat het zelfs mogelijk is om met behulp van het PDA systeem de rotationele structuur op te lossen van dit 20-atomige molecuul. Dankzij de hoge spectrale helderheid van het PDA systeem zijn niet alleen elektrische dipool overgangen waargenomen maar ook de zeer veel zwakkere elektrische quadrupool overgangen.

Hoofdstuk 6 laat zien dat het PDA systeem niet alleen gebruikt kan worden om spectroscopische informatie te verkrijgen. In het experiment beschreven in dit hoofdstuk wordt CO dat zich in de electronische grondtoestand bevindt in de aanwezigheid van een elektrisch veld opgepompt naar de laagst gelegen metastabiele toestand. Dankzij de smalle bandbreedte van het lasersysteem is het

mogelijk één bepaald  $M$ -niveau in de aangeslagen toestand te bezetten. Op deze manier kunnen CO moleculen worden georiënteerd ten opzichte van het aangelegde elektrische veld. Doordat de levensduur van het metastabiele niveau enkele milliseconden bedraagt is het bovendien mogelijk een bundel van georiënteerd metastabiel CO te produceren.

Het laatste gedeelte van dit proefschrift beschrijft experimenten aan hoog aangeslagen elektronische toestanden van het CO molecule. De spectroscopie aan deze toestanden wordt bemoeilijkt door het gebrek aan intense smalbandige afstembare lichtbronnen in het VUV en XUV gedeelte van het elektromagnetische spectrum. Door echter gebruik te maken van verschillende spectroscopische technieken, zoals multifoton en dubbel-resonantie spectroscopie kunnen deze toestanden toch op een relatief eenvoudige manier bestudeerd worden.

In het experiment beschreven in hoofdstuk 7 zijn hoog aangeslagen elektronische toestanden van CO in de aanwezigheid van een sterk elektrisch veld bestudeerd met behulp van twee-foton spectroscopie. Door de verschuivingen en opsplitsingen van de rotationele niveaus ten gevolge van het Stark effect als functie van het elektrische veld te bestuderen konden de permanente elektrische dipool momenten van de verschillende elektronische toestanden worden bepaald. Tevens konden aan de hand van levensduur metingen de overgangswaarschijnlijkheden van deze hoog gelegen toestanden naar lager gelegen toestanden worden bepaald.

Hoofdstuk 8 beschrijft de spectroscopie aan Rydberg toestanden van CO met een energie van ongeveer  $103\,000\text{ cm}^{-1}$ . Deze toestanden zijn bestudeerd in een dubbel-resonantie experiment waar in een eerste stap individuele rotatie-niveaus in de hoog gelegen  $B\ ^1\Sigma^+(v = 0)$  toestand zijn bezet via een twee-foton overgang. Vervolgens zijn de overgangen vanaf deze niveaus naar de Rydberg toestanden onderzocht met behulp van het PDA systeem. Uit de waargenomen Fourier begrensde lijnbreedtes konden de levensduren en predissociatie snelheden van de verschillende Rydberg toestanden worden bepaald.

Hoofdstuk 9 tenslotte beschrijft een soortgelijk experiment aan de  $A\ ^1\Pi(v = 0)$  toestand van CO. Echter in dit experiment is het PDA systeem vervangen door een smalbandige kleurstoflaser. Op deze manier kon nauwkeurige spectroscopische informatie over de  $A\ ^1\Pi(v = 0)$  toestand van CO worden verkregen.

# Curriculum Vitae

---

Op 31 maart 1966 ben ik geboren te Venray. Na het behalen van mijn VWO diploma Gymnasium- $\beta$  aan het "Boschveld College" te Venray in 1984 begon ik in datzelfde jaar met mijn studie Natuurkunde aan de Katholieke Universiteit Nijmegen. Na een afstudeerstage binnen de vakgroep "Molecule- en Laserfysica" werd het doctoraal diploma Experimentele Natuurkunde op 9 februari 1989 behaald. Aansluitend begon ik in dienst van de stichting voor Fundamenteel Onderzoek der Materie (FOM) aan mijn promotie-onderzoek op dezelfde afdeling onder begeleiding van Prof. Dr. J. Reuss, Dr. J.J. ter Meulen en Dr. W.L. Meerts. De resultaten van dit onderzoek staan in dit proefschrift beschreven.





*A far infrared laser sideband spectrometer in the frequency region 550-2700 GHz*

P. Verhoeve, E. Zwart, M. Versluis, M. Drabbels, J.J. ter Meulen, W.L. Meerts, A. Dymanus and D. McClay

Review of Scientific Instruments **61**, 1612 (1990)

*Frequency calibration in the ArF excimer laser tuning range using laser-induced fluorescence of NO*

M. Versluis, M. Ebben, M. Drabbels and J.J. ter Meulen

Applied Optics **30**, 5229 (1991)

*The first LIF spectrum of SiC*

M. Ebben, M. Drabbels and J.J. ter Meulen

Chemical Physics Letters **176**, 404 (1991)

*The  $C^3\Pi(v'=0-6) \leftarrow X^3\Pi(v''=0)$  transition in SiC*

M. Ebben, M. Drabbels and J.J. ter Meulen

Journal of Chemical Physics **95**, 2292 (1991)

*Acetone, a laser induced fluorescence study with rotational resolution at 320 nm*

H. Zuckermann, Y. Haas, M. Drabbels, J. Heinze, W.L. Meerts, J. Reuss and J. van Bladel

Chemical Physics **163**, 193 (1992)

*Production of an intense pulsed beam of oriented metastable CO a  $^3\Pi$*

M. Drabbels, S. Stolte and G. Meijer

Chemical Physics Letters **200**, 108 (1992)

*High resolution laser induced fluorescence study of a cage molecule,*

*1,4-diazabicyclo[2,2,2]octane, DABCO*

D. Consalvo, M. Drabbels, G. Berden, W.L. Meerts, D.H. Parker and J. Reuss

Accepted for publication in Chemical Physics

*High resolution double resonance spectroscopy on Rydberg states of CO*

M. Drabbels, J. Heinze, J.J. ter Meulen and W.L. Meerts

Accepted for publication in *Journal of Chemical Physics*

*Determination of electric dipole moments and transition probabilities of low-lying singlet states of CO*

M. Drabbels, W.L. Meerts and J.J. ter Meulen

Accepted for publication in *Journal of Chemical Physics*

*A study of the singlet-triplet perturbations in the  $\bar{A}^1A_u$  state of acetylene by high resolution UV spectroscopy*

M. Drabbels, J. Heinze and W.L. Meerts

To be published



